AD-A118 884 GENERAL MOTORS CORP INDIANAPOLIS IN DETROIT DIESEL A--ETC F/G 21/5
TIME-VARIANT AERODYNAMICS FOR TRANSLATIONAL MOTION OF LARGE-TUR--ETC(U)
FEB 82 R L JAY, M J GRITTON, M D ROTHROCK N00019-80-C-0430

UNCLASSIFIED NL

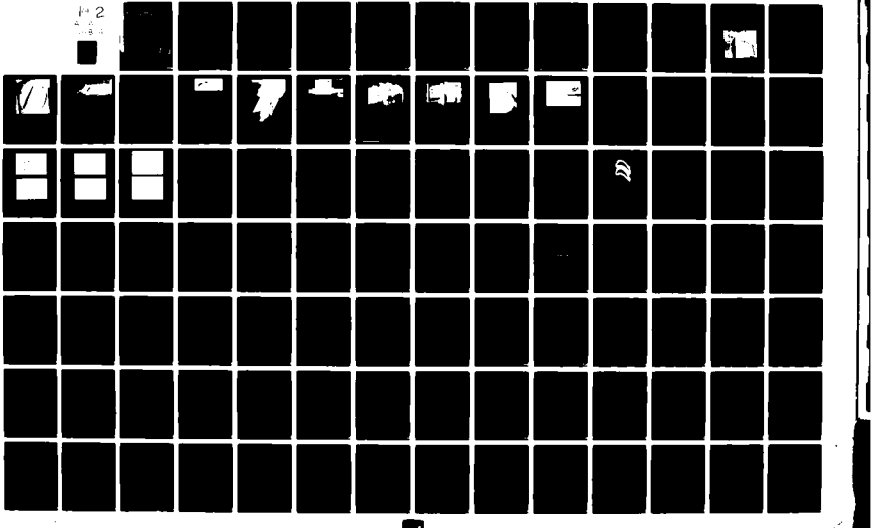

DDA EDR 10992 AD A118884

(12)

TIME-VARIANT AERODYNAMICS FOR TRANSLATIONAL MOTION OF LARGE-TURNING AIRFOILS

R. L. Jay
M. J. Gritton
M. D. Rothrock

Detroit Diesel Allison Division
General Motors Corporation
Indianapolis, Indiana 46206

February 1982

Final Report for Period October 1980 - February 1982

Prepared for
DEPARTMENT OF THE NAVY
NAVAL AIR SYSTEMS COMMAND
Washington, D. C. 20361

UNCLASSIFIED

SECURITY CLASSIFICATION OF THIS PAGE (When Data Entered)

REPORT DOCUMENTATION PAGE	READ INSTRUCTIONS BEFORE COMPLETING FORM
1. REPORT NUMBER	2. GOVT ACCESSION NO. AD-A118884 / 3. RECIPIENT'S CATALOG NUMBER
4. TITLE (and Subtitle) Time-Variant Aerodynamics for Translational Motion of Large-Turning Airfoils	5. TYPE OF REPORT & PERIOD COVERED Final Report
	6. PERFORMING ORG. REPORT NUMBER EDR 10992
7. AUTHOR(s) R. L. Jay, M. J. Gritton, M. D. Rothrock	8. CONTRACT OR GRANT NUMBER(s) N00019-80-C-0430
9. PERFORMING ORGANIZATION NAME AND ADDRESS Detroit Diesel Allison, Division of General Motors Corporation, Indianapolis, Indiana 46206	10. PROGRAM ELEMENT, PROJECT, TASK AREA & WORK UNIT NUMBERS
11. CONTROLLING OFFICE NAME AND ADDRESS Department of the Navy, Naval Air Systems Command, Washington, D.C. 20361	12. REPORT DATE January 1982
	13. NUMBER OF PAGES
14. MONITORING AGENCY NAME & ADDRESS(if different from Controlling Office)	15. SECURITY CLASS. (of this report) Unclassified
	15a. DECLASSIFICATION/ DOWNGRADING SCHEDULE

16. DISTRIBUTION STATEMENT (of this Report)

APPROVED FOR PUBLIC RELEASE
DISTRIBUTION UNLIMITED

17. DISTRIBUTION STATEMENT (of the abstract entered in Block 20, if different from Report)

18. SUPPLEMENTARY NOTES

19. KEY WORDS (Continue on reverse side if necessary and identify by block number)

Cascades, Unsteady Aerodynamics, Forced Response, Time-Variant Data

20. ABSTRACT (Continue on reverse side if necessary and identify by block number)

A cascade of five airfoil sections modelling the hub section of an advanced design turbine featuring a high inlet Mach number and 112 degrees of turning was evaluated at 4 steady-state conditions of varying exit Mach number and expansion ratio. The resulting steady-state airfoil surface pressures were compared to a state-of-the-art analytical prediction.

(Continued)

DD FORM 1 JAN 73 1473 EDITION OF 1 NOV 65 IS OBSOLETE

UNCLASSIFIED

SECURITY CLASSIFICATION OF THIS PAGE (When Data Entered)

20. ABSTRACT (Cont)

A time-variant investigation was conducted at the 4 operating conditions of the steady-state experiment. Data from high response pressure transducers imbedded along the surfaces of the center airfoil was acquired by individually oscillating each airfoil of the cascade normal to its chord. From this data, the time-varying surface pressures as functions of interblade phase angle were quantified and compared with a current unsteady analysis.

SUMMARY

A cascade of five airfoils featuring a high inlet Mach number and 112 degrees of turning was tested in the turbine cascade facility at Detroit Diesel Allison Division of General Motors Corporation. This cascade was the same as that investigated under Naval Air Systems Command Contract N00019-79-C-0087. The cascade was investigated at four steady-state conditions of varying exit Mach number. Data acquired from fixed instrumentation on the airfoil surface and tunnel sidewalls were used along with data from an exit cone probe to determine aerodynamic operation of the cascade. Separation along the airfoil surfaces was investigated by using alcohol injected through static pressure taps located on the surfaces. Schlieren photographs were used as a visual aid in analyzing surface data. The experimental results were compared to an advanced aerodynamic analysis and the correlation indicated excellent agreement, except in separated flow regions.

Following the steady-state experiment, an airfoil instrumented with twelve flush mounted pressure transducers was installed as the center airfoil of the cascade. At the conditions investigated in the steady-state studies, each airfoil was oscillated in translational motion normal to the chordline. Data acquired from the transducers located on the instrumented airfoil were vectorially summed to furnish information relative to the effect of interblade phase angle. These results were compared with an existing flat plate analysis. Several groupings of data were used in these comparisons. The analytical model trends with interblade phase angle for both pressure magnitude and phase lags on the center airfoil surfaces agree favorably with experimental results. The experimental data suggest the existence of a narrow range of interblade phase angles for which the cascade could be unstable in the translational mode.

Conclusions and recommendations based on the reported data are presented for consideration.

TABLE OF CONTENTS

LIST OF ILLUSTRATIONS

LIST OF TABLES

I. INTRODUCTION

The calculation of alternating stresses in turbomachinery airfoils created by resonant vibratory behavior is a necessary step in designing aircraft turbine engines. Failure to account for vibratory behavior can lead to premature engine failures, development cost overruns, increased procurement cycle timing, and reduced engine life. However, a validated technique for prediction of these stresses has not been established to date.

The structural behavior of turbine engine airfoils in terms of frequencies and mode shapes can be made from geometric and material considerations. Frequency and mode shape predictions from the structural models compare favorably with measurements made both in bench and engine test programs. However, the overall vibratory response of the airfoil is influenced not only by structural dynamics, but also by the aerodynamics around the airfoil. A predictive capability for the unsteady aerodynamics field created by periodic disturbances in the airstream or by blade motion has not been established to date, except for specialized cases.

A general analytical model of the unsteady aerodynamic field in which airfoils operate would include proper representation of the steady flow field, the loading on the airfoil due to disturbances which exist in that field, and the loading created by movement of the airfoil in the flow field. Analyses have been presented which model uncambered, zero thickness airfoils in a cascade operating at zero incidence angle in both subsonic and supersonic flow fields (References 1, 2, 3, 4, and 5).* For special cases, such as forced response of thin compressor airfoils operating at low loadings and supersonic flutter of fan stages, these models have yielded good results.

In general, however, airfoils are cambered and have significant thickness. Additionally, blading typically operates with regions of subsonic, transonic, and supersonic flow. Therefore, a critical need exists for the development of more general unsteady aerodynamic analyses which include cambered, loaded airfoils operating in varied aerodynamic fields.

In October 1980, a joint NASA/AF/Navy Symposium entitled "Aeroelasticity of Turbine Engines" was held at NASA-Lewis Research Center in Cleveland, Ohio. This symposium brought together investigators whose studies focus on aspects of turbine engine aeroelasticity. Caruthers (Reference 6) and Caspar and Verdon (Reference 7) reported progress on two-dimensional, subsonic cascade analyses which consider thick, cambered airfoils operating at incidence. Caruthers presented limited correlations for wake excitation of NACA 65 series airfoils. Williams and Dowell (Reference 8) reported on progress at Princeton on small amplitude disturbances in transonic cascades. In discussion, the model which Dr. Williams was developing would be capable of computing, arbitrary, small amplitude, unsteady flows in two dimensional cascades of finitely loaded blades at transonic speeds. In this model, both blade vibration and inflow disturbances are considered. Platzer and Adamson (Reference 9) described a method of characteristics approach to analyze a finite oscillating supersonic cascade with thickness effects. This model is established to analyze flutter for arbitrary blade geometry with sharp leading and trailing edge restrictions.

*The references are listed in Section IV of this report.

These three sets of analyses tend to highlight the "missing links" in a truly predictive aeroelasticity design system. Models such as these, plus improvements and removal of restrictions in the models, are needed. Additionally, basic experimental data must be available in a timely fashion for the correlation of these models. Not only does experimental data furnish benchmark correlative data, but also provides insight into the physical phenomena governing the processes.

For the acquisition of data designed uniquely to furnish results for analytical model improvement and guidance, rectilinear and annular cascades are necessary. In the cascade environment, separation of parameters involved in aeroelasticity can be obtained. Researchers including Carta and St. Hillaire (Reference 10), Boldman and Buggele (Reference 11), Riffel and Rothrock (Reference 12), Jay, Rothrock, Riffel and Sinnet (Reference 13), Jay and Bennett (Reference 14), and Szechenyi, Loiseau, and MaQuennehan (Reference 15) have presented results from detailed measurements made in cascades of turbomachinery airfoils. Flow regimes including subsonic, transonic, and supersonic have been investigated in part. Platzer (Reference 16) examined the unsteady aerodynamic field with regards to needs and current state of the art in 1977. The "Aeroelasticity in Turbine Engines" symposium in late 1980 updated this summary paper and examined the current state of the art in aeroelasticity and again presented problem areas which must be investigated. Among these was the development of transonic models of the unsteady aerodynamics of loaded compressor and turbine stages. To this end, experimental investigations carried out in a high turning turbine cascade were needed.

Under Naval Air Systems Command (NASC) funding, Detroit Diesel Allison (DDA) has acquired data from a five-bladed cascade of turbine airfoils oscillating in a torsional mode (Reference 13). Operation of the airfoils at varying flow conditions resulted in flows around the airfoil which encompassed the subsonic, transonic, and supersonic ranges. The steady-state aerodynamics were documented along with the time-varying pressures on the airfoil surfaces resulting when torsional oscillations of the airfoils in prescribed phase patterns were created.

In order to provide similar information in a translational mode, NASC funded the program described in this report. The experimental program consisted of acquisition of steady-state and time-varying data from the cascade of five airfoils used in execution of the contract described in Reference 13. Aerodynamic conditions investigated were the same as in Reference 13 and exit Mach numbers ranged from subsonic to supersonic. Data from high response pressure transducers imbedded along the surfaces of the center airfoil was acquired by oscillating each airfoil of the cascade individually. From these data, the time-varying surface pressures as functions of interblade phase angle were quantified. A discussion of the experiment, including hardware and data acquisition descriptions, is included along with comparisons of the experimental data with a current unsteady aerodynamic analysis. The trends noted from the data are presented along with a listing of results, conclusions, and recommendations.

II. DISCUSSION

EXPERIMENTAL FACILITY

The Detroit Diesel Allison (DDA) rectilinear turbine cascade facility (Figure 1) was conceived and built as a research tool to evaluate the steady and time-variant aerodynamic characteristics of turbine blade sections having high turning. The facility is a continuous-flow, nonreturn, pressure-vacuum-type wind tunnel; the test section is evacuated by two primary steam ejectors. Up to 10 lbm/sec of filtered, dried, and temperature-controlled air can be used.

The major features of this facility include the following:

- o Continuous operation for extended time periods
- o A mechanized test section for changing cascade incidence angle
- o A schlieren optical system for visual observation and photography of the facility in both steady and unsteady operation
- o Bleed systems on all four cascade inlet sidewalls
- o A sophisticated instrumentation system centered around a digital minicomputer

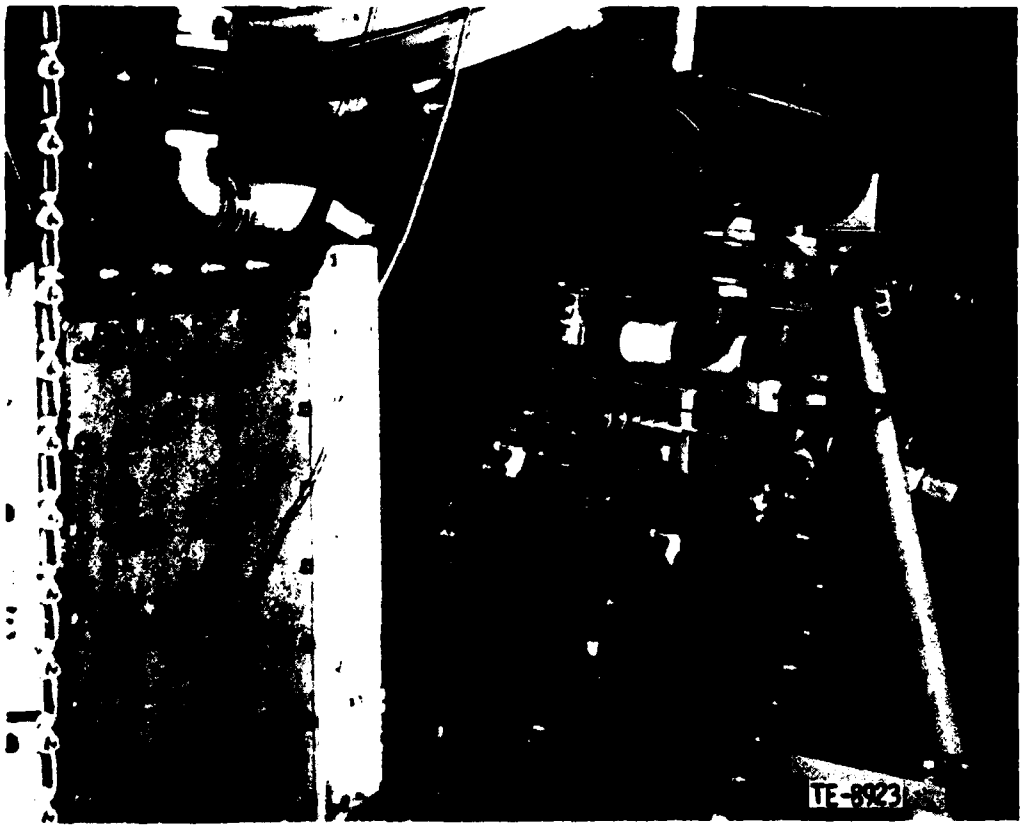

Figure 1. Detroit Diesel Allison rectilinear turbine cascade facility.

In the cascade facility, the entrance flow to the test section is generated by parallel nozzle blocks (Figures 2 and 3) which set the inlet flow direction. The upper nozzle block is movable to ensure that all the flow is directed through the cascade. The cascade inlet Mach number is determined by the cascade geometry under test.

To aid in the establishment of the cascade inlet periodicity, bleed chambers are provided in the upper and lower nozzle blocks. Adjustment of the bleed rate through these chambers allows the inlet flow field to the cascade to be affected.

Active cascade-inlet sidewall boundary-layer control capability to ensure the two-dimensionality of the cascade flow field is effected by the use of suction strips in the cascade sidewalls. Two bleed-hose connections on each strip with separately variable valves provide appropriate bleed flows to the front and rear portions of the sidewall. A third, smaller steam ejector is used to evacuate all of the bleed system used.

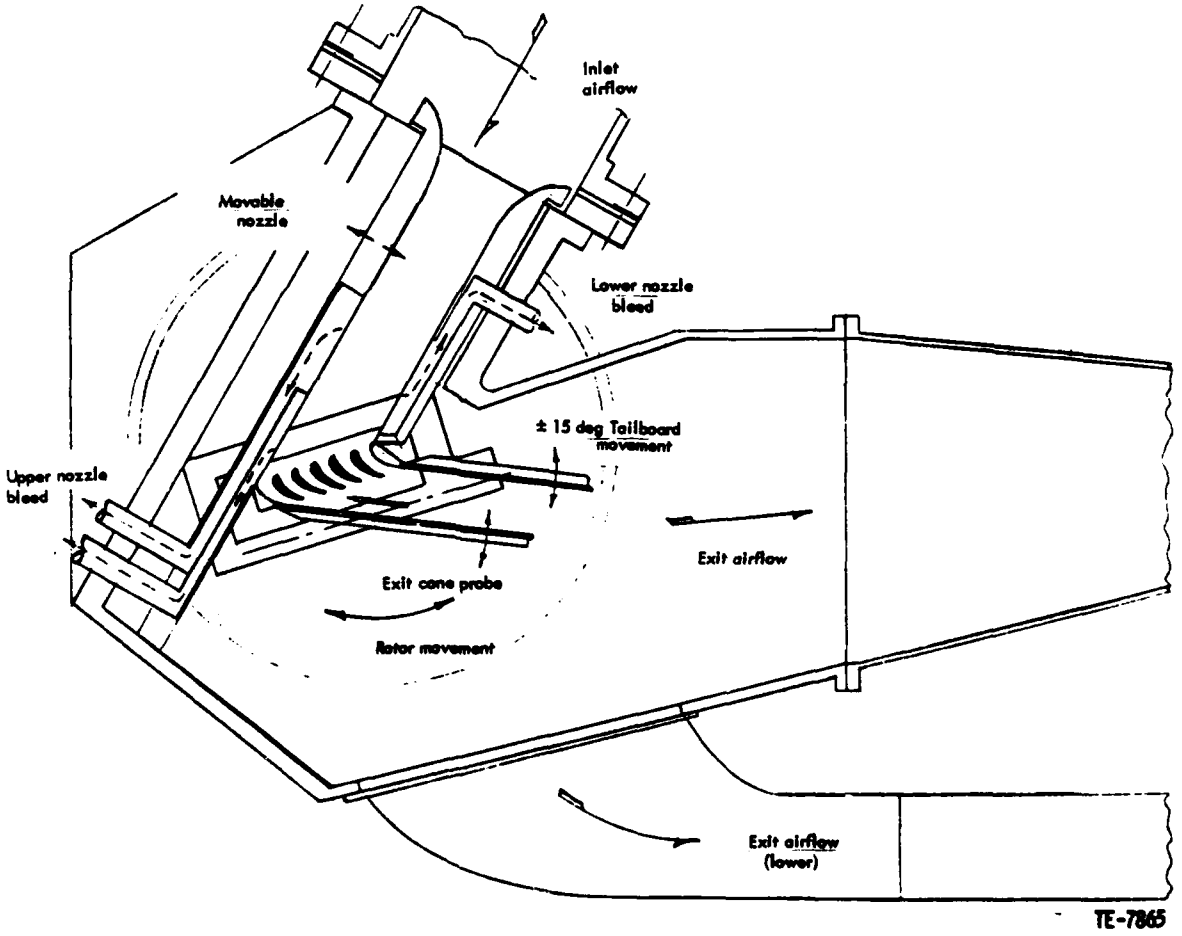

Figure 2. Schematic of turbine rotor cascade hardware.

Figure 3. Photograph of turbine rotor cascade hardware.

The cascade has dummy end blades presenting one surface to the flow, as shown in Figures 3 and 4. The front dummy blade slides along the movable upper nozzle block as the incidence angle is changed. Adjustable porous tailboards are hinged on the aft ends of the dummy blades, serving to set expansion ratio and exit periodicity. The porous tailboards generate a bleed effect because of the lower exit plenum pressure on their outside surfaces. This bleed prevents shock wave reflections back into the cascade during transonic exit operation.

To acquire the steady-state and dynamic data from this facility requires the use of a minicomputer interfaced to both a Scanivalve pressure cabinet and crossbar scanner and a high-speed analog-to-digital multiplexer. Other facility equipment includes racks of amplifiers and signal conditioners for strain gages and pressure transducers and a 14-channel magnetic tape recorder. This equipment is used for the time-variant testing.

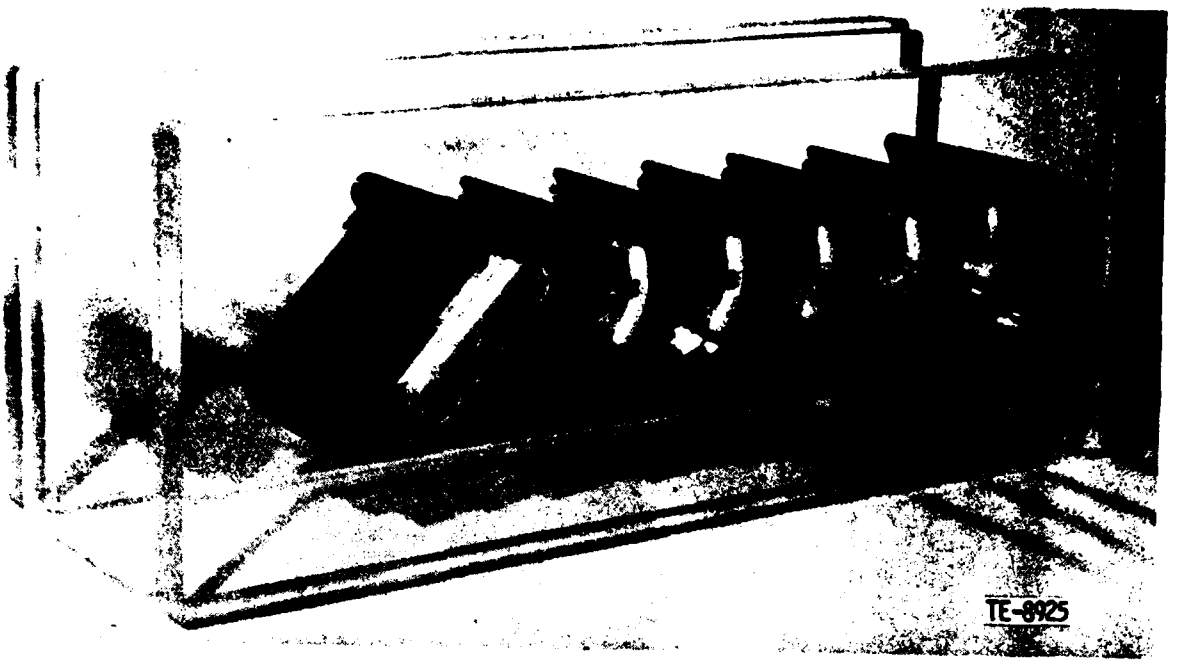

Figure 4. Airfoil cascade in windows.

AIRFOIL CASCADE AND INSTRUMENTATION

The two-dimensional cascade used in this investigation comprises five airfoils that have the profile of a high-turning turbine rotor hub section, as shown in Figure 5. Trunnions have been attached to both ends of each airfoil for support in the cascade sidewalls. The physical dimensions of the airfoils are a 3.00-in. span, and a 2.59-in. chord, a maximum thickness of 0.53 in., and 112° of turning. The cascade physical parameters and the manufacturing coordinates are listed in Table 1.

The cascade airfoils consist of injection-molded fiberglass with a Kevlar outer wrap. Steel trunnions have been attached to both ends of each airfoil with screw clamps and pins. Spacers inserted into the plexiglass windows were used to support and locate the airfoils, while their setting angles were maintained by clamping the trunnions together. Paths for the instrumentation wires and pressure tubes were machined into the blade surface, and the instrumented airfoil trunnions were hollow to allow the wires and tubes to exit the cascade.

The instrumentation used to describe the steady-state aerodynamic performance of the cascade included sidewall static pressure taps at the inlet and exit, upstream total pressure and temperature probes, and a five-hole conical probe to survey the exit. Schlieren flow visualization was also used to help establish exit periodicity in the transonic cases.

TABLE 1. DESCRIPTION OF TURBINE AIRFOIL CASCADE.

Physical Parameters

Chord	2.59 in.
Solidity	1.891
Setting Angle	25.5 deg
Maximum Thickness/Chord	0.205
Leading Edge Radius/Chord	0.024
Trailing Edge Radius/Chord	0.009
Axial Chord Projection	2.34 in.
Torsion Axis Location	35.5% (From L.E.)

Manufacturing Coordinates

Leading Radius 0.06323			Trailing Radius 0.02371		
Station	x	y	Station	x	y
1	-0.8429	0.5398	31	1.7245	0.5398
2	-0.7226	0.5671	32	1.7147	0.5206
3	-0.6766	0.4820	33	1.6137	0.4486
4	-0.6218	0.4024	34	1.5116	0.3780
5	-0.5483	0.3241	35	1.4086	0.3090
6	-0.4861	0.2652	36	1.3045	0.2414
7	-0.4070	0.2097	37	1.1995	0.1754
8	-0.3220	0.1637	38	1.0935	0.1109
9	-0.2326	0.1268	39	0.9865	0.0480
10	-0.1401	0.0987	40	0.8786	-0.0132
11	-0.0456	0.0785	41	0.7697	-0.0727
12	0.0502	0.0654	42	0.6600	-0.1306
13	0.1467	0.0590	43	0.5492	-0.1864
14	0.2434	0.0583	44	0.4371	-0.2397
15	0.3400	0.0631	45	0.3234	-0.2893
16	0.4362	0.0727	46	0.2074	-0.3334
17	0.5319	0.0868	47	0.0889	-0.3698
18	0.6268	0.1051	48	-0.0324	-0.3956
19	0.7210	0.1272	49	-0.1559	-0.4075
20	0.8142	0.1530	50	-0.2797	-0.4018
21	0.9064	0.1820	51	-0.4007	-0.3754
22	0.9976	0.2142	52	-0.5145	-0.3264
23	1.0878	0.2492	53	-0.6159	-0.2553
24	1.1768	0.2869	54	-0.7007	-0.1650
25	1.2648	0.3272	55	-0.7663	-0.0599
26	1.3516	0.3697	56	-0.8124	0.0551
27	1.4374	0.4144	57	-0.8404	0.1759
28	1.5220	0.4611	58	-0.8528	0.2992
29	1.6057	0.5097	59	-0.8524	0.4233
30	1.6883	0.5599	60	-0.8425	0.5469

Figure 5. High-turning turbine rotor hub section.

For the steady-state testing, the center blade of the cascade was instrumented with nine static pressure taps per surface for definition of the surface pressure distributions at each operating condition. For the time-variant phase of the experiment, the center blade of the cascade was instrumented with 12 miniature high-response Kulite pressure transducers. These Kulites were staggered across the center 50% span of the airfoil, five on the pressure surface and seven on the suction surface. The locations of the static pressure taps and Kulite dynamic pressure transducers are given in Table 2.

TABLE 2. PRESSURE MEASUREMENT LOCATIONS IN TERMS OF PERCENT PROJECTED CHORD.

Pressure surface		Suction surface	
Static taps	Kulites	Static taps	Kulites
1.3	10	5	5
5	30	10	15
10	60	20	30
20	75	30	55
30	90	45	70
45		60	80
60		70	92.5
80		80	
95		90	

The Kulite pressure transducers are embedded in the airfoil and covered by a perforated metal screen made flush with the airfoil surface, as shown in Figures 6 and 7. By covering the transducer diaphragm with a metal screen instead of the usual RTV coating there is no increase in its effective mass. This results in a reduction of the perpendicular acceleration sensitivity of the transducer.

Figure 6. Kulite transducer installation--suction surface.

TRANSLATIONAL MODE DRIVE SYSTEM

Each airfoil in the cascade was designed to be oscillated individually by using a common translational mode drive system. Resulting time-variant surface pressures measured at the center airfoil can then be superimposed vectorially to obtain the total time-variant surface pressures, which would result if all five airfoils were driven simultaneously at different interblade phase angles. Since only one set of drive system hardware was installed on the cascade, spacing problems caused by the cascade geometry were alleviated. Also, large blade deflections could be obtained at higher resonant frequencies.

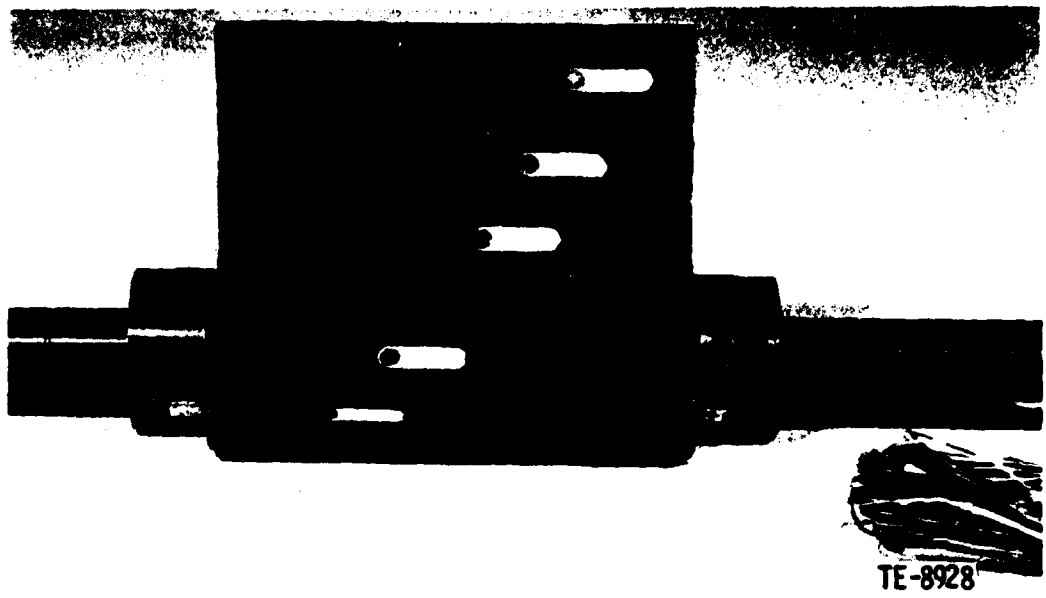

Figure 7. Kulite transducer installation--pressure surface.

The translational mode drive system is a spring bar and hammer arrangement with a driving electromagnet. The airfoil is held on both sides by "battery" clamps which are attached to supporting spring bars. The spring bars are aligned parallel to the airfoil chord. To ensure pure translational motion the spring bars are clamped at both ends and along with the hammers are centered about the trunnion. The hammers are driven by electromagnets aligned normal to the chord. Figures 8 and 9 show the translational mode drive system assembled on a bench rig for test and calibration.

In operation, the electromagnets are powered by a power supply which is switched on and off at the resonant frequency of the translational system by an oscillator. The hammers oscillate normal to the airfoil chord resulting in a rigid body translational deflection of the airfoil. Strain gages are attached to both spring bars at four locations and are calibrated to indicate the amplitude of the deflection. The magnet to hammer air gap and power supply voltage are adjusted to obtain a peak airfoil deflection. The drive system spring bars, designed to a resonant frequency of 205 Hz, allowed a peak amplitude of .010 inches while installed in a bench rig.

During time-variant testing the drive system is installed to oscillate a single cascade airfoil, as shown in Figure 10, in which the fifth airfoil is to be oscillated. The other four airfoils are supported by locating spacers inserted into the trunnion clearance holes of the plexiglass windows. The airfoils are held in place by clamping the trunnions to each other. The cascade is sealed from the outside by a "boot" seal placed over the trunnion and attached to the plexiglass with RTV. This minimizes the damping added to the system. A cooling air system is installed to prevent magnet overheating and local heating of the cascade windows. An enlarged view of the installed translational mode drive system is shown in Figure 11.

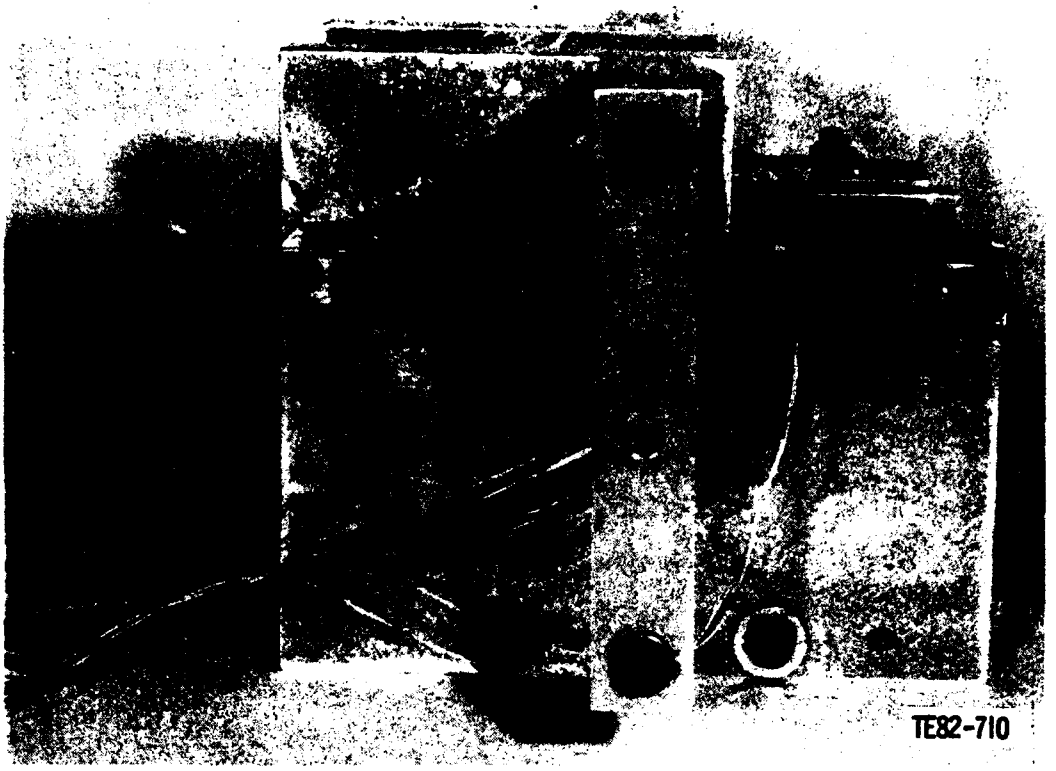

Figure 8. Translational mode drive system bench rig.

CALIBRATION PROCEDURES

Calibrations were performed before the time-variant data were acquired so that the transfer functions throughout the measurement system could be determined. Included in these calibration measurements were strain gage dynamic sensitivities, Kulite static sensitivities, Kulite amplitude and phase shift components due to oscillator, amplifier and signal conditioner gains and phase shifts, and phase shifts between channels of the magnetic tape recorder.

The translational drive system bench rig, shown in Figures 8 and 9, was used to calibrate the spring bar strain gages. The system was oscillated at the translational resonant frequency while the amplitude of the strain gage signals were being read by the mini computer. The amplitude of the airfoil motion was obtained using a dial indicator and height gage to measure the difference between the blades upward peak height and its rest position and the difference between its downward peak height and its rest position. The amplitude of the translational deflection was the sum of these measurements. The strain gage sensitivities were then calculated.

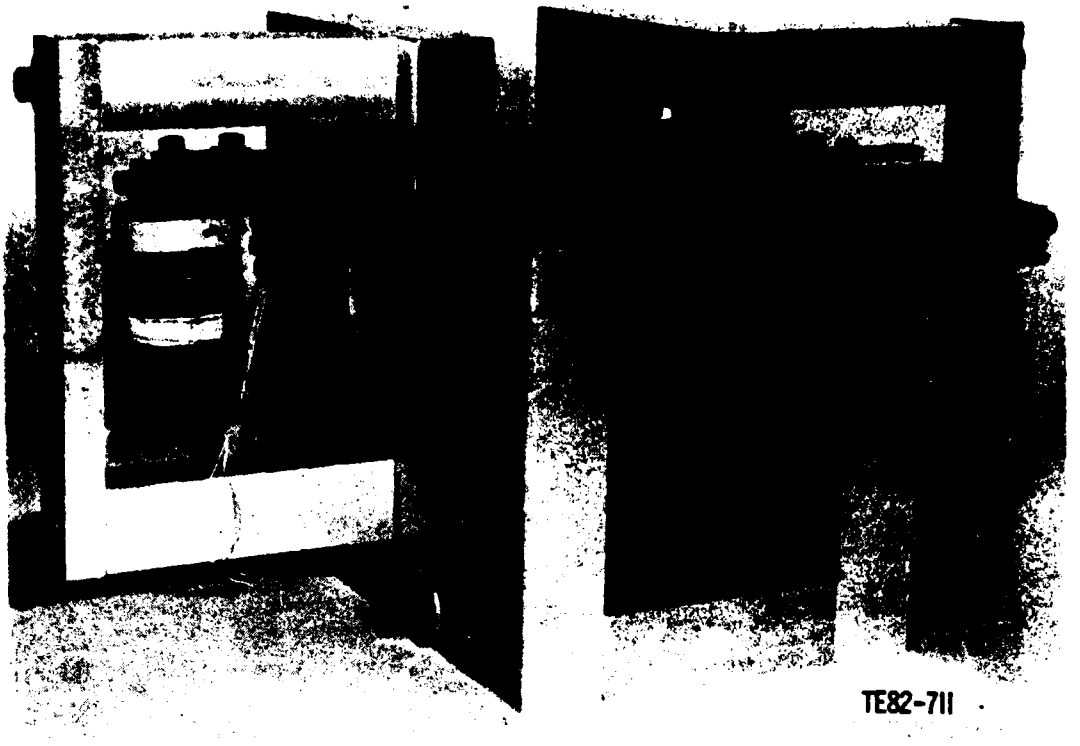

Figure 9. Translational mode drive system bench rig.

The Kulite pressure transducer static sensitivities were obtained with a vacuum-jar calibration rig. The jar, containing the Kulite instrumented airfoil, was evacuated to a desired pressure and the resulting d-c voltage output of each Kulite transducer was recorded. By evacuating over a range of pressures a voltage vs. pressure plot was obtained for each Kulite. The sensitivities in MV/PSI were the slopes of these linear plots. The sensitivities compared closely with manufacturer supplied data.

A Kulite pressure transducer mounted on an oscillating airfoil is subjected to forces resulting from acceleration of the transducer diaphragm and strain transmitted to the transducer through its mounting as well as to forces from the pressure to be measured. To determine the acceleration/strain contribution to the Kulite signal, the instrumented blade was oscillated in the bench rig in a vacuum. Under these conditions, no pressure-induced signal was present. The remaining signal was therefore the result of acceleration/strain effects alone. The minicomputer was used to measure the amplitude and phase shift of each Kulite signal over a range of translational blade amplitudes. The data plots of signal versus translational amplitude were linear. A calibration of acceleration effects was thus obtained and stored in the computer data analysis program to allow corrections to the final data. These effects were less than 5% of a typical pressure measured during time-variant testing.

Figure 10. Translational drive system installed on cascade.

The dynamic response of the blade-mounted Kulites to an oscillating pressure was not obtained. Experience with mounted Kulites has shown that the dynamic characteristics of the Kulites are sufficient for measurements at the frequency used in this testing.

To complete the calibration of the equipment, the gains and phase shifts of all other electronics were determined and stored in the computer for on-line corrections.

DATA ACQUISITION AND ANALYSIS

The primary components of the data acquisition system, including the equipment for on-line and off-line analysis, are shown in Figure 12.

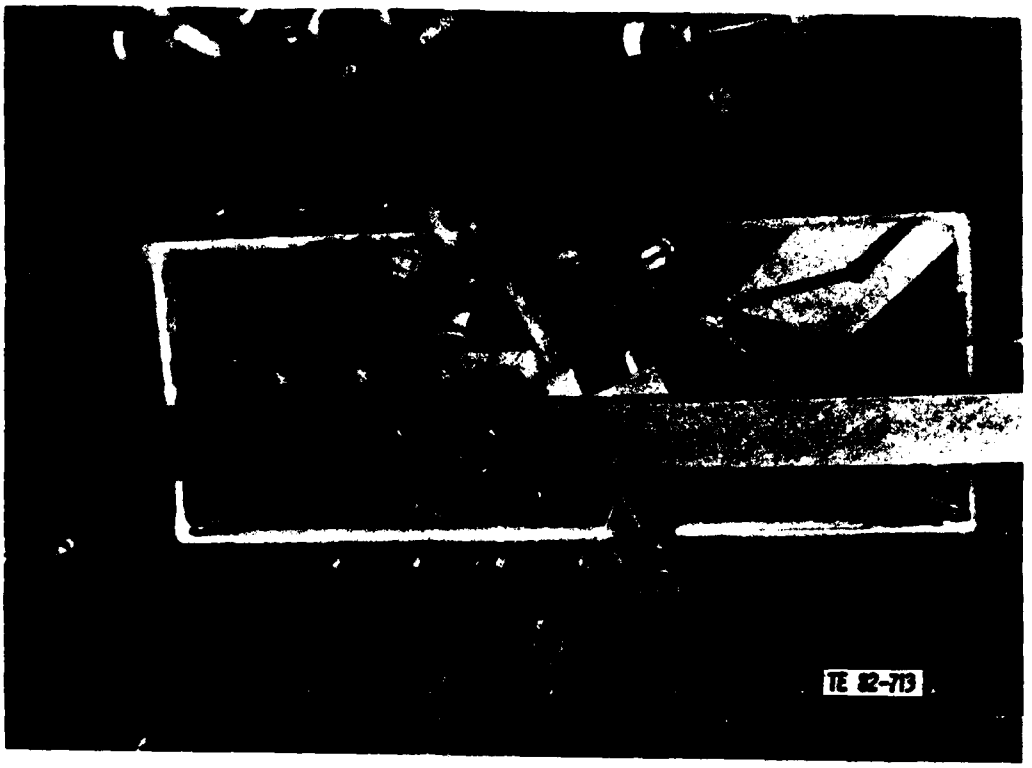

Figure 11. Translational drive system installed on cascade.

With the tunnel in operation, steady-state data were measured using the minicomputer system interfaced with a Scanivalve pressure cabinet and crossbar scanner. Steady-state periodicity was established at the desired operating point and a cone probe exit survey was made yielding aerodynamic performance, wake definition, and mass-averaged properties. The computer listed each measured pressure, including the surface static pressures of the instrumented airfoil. At each operating point schlieren photographs were taken to show trailing edge shock structures. Regions of flow separation were identified by injecting alcohol through the static pressure taps of the center airfoil.

For the time-variant phase of the experiment, the concept of oscillating each blade individually and measuring from the reference center airfoil was used. Figures 13 and 14 present time-variant surface pressure data acquired while simultaneously oscillating in torsion all airfoils compared to the data acquired from oscillating in torsion each airfoil in turn and vectorially superimposing each blade's effect on the total time-variant surface pressure. The comparison is seen to be very close, both in amplitude and phase. Note that in these Figures, the pressures have been normalized to and phased with the motion of the center airfoil. This study was performed using the same cascade as that used in this experiment.

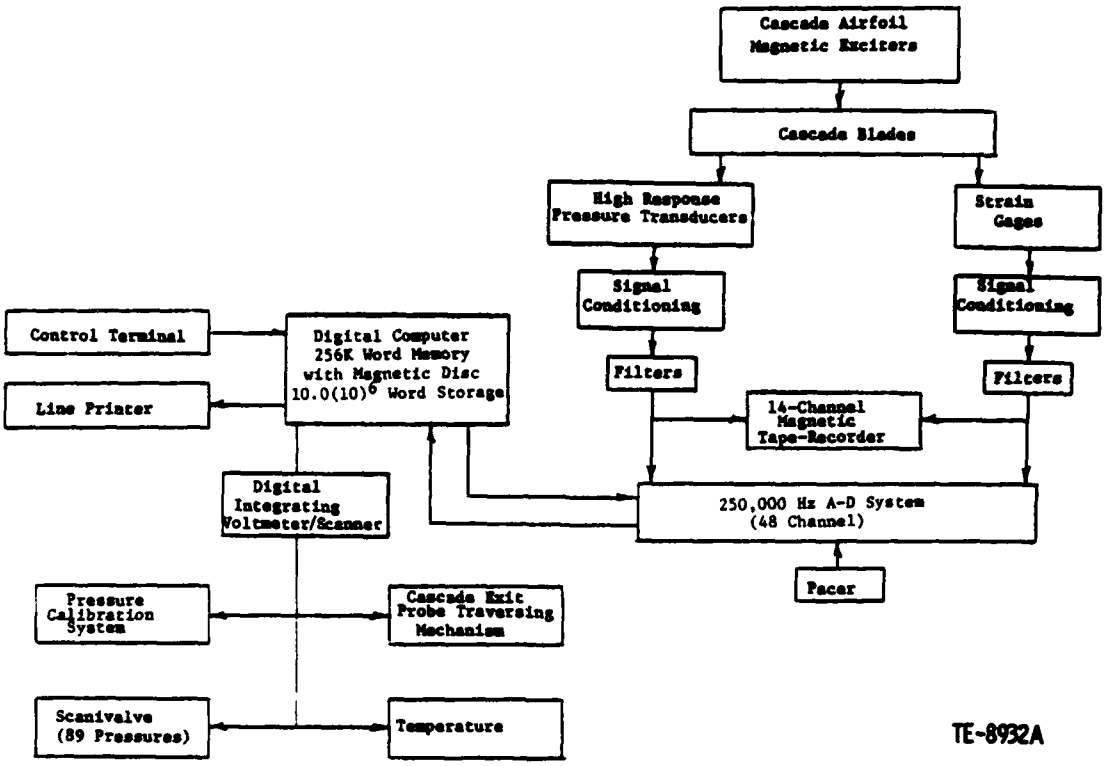

Figure 12. Schematic of data acquisition system.

During time-variant testing the center airfoil was instrumented with Kulite high-response miniature pressure transducers. Each blade was driven individually at each of the four operating conditions described by the steady-state data. Maximum blade deflections were established by magnet to hammer air gap and power supply adjustments. The time-variant signals from Kulites and strain gages were recorded on magnetic tape for each driven blade sequence at each operating condition.

The recorded signals were analyzed off-line by using the analog to digital converter to digitize data, and using these data in specialized digital analysis software. A signal enhancement technique is used whereby three hundred ensembles are collected. Each ensemble contained the same number of points and was acquired by using a signal generated from the blade driven oscillator. This "trigger" initiated the digitalization process of each ensemble. The ensembles were stored and on a point by point basis averaged over the three hundred ensemble sampling. This yielded an enhanced signal by effectively averaging out random signals. This technique is used regardless of signal strength or signal to noise ratio.

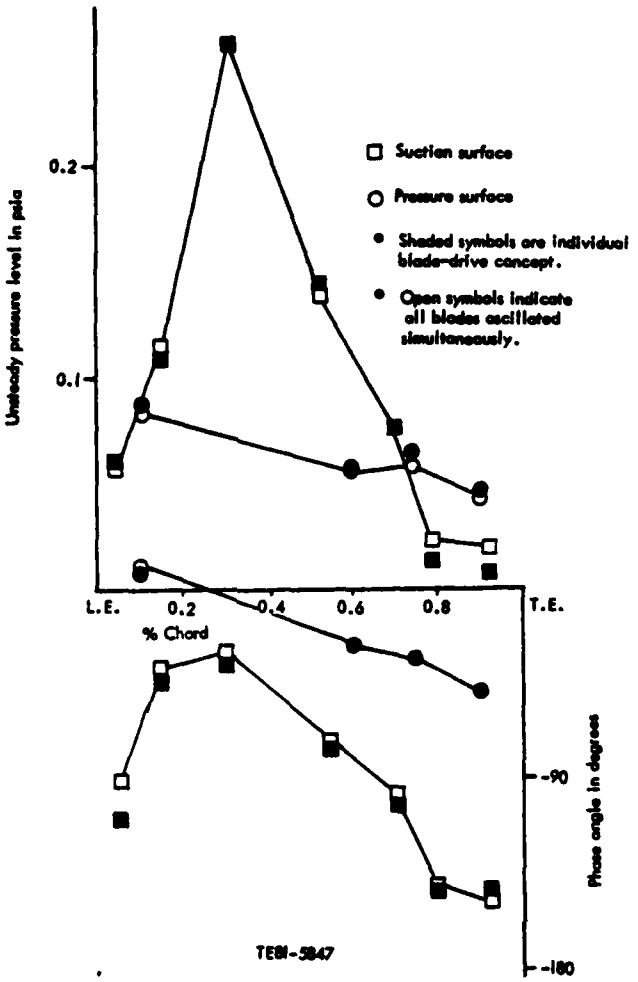

Figure 13. Comparison of dynamic data techniques at Re = 2.3, -45 degrees phase.

The averaged ensemble was subjected to both auto- and cross-correlation analyses and a Fourier analysis. Both techniques yield the uncorrected amplitude and phase angle of the particular time-varying signal of interest. Corrections were made to these quantities based on the information obtained during the calibration phase.

The Kulite data acquired from the center airfoil of the cascade was normalized by the translational deflection of the particular oscillating airfoil. By using a linear superimposition, these data were arranged to yield data at different interblade phase angles for the four expansion ratios.

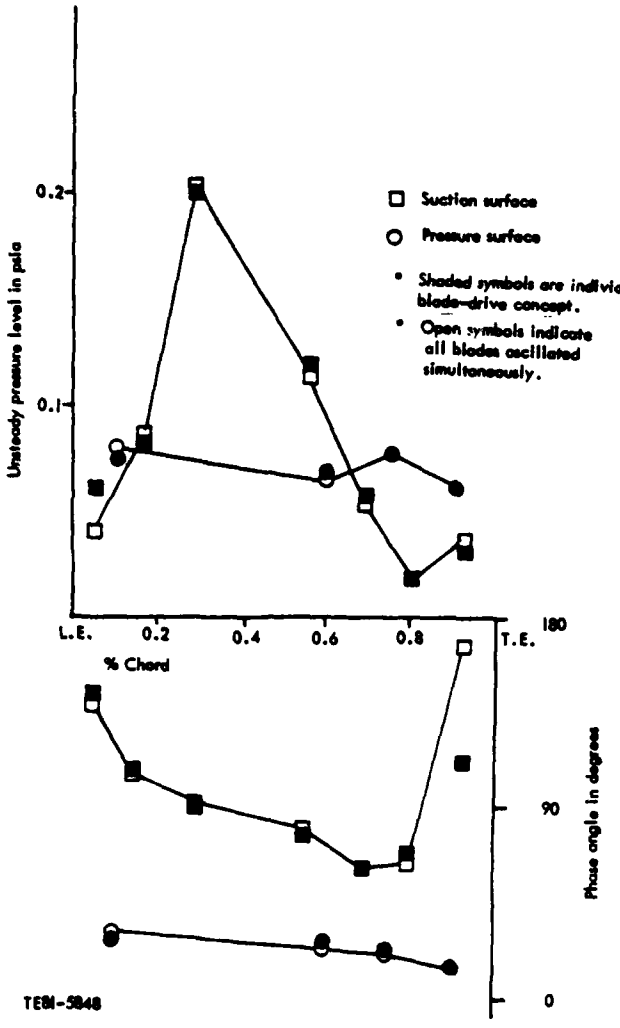

Figure 14. Comparison of dynamic data techniques at Re = 2.3, -45 degrees phase.

RESULTS

Steady-State Operation

The steady-state phase of the experimental research program involved the operation of the cascade at the same four operating conditions used in the torsional cascade test program (Reference 13). The four points were duplicated by controlling the cascade inlet temperature and pressure to match the previous data. The desired expansion ratio was obtained by adjusting the exit tailboards and exit air throttling valve to give the correct cascade back pressure. Inlet and exit periodicity, as determined by static pressure taps and Schlieren flow visualization, was closely maintained. The four cascade operating points are summarized in Table 3.

TABLE 3. STEADY-STATE OPERATING POINTS.

Ideal inlet total to exit static expansion ratio	Mass-averaged expansion ratio	Inlet Mach number	Inlet static pressure (psia)	Cascade incidence angle (deg)	Mass-averaged exit Mach number
1.5:1	1.51	0.50	12.66	-6.6	0.77
1.8:1	1.82	0.53	12.08	-6.6	0.94
2.3:1	2.21	0.53	11.98	-6.6	1.10
2.8:1	2.57	0.53	12.18	-6.6	1.22

The turbine cascade geometry is depicted schematically in Figure 15, which shows the air and metal angles and the airfoil numbering system. Figures 16 through 19 are Schlieren photographs of the cascade, from the viewpoint of Figure 15, at the four operating conditions. Trailing edge shocks are visible for the upper three expansion ratios. The periodicity of the exit flow is evidenced by the identical appearance of each shock structure. As the exit mass-averaged mach number decreased from 1.22 (Fig. 19) to 0.94 (Fig. 17) the shock waves impinging on the suction surface of each airfoil are seen to become more nearly normal. The normal shock wave position shown in Figure 19 for the 1.8 expansion ratio case was somewhat unsteady, possibly attributed to the local flow being almost sonic. Figures 20 and 21 are close-ups of the leading and trailing edge regions for the 2.3 expansion ratio case.

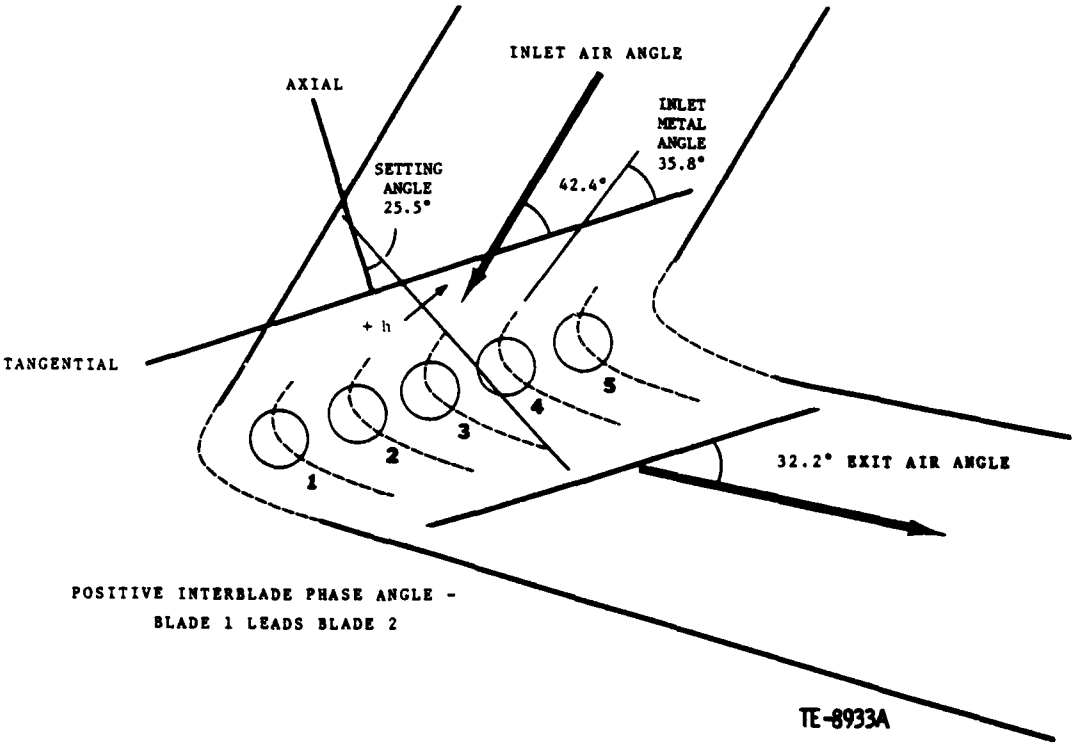

Figure 15. Translation cascade geometry.

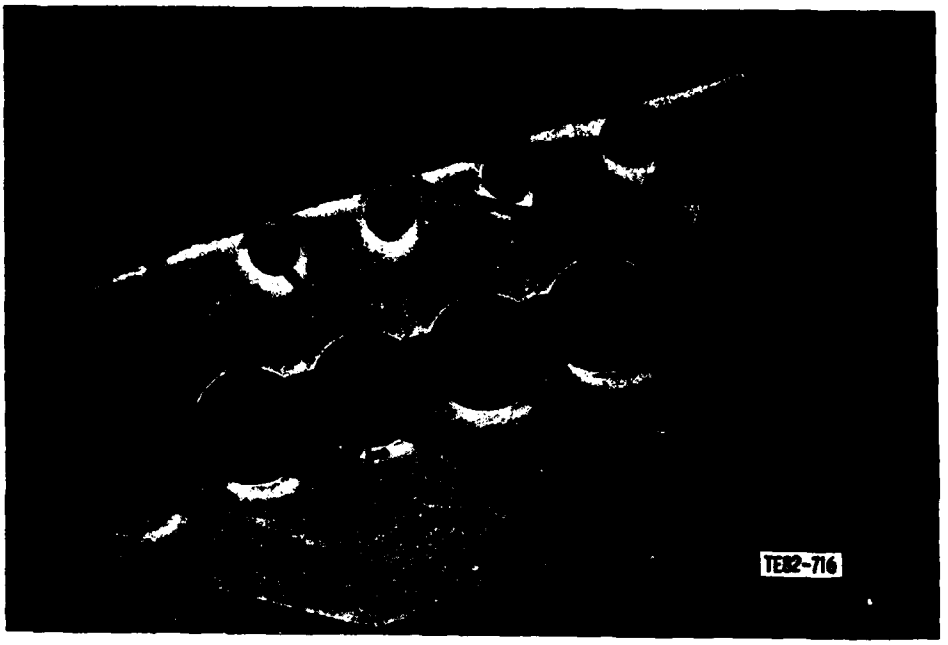

Figure 16. Schlieren photograph at 1.5 expansion ratio.

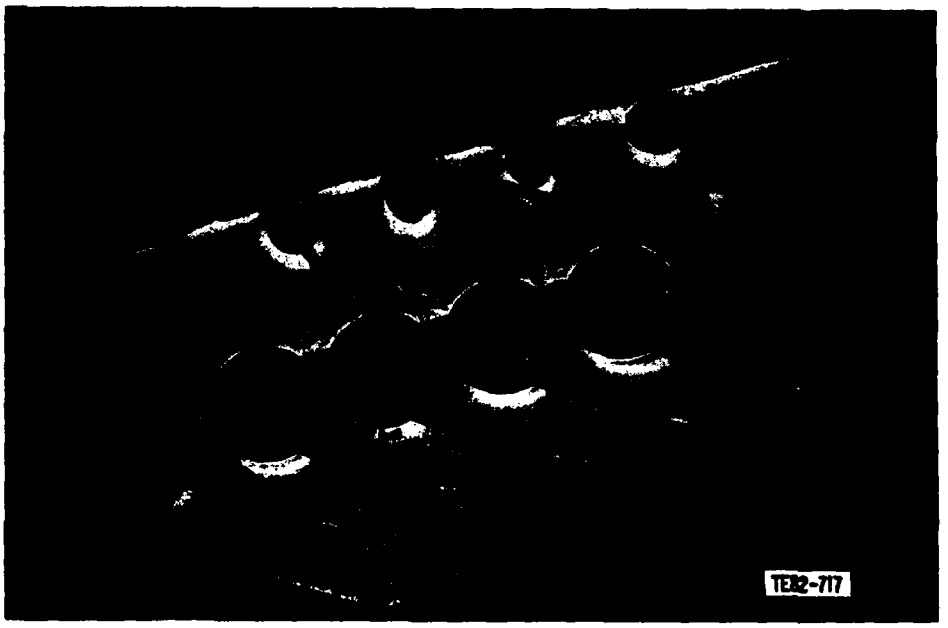

Figure 17. Schlieren photograph at 1.8 expansion ratio.

Figure 18. Schlieren photograph at 2.3 expansion ratio.

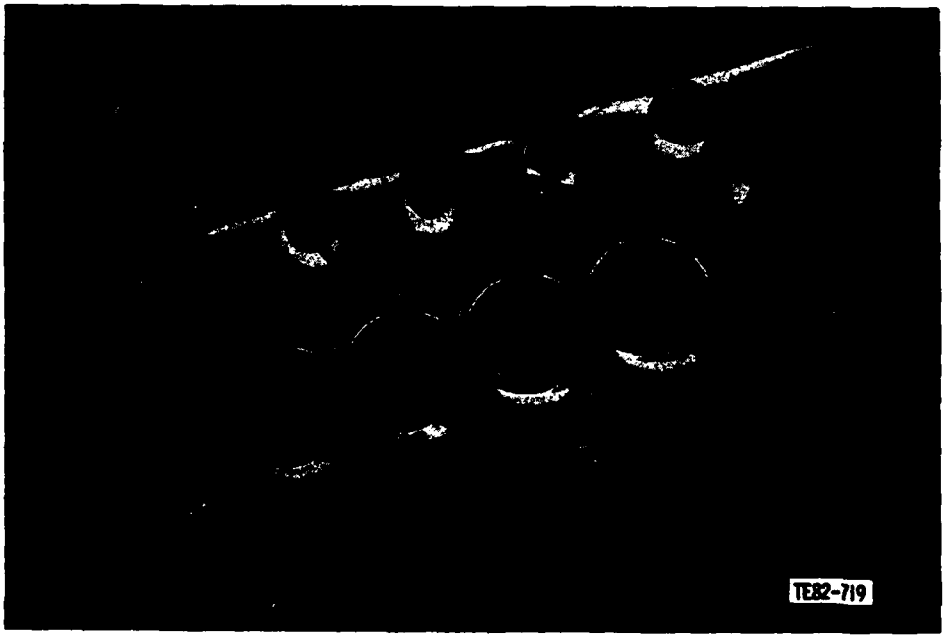

Figure 19. Schlieren photograph at 2.8 expansion ratio.

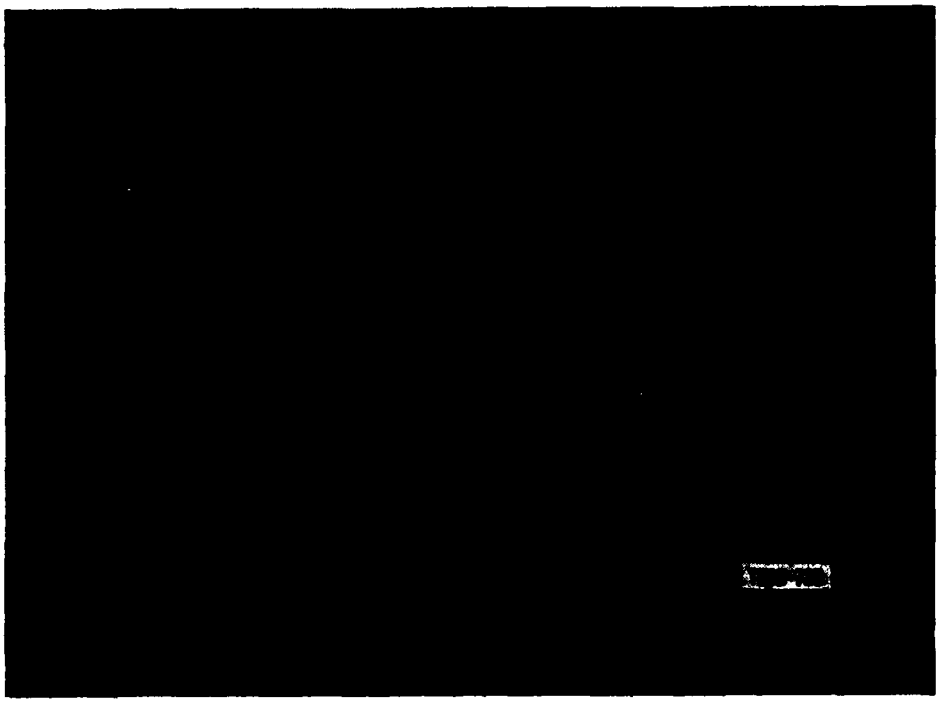

Figure 20. Close-up of leading edge.

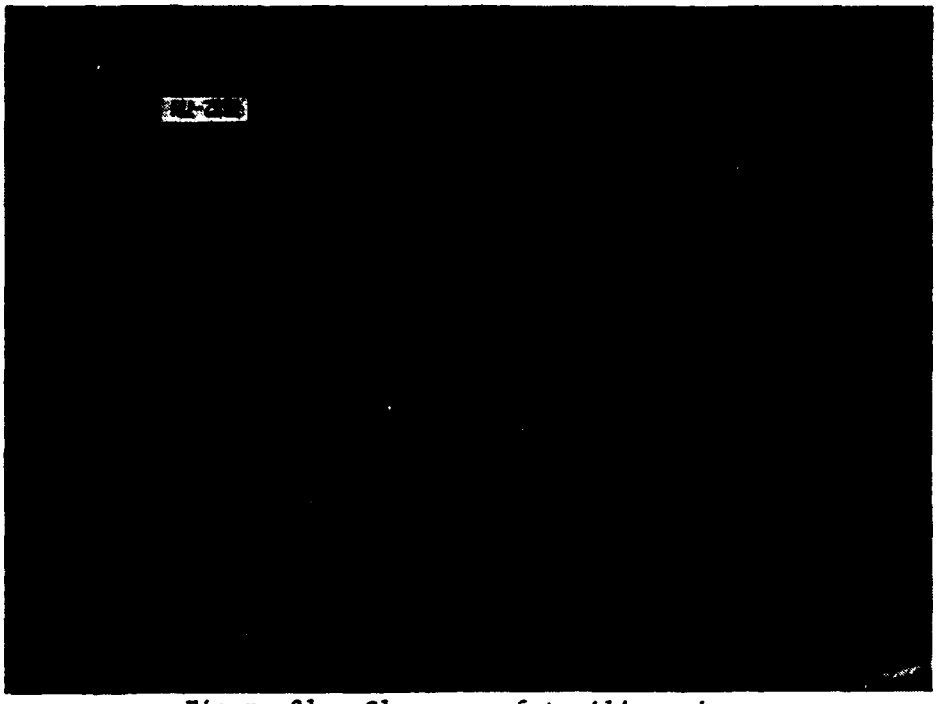

Figure 21. Close-up of trailing edge.

An alcohol injection technique was used to identify regions of flow separation. This technique involved injecting alcohol through static pressure taps on an instrumented airfoil and observing the direction of flow of the alcohol on the blade surface. The technique clearly showed the flow to be separated on the pressure surface leading edge from approximately 3 to 25 percent projected chord for all four operating conditions. It was also observed that the shock wave impinging on the suction surface of the airfoil caused local separation of the flow for the 2.8 and 2.3 expansion ratios. At the 2.8 expansion ratio, the flow becomes reattached while for the 2.3 expansion ratio condition no reattachment occurs. At the 1.5 and 1.8 expansion ratio operating points, the flow does not separate on the suction surface.

Exit surveys were made at each operating point with a traversing five-hole cone probe. Figure 22 shows the wake profiles in terms of total pressure ratios. The probe was traversed from midway between blades 3 and 4 to midway between blades 2 and 3. As expansion ratio was increased the pressure deficit became more pronounced as a result of the increased exit mach number, and shifted due to the decreased turning. The peaks at approximately 80% passage for the 2.3 and 2.8 expansion ratio cases are attributable to the presence of a shock wave from the trailing edge of blade 3.

Blade 3 was instrumented with 18 static pressure taps, 9 on each surface, for the steady-state testing. The surface static pressure distributions obtained for the four operating conditions are shown in Figures 23 through 26. Zero percent projected chord corresponds to the airfoil leading edge. A DDA steady-state, transonic flow analysis (Reference 17) was performed for each point and is presented for comparison with the experimental data. The analysis is in excellent agreement with the data for all four cases except over the

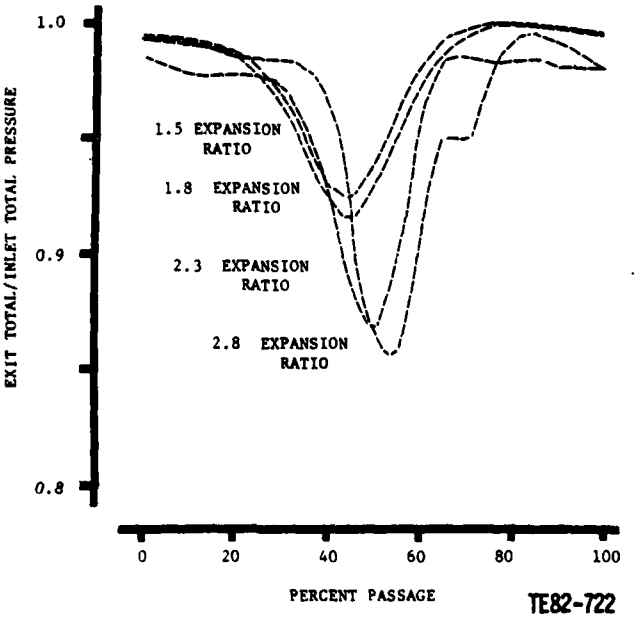

Figure 22. Steady-state cascade wake survey.

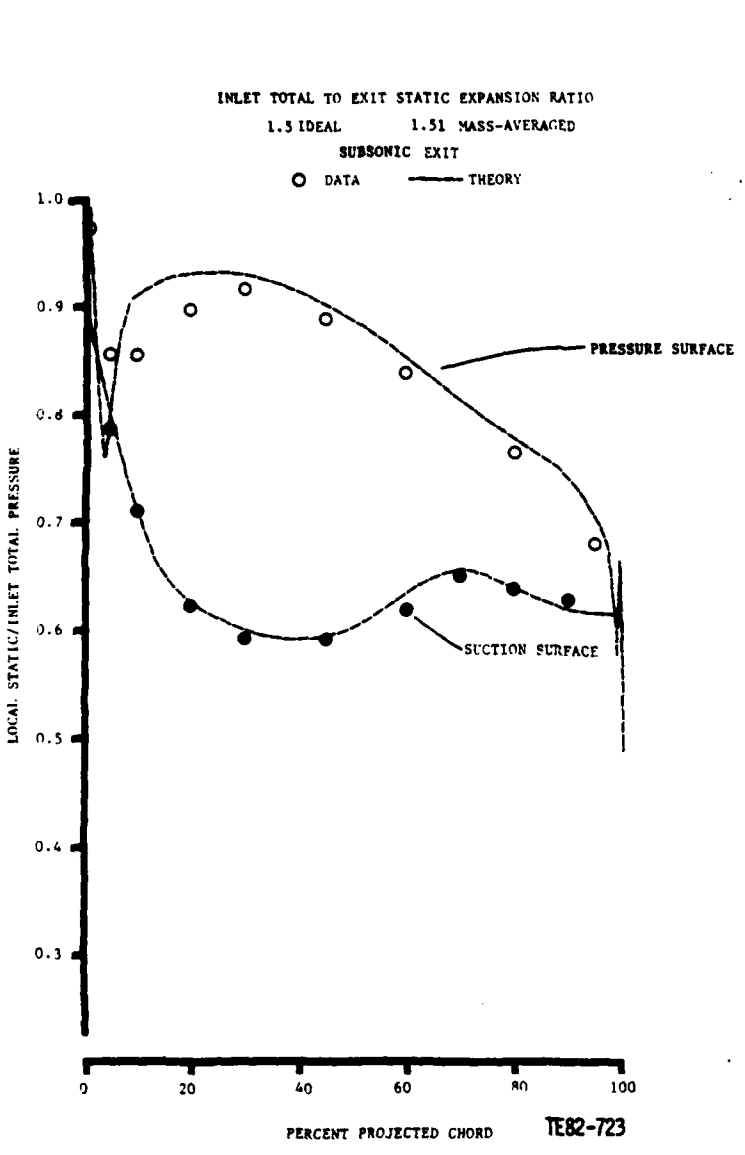

Figure 23. Steady-state airfoil surface static pressures for 1.5 expansion ratio.

separated regions of the airfoil surface identified by the alcohol injection investigation. Figure 27 shows the solution grid used by the analysis for the high turning airfoils of this cascade.

Time-Variant Testing

The time-variant phase of the experimental research program was conducted by installing the Kulite instrumented airfoil as blade 3 of the cascade and measuring the dynamic pressures generated on the airfoil surface while driving each blade individually. Pressure phase lags referenced to the driven blade and peak pressure amplitudes were obtained along the pressure and suction surfaces of the instrumented airfoil at each operating condition for each blade driven. The peak translational amplitude of the driven blade was measured

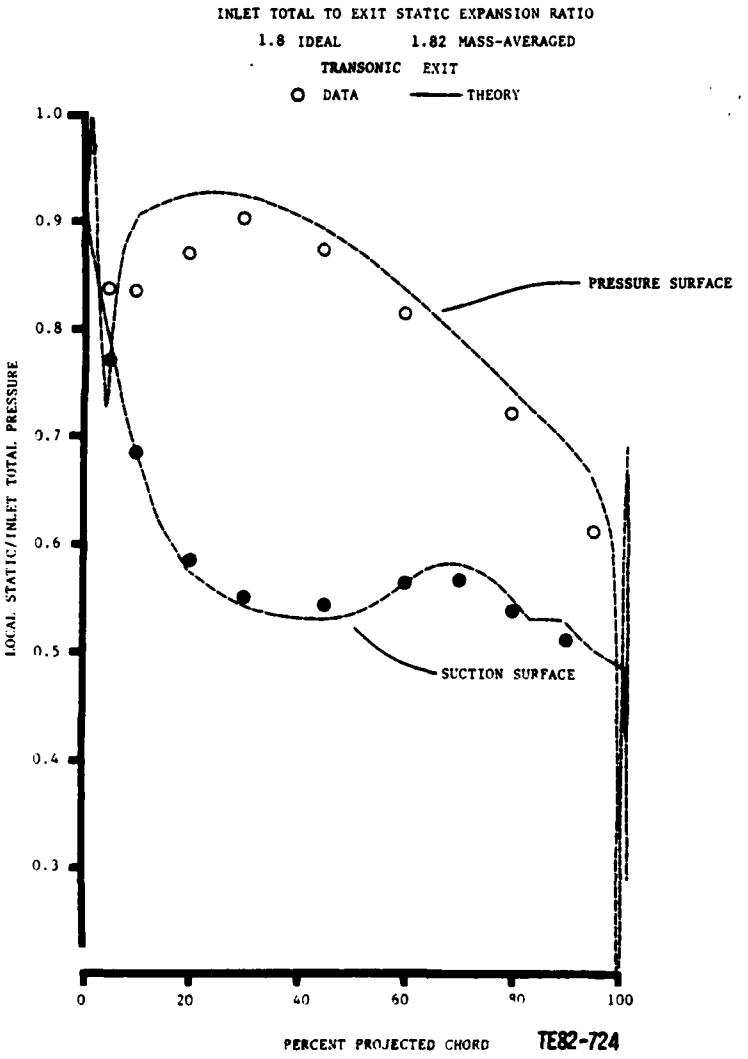

Figure 24. Steady-state airfoil surface static pressures for 1.8 expansion ratio.

and used to normalize the peak pressure amplitudes. The individually driven blade results were then superimposed vectorially at each operating condition to yield results for 8 interblade phase angles.

A summary of the individually oscillating airfoil results is given in Table 4. At each operating condition the peak pressure amplitudes and aerodynamic phase lags measured by each Kulite for each oscillating airfoil are listed. Also shown is the driven airfoils peak translational amplitude and the frequency of oscillation. The Kulite located at 30% projected chord on the pressure surface ceased to function before any time-variant data could be taken.

TABLE 4. INDIVIDU

IDEAL TOTAL TO STATIC EXPANSION RATIO	SINGLE OSCILLATING AIRFOIL	FREQUENCY (HZ)	O-P BLADE AMPLITUDE (THOUSANDTHS)	PRESSURE SURFACE P_1	P_3	P_4	PRESSURE P_5
1.5	1	202.5	4.252	.0026 140.22	.0025 90.14	.0054 85.92	.009 87.84
	2		6.019	.0020 146.16	.0006 61.95	.0019 28.75	.004 78.41
	3		4.931	.0187 -49.82	.0199 -110.33	.0194 -114.31	.014 -117.08
	4		5.214	.0095 104.74	.0155 64.66	.0248 39.45	.022 45.73
	5		5.199	.0026 47.97	.0028 48.61	.0040 36.15	.003 32.99
1.8	1	202.4	4.828	.0007 -144.75	.0014 54.38	.0011 -34.30	.000 150.87
	2		4.946	.0014 178.88	.0012 -101.26	.0019 -77.36	.000 162.01
	3		4.043	.0162 -49.04	.0158 -109.36	.0165 -108.49	.013 -102.96
	4		4.630	.0074 91.36	.0137 52.21	.0246 32.94	.018 44.32
	5		4.828	.0022 45.82	.0020 61.09	.0020 47.00	.001 63.58
2.3	1	202.1	4.966	.0007 -132.07	.0016 -45.88	.0018 -37.86	.000 -89.23
	2		5.007	.0112 130.42	.0034 -172.49	.0025 -95.24	.002 -56.05
	3		5.177	.0153 -57.92	.0175 -121.89	.0182 -123.06	.013 -118.55
	4		4.300	.0066 64.02	.0118 33.15	.0232 25.89	.013 37.60
	5		3.694	.0014 63.43	.0016 71.38	.0015 44.00	.0016 60.52
2.8	1	206.0	3.806	.0003 -107.76	.0010 -57.56	.0010 -44.56	.0004 -171.00
	2		5.078	.0023 171.64	.0009 -131.33	.0013 -88.24	.0017 -138.05
	3		4.948	.0130 -63.16	.0179 -128.67	.0188 -129.32	.0137 -125.80
	4		2.668	.0045 57.60	.0079 39.60	.0168 16.66	.007 27.15
	5		4.456	.0018 51.59	.0015 56.98	.0019 35.81	.0016 39.19

DUAL BLADE DRIVER RESULTS.

URE AMPLITUDE (PSIA)/AERODYNAMIC PHASE LAG (DEGREES)

				SUCTION SURFACE			
S_5	S_1	S_2	S_3	S_4	S_5	S_6	S_7
.0096	.0110	.0042	.0056	.0112	.0126	.0153	.0188
.84	-59.84	-43.16	87.37	86.05	73.42	61.60	75.76
.0042	.0260	.0655	.0806	.0333	.0129	.0140	.0157
.41	33.71	22.28	22.55	-29.18	-19.54	34.06	60.72
.0148	.0530	.0759	.0645	.0231	.0103	.0068	.0029
.08	172.27	170.80	165.33	142.95	116.63	110.46	-100.89
.0229	.0110	.0059	.0056	.0068	.0067	.0077	.0064
.73	19.40	54.00	42.77	49.07	37.03	30.43	69.88
.0035	.0043	.0031	.0028	.0030	.0032	.0040	.0038
.99	28.12	35.02	46.61	38.20	29.48	18.29	15.82
.0007	.0116	.0080	.0022	.0008	.0010	.0049	.0070
.87	-56.91	-56.74	-59.33	-98.91	-111.45	12.38	126.65
.0009	.0214	.0523	.0650	.0299	.0170	.0077	.0112
.01	-37.58	-24.73	-26.57	-43.38	-47.85	156.41	45.58
.0131	.0382	.0543	.0431	.0139	.0093	.0028	.0079
.96	169.11	164.78	158.23	121.81	143.33	34.31	-138.89
.0183	.0084	.0042	.0040	.0034	.0026	.0018	.0083
.32	15.38	50.82	34.53	46.74	28.84	44.47	152.67
.0018	.0032	.0020	.0012	.0014	.0012	.0016	.0022
.58	33.60	52.41	49.16	43.19	39.93	64.25	149.52
.0006	.0113	.0080	.0028	.0014	.0014	.0015	.0045
.23	-57.56	-56.50	-53.90	-72.55	-99.82	-74.51	-122.14
.0021	.0238	.0490	.0590	.0300	.0176	.0087	.0132
.05	-39.13	-25.75	-34.17	-62.16	-59.77	-80.15	-32.86
.0139	.0376	.0545	.0413	.0152	.0075	.0038	.0184
.55	160.49	136.21	145.76	103.64	127.48	103.57	-153.16
.0130	.0063	.0028	.0046	.0033	.0025	.0030	.0011
.60	12.53	36.14	20.97	32.35	23.71	18.93	157.17
.0016	.0022	.0015	.0008	.0011	.0011	.0008	.0014
.52	37.70	67.56	60.97	62.65	57.60	36.38	94.66
.0004	.0084	.0058	.0015	.0009	.0011	.0010	.0456
.00	-65.10	-66.28	-72.72	-98.42	-121.90	-84.98	69.20
.0017	.0214	.0531	.0672	.0318	.0176	.0092	.0555
.05	-106.90	-25.10	-27.46	-43.65	-47.21	-65.59	66.42
.0137	.0316	.0461	.0333	.0132	.0050	.0026	.0326
.80	-159.68	155.06	141.68	85.41	125.49	114.99	75.17
.0078	.0037	.0018	.0027	.0019	.0018	.0024	.0002
.15	16.78	51.63	-1.59	18.32	4.89	-.23	89.16
.0016	.0022	.0019	.0018	.0013	.0012	.0009	.0020
.19	48.70	63.95	42.82	50.83	58.50	44.05	165.45

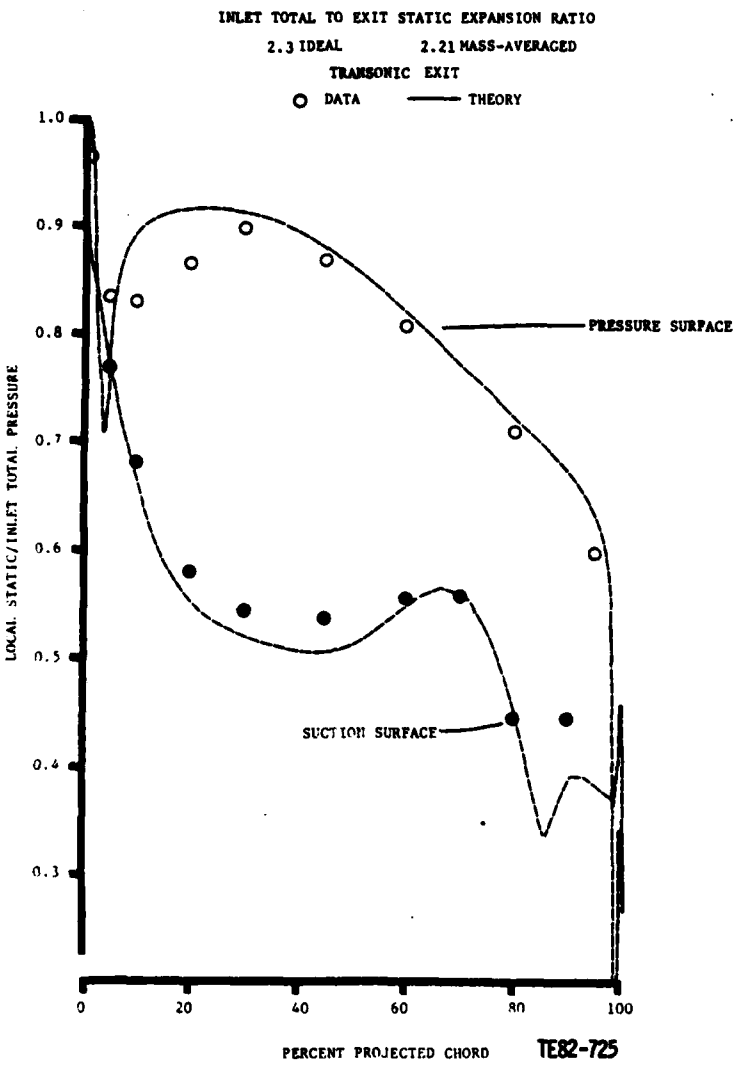

Figure 25. Steady-state airfoil surface static pressures for 2.3 expansion ratio.

The data shows that the primary unsteady pressure effects on the center airfoil are due to its own oscillation. The oscillation of blades 1 and 2 result in large unsteady pressures along the suction surface while the pressure surface is effected by the motion of blade 4. Blade 5 oscillating results in very small unsteady pressures all along the blade surface.

Figures 28 and 29 are examples of the superimposed peak time-variant surface pressure amplitude results. These two plots are for the 1.5 and 2.8 expansion ratios with an interblade phase angle of 0 deg. Unsteady peak pressure amplitude normalized with blade translational amplitude is plotted versus percent projected chord for the pressure and suction surfaces of the center airfoil. The large amplitude at 92.5% projected chord is due to an impinging shock wave from blade 2.

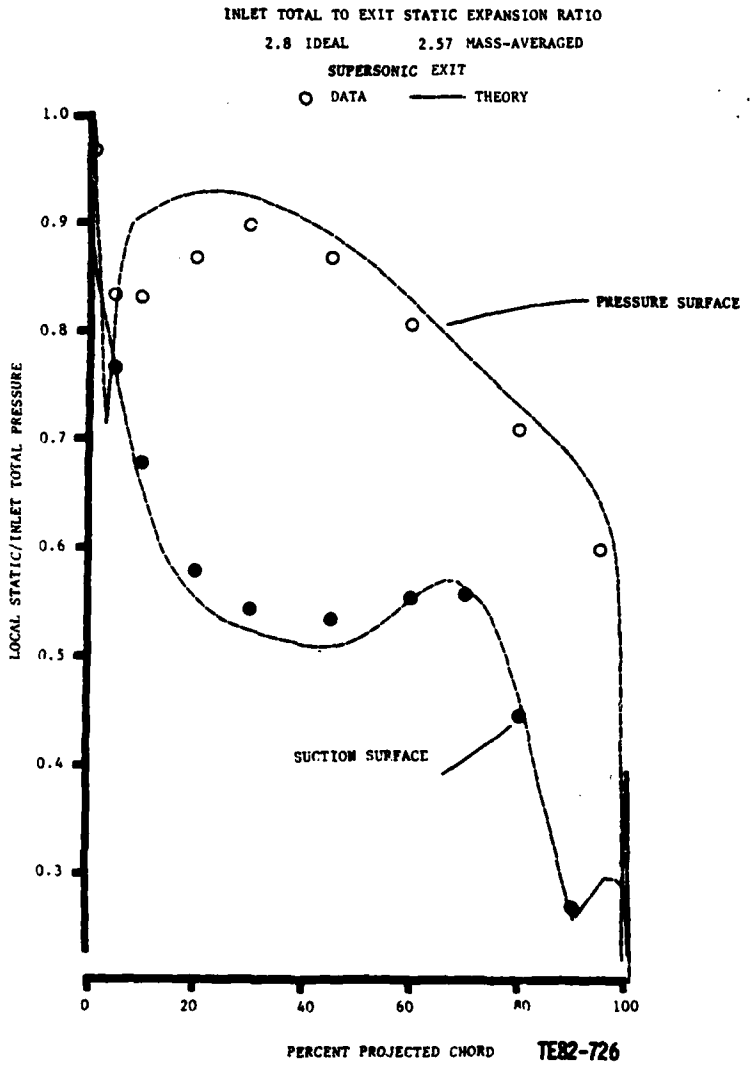

Figure 26. Steady-state airfoil surface static pressurs for 2.8 expansion ratio.

Figures 30 and 31 show the surface pressure phase lags of the time-variant pressure results referenced to the motion of blade 3. The translational motion of the blade is positive when it moves normal to the airfoil chord as shown in Figure 15. Aerodynamic phase lag is plotted versus percent projected chord for the pressure and suction surfaces of the center airfoil.

Peak pressure amplitude and aerodynamic phase lag calculated for each Kulite on the center airfoil at interblade phase angles of 0 deg, 180 deg, $\pm$90 deg, $\pm$45 deg, and $\pm$135 deg are given in Appendix A for each operating condition. The interblade phase angle is positive in sign when the motion of blade 1 is leading the motion of blade 2 as defined in Figure 15.

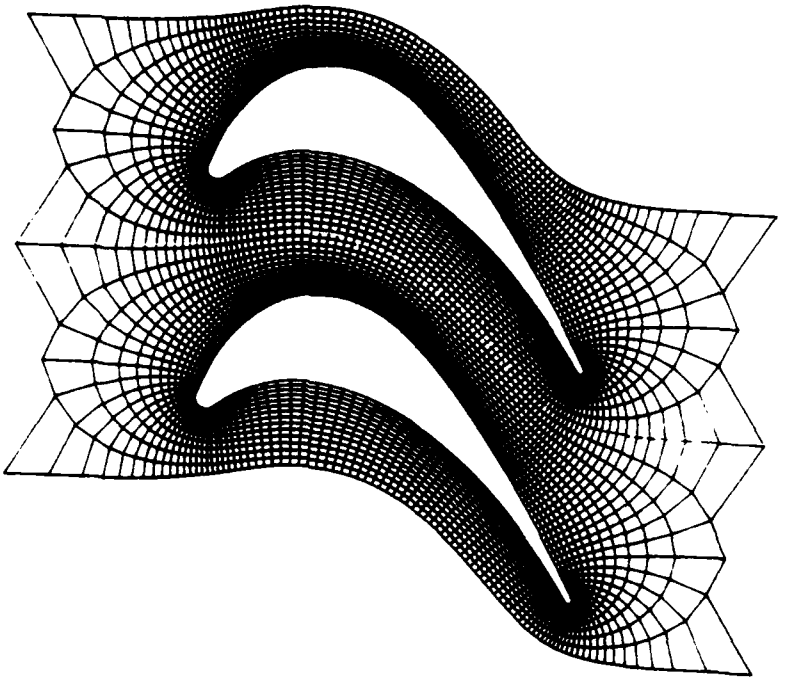

TE82-727

Figure 27. Solution grid for steady-state cascade analysis.

Theoretical calculations and superimposed time-variant results were compared for each operating condition. An internally developed code based on the method outlined by Smith (Reference 2) was used for the theoretical calculations. Since the analytical code is restricted to flat plate cascades, the highly cambered airfoils were represented by flat plate airfoils aligned with the blade setting angle as shown in Figure 32. This allowed the flat plate cascade to translate normal to the actual cambered airfoil's chord. The parameters necessary to analyze this assumed cascade were based on an average fluid velocity along the meanline from the leading to the trailing edge. Table 5 lists the input parameters used. Figure 33 depicts the flat plate cascade arranged in a more conventional manner. Only the 1.5 expansion ratio theoretical results will be presented in the following discussion.

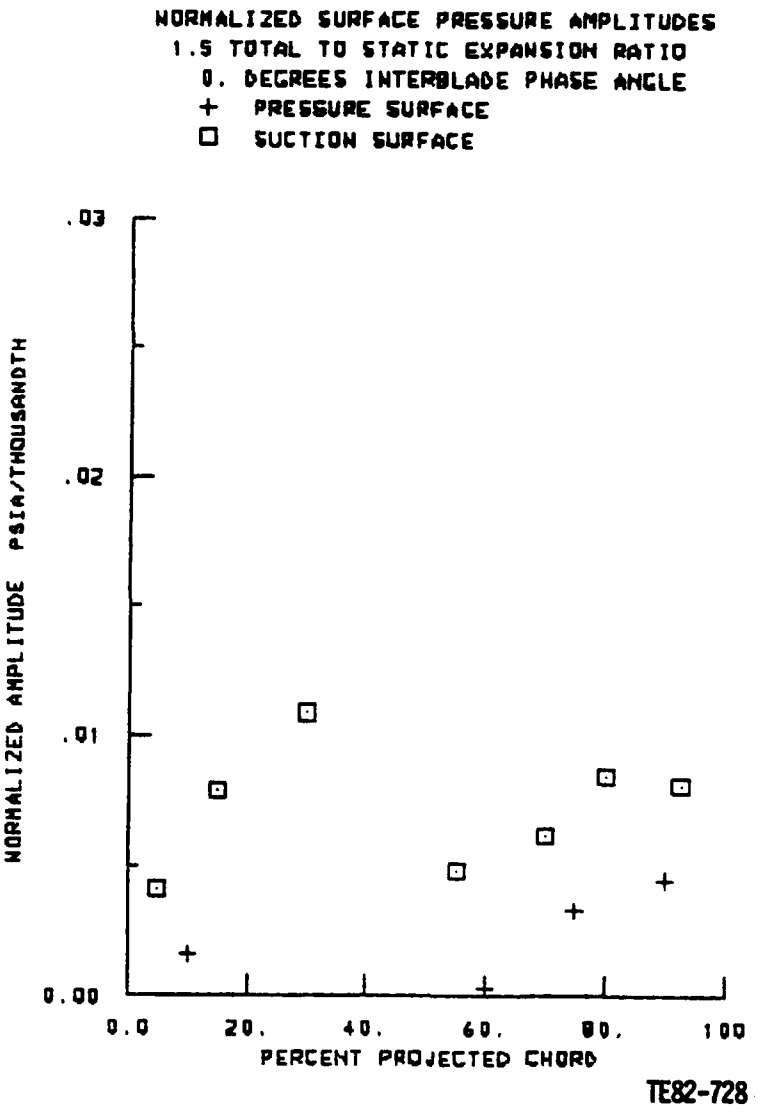

Figure 28. Time-variant surface pressure amplitude plot for 1.5 expansion ratio and 0° interblade phase angle.

TABLE 5. CONDITIONS ASSUMED FOR ANALYTICAL STUDY.

Parameter	Flat plate cascade
Solidity (chord/spacing)	1.890
Reduced frequency (based on chord)	0.485
Setting angle, degrees	25.5
Mach number	0.502
Interblade phase angle	Variable

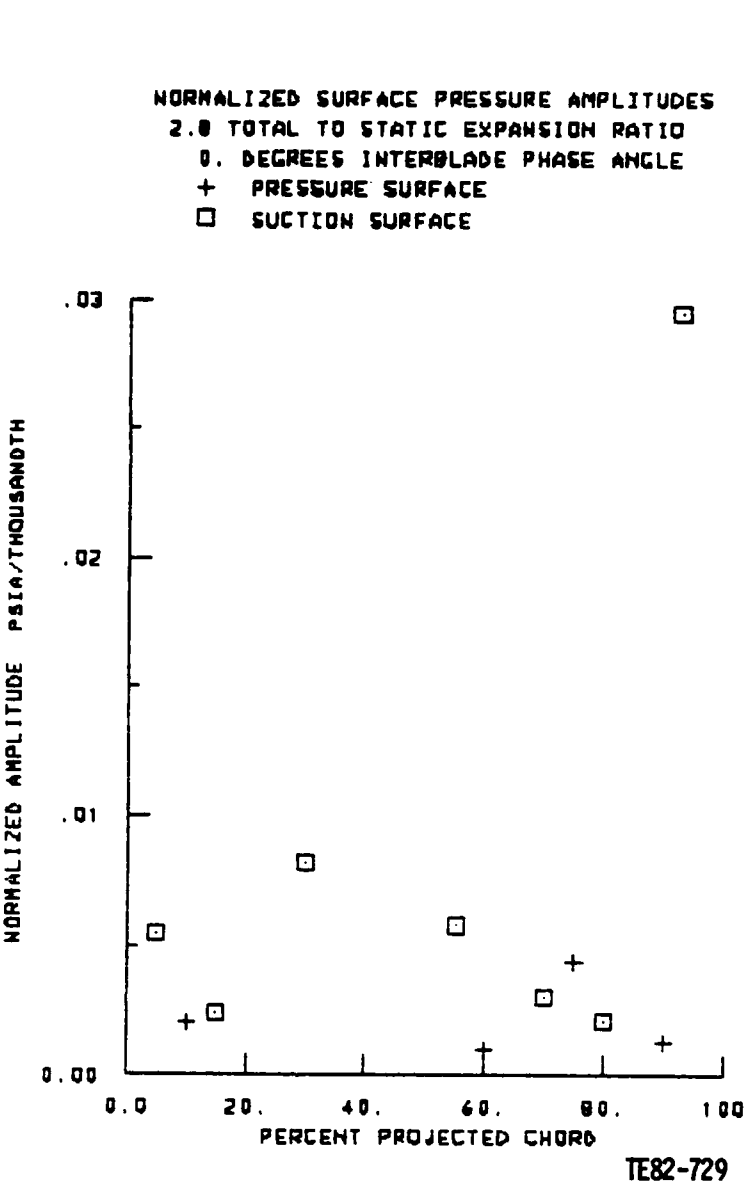

Figure 29. Time-variant surface pressure amplitude plot for 2.8 expansion ratio and 0° interblade phase angle.

Figures 34 through 37 are plots of normalized pressure coefficient and phase lag versus normalized length along the airfoil meanline for interblade phase angles of 0 and 180 degrees. The plots were obtained by vectorially subtracting the suction surface time-variant pressure from the pressure surface time-variant pressure at locations along the airfoil meanline. The magnitude of this time-variant pressure difference across the airfoil was normalized by dividing by the product of twice the dynamic head and the ratio of the peak blade velocity to the inlet air velocity. The phase lag plotted in the curves is referenced to the motion of the instrumented center airfoil. Normalized pressure coefficient and phase lag plots for interblade phase angles of $\pm$135 deg, $\pm$90 deg, and $\pm$45 deg are given in Appendix B.

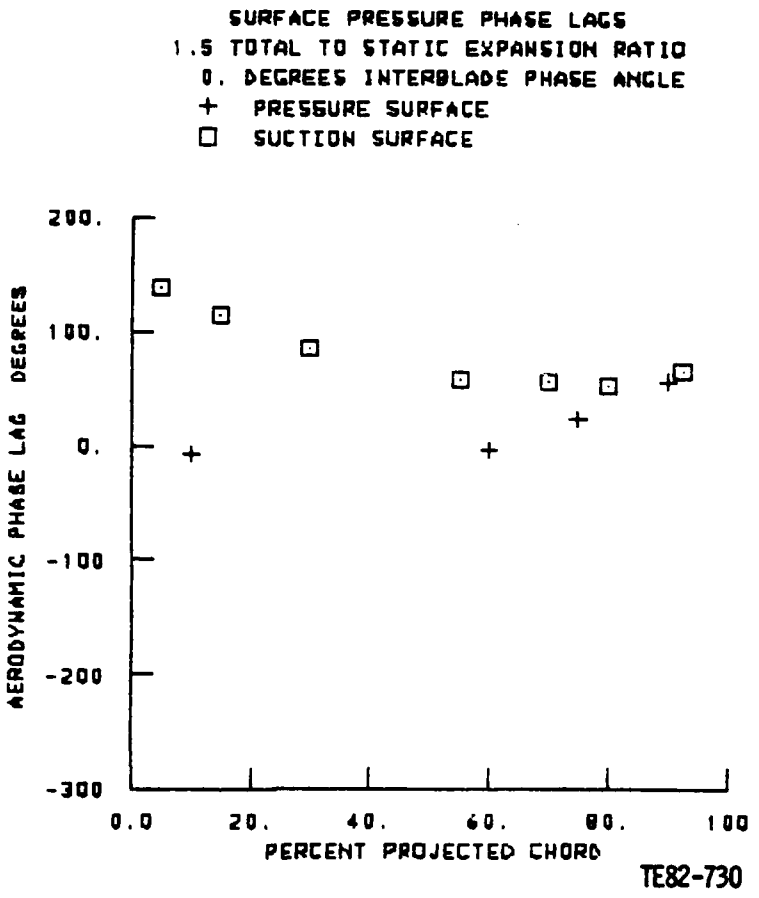

Figure 30. Time-variant surface pressure phase lag plot for 1.5 expansion ratio and 0° interblade phase angle.

Figures 34 and 35 are normalized pressure coefficient plots for the 0 and 180 deg interblade phase angles. The plots show the amplitude of the data to be an order of magnitude higher than that predicted by the flat plate model. However, the theoretical results and the data both show the same trends except near the airfoil trailing edge. The large amplitude pressure coefficient at 88.5% meanline for an expansion ratio of 2.8 is due to an impinging shock wave from blade 2. The effect of the impinging shock wave is not evident in the phase lag plots shown in Figures 36 and 37. The 180-deg phase lag data agrees very well with the theoretical flat plate calculations while the 0 deg data shows a difference in magnitude but still follows the general trend predicted by the theoretical calculations.

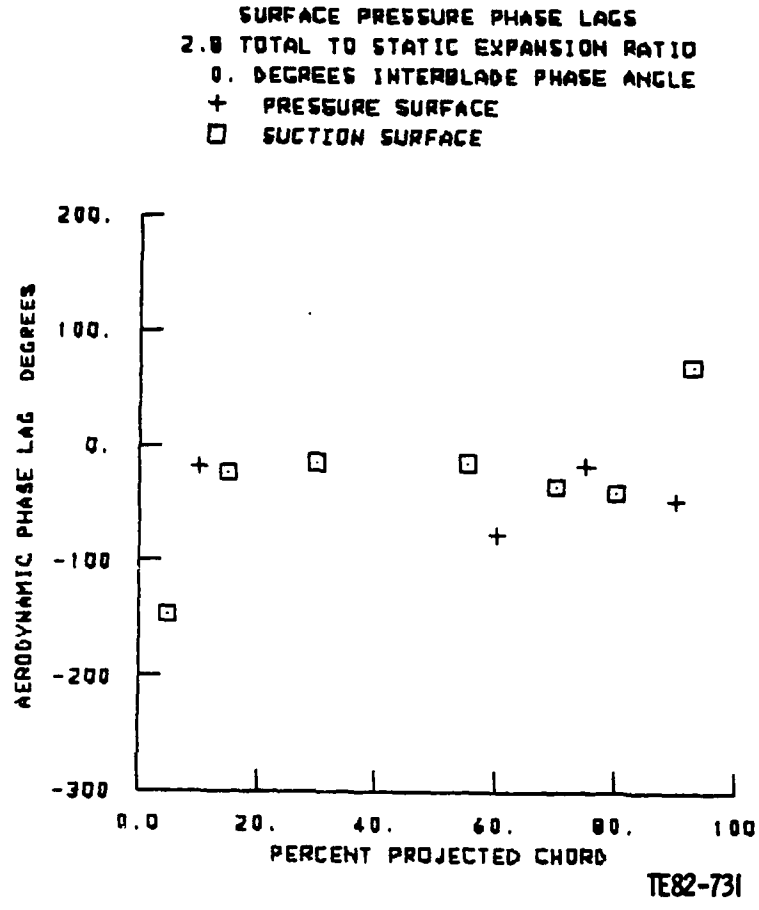

Figure 31. Time-variant surface pressure phase lag plot for 2.8 expansion ratio and 0° interblade phase angle.

The data were arranged to present trends with regards to interblade phase angle. Normalized pressure coefficients at the 8, 57.7, 71.2, and 88.5% meanline stations are presented in Figures 38 through 41, respectively. Data for each of the expansion ratios are preaented at each meanline station.

In Figure 38, data for the leading edge (8% normalized meanline) location are presented along with the theoretical results. Very obviously the experimental data indicate that minimum pressure coefficients occur in the -45 to +45 deg interblade phase angle region. This is in agreement with the trend noted for the analytical model. At the 57.7% meanline location, Figure 39, the minimum pressure coefficients occur between 0 deg and +90 deg interblade phase, dependent on expansion ratio. In general the overall level is reduced from that of

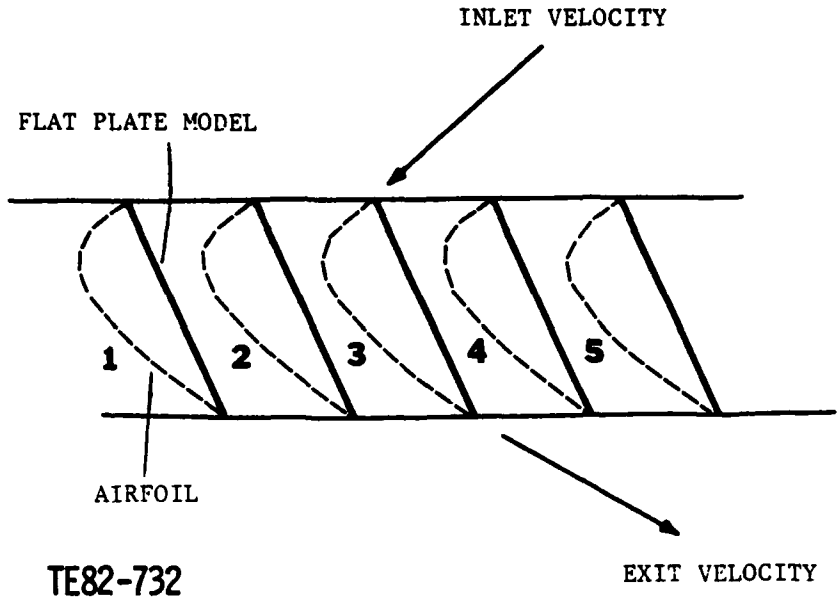

Figure 32. Assumed flat plate cascade.

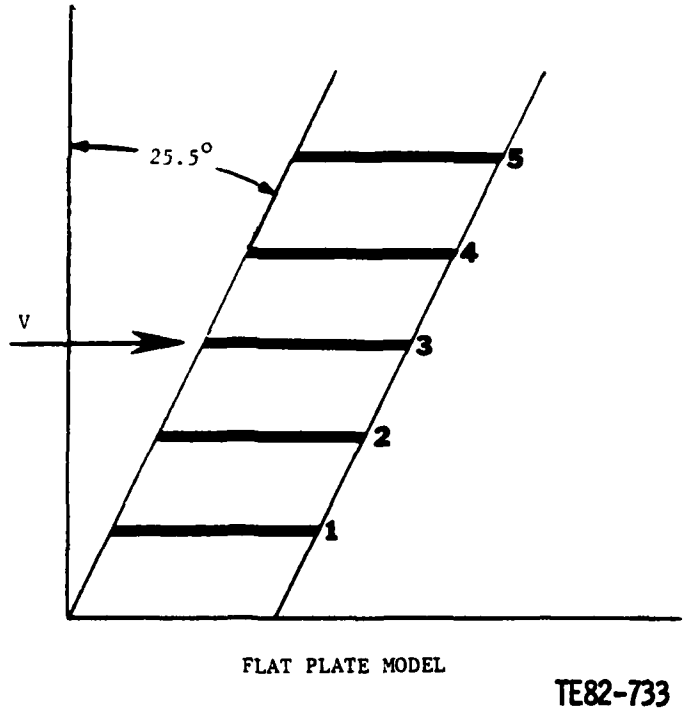

Figure 33. Description of flat-plate cascade.

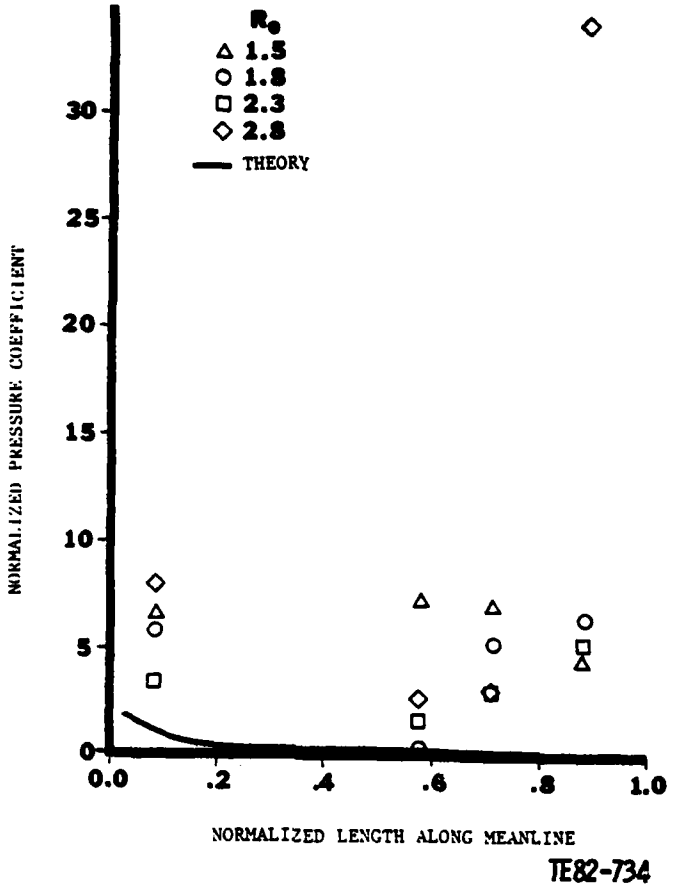

Figure 34. Normalized pressure coefficients for 0° interblade phase angle.

the leading edge. The theoretical model indicates the minimal pressure coefficient should occur near 0 deg. In Figure 40, results from the 71.2% meanline station are presented. Experimental data here are tightly grouped and minimum pressure coefficients occur in the region from +45 deg to +90 deg interblade phase angle. The 88.5% meanline results, Figure 41, are clouded by the presence of the shock wave from the adjacent airfoil, especially notable in the 2.8 expansion ratio results. The trend with interblade phase angle is not clearly defined at this location. In each of Figures 38 through 41, the maximum pressure coefficient lies in the range from -135 deg to 180 deg, in the negative part of the spectrum.

In summary of these plots, the largest coefficients result when blade to blade relative motion is large, such as the condition existing at 180 deg interblade phase angle. When blades are nearly in phase or moving as an assembly, the pressure coefficients tend to be at a minimum.

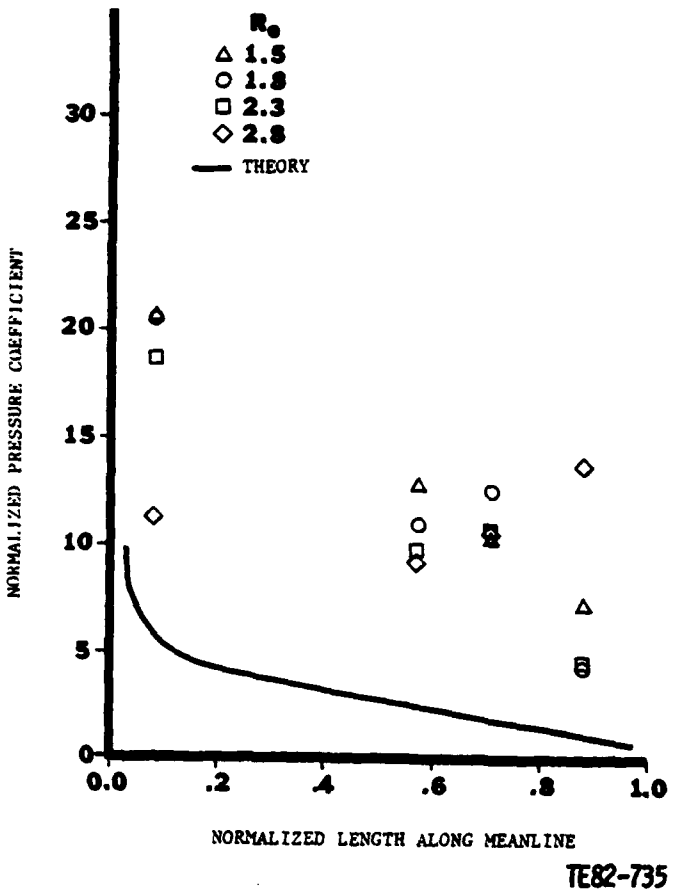

Figure 35. Normalized pressure coefficients for 180° interblade phase angle.

To portray corresponding trends for the phase lag of the pressure differences across the airfoil at various meanline positions, Figures 42 through 45 are presented. Figure 42 presents results from data acquired at the 8% meanline location, along with the phase lag trend of the pressure difference (with respect to the displacement of the center airfoil) from the theoretical analysis. Examining Figure 42, the experimental data agree well in trend with the theoretical results. Both experimental and analytical results indicate almost anomalous behavior near the 0 deg interblade phase angle. Theoretical results were obtained at 9 deg increments to ensure that discontinuities did not exist. The level of phase lag indicates an approximate 60 deg difference between the measured and calculated data.

Results for the 57.7% meanline location are shown in Figure 43. The theoretical results indicate a sharp notch in the pressure phase angle near 0 deg interblade phase angle. A similar trend in the experimental data are noted at +45 deg interblade phase angle. Levels of the phase lag agree fairly well between the experimental and analytical data except in the "notch" region.

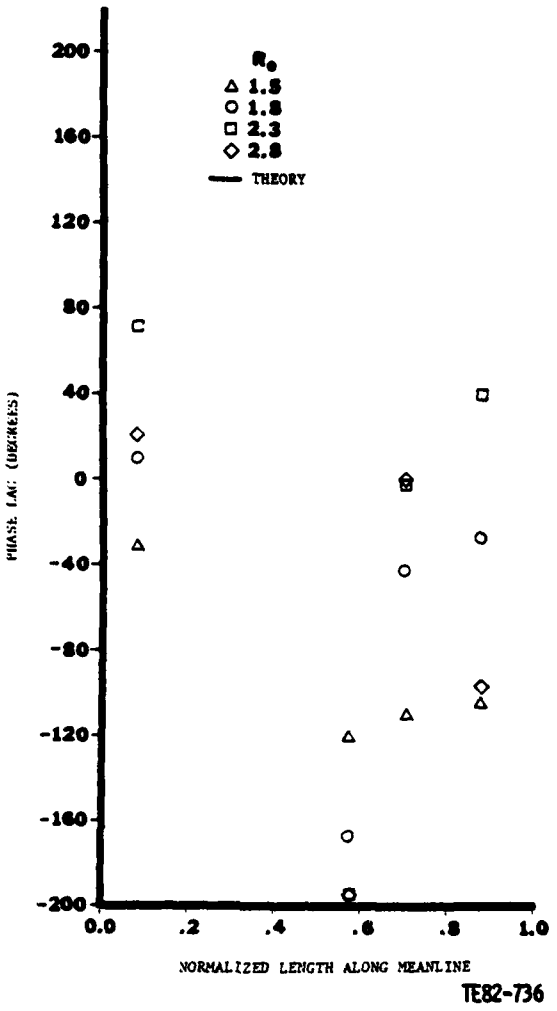

Figure 36. Phase lag for 0° interblade phase angle.

Figures 44 and 45 present similar data for the 71.2% and 88.5% meanline stations, respectively. Both curves exhibit the behavior noted in Figure 43, a "notch" in the data, analytical and experimental, occurring in the 0 deg to +45 deg interblade phase angle region.

The previous two sets of figures, trends of pressure coefficient magnitude and phase lag with respect to interblade phase angle, are necessary to present correlation type data. In order to gain somewhat more insight into the meaning of the experimental data gathered, the real and imaginary portions of the pressure differences across the center airfoil at four normalized meanline positions were calculated versus interblade phase angle. The imaginary portion of this pressure difference is presented in Figures 46 through 49.

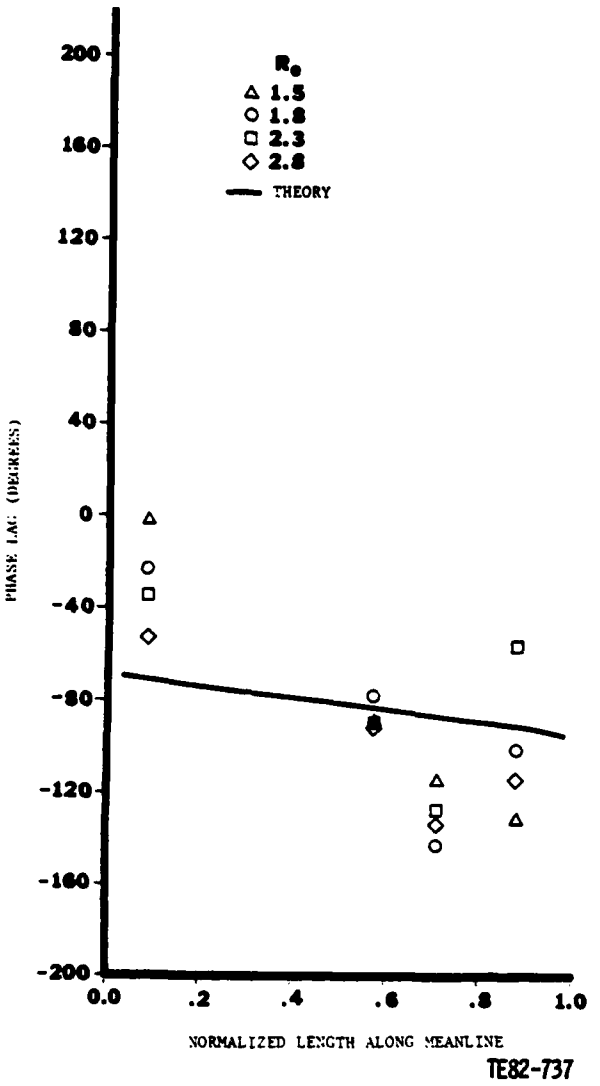

Figure 37. Phase lag for 180° interblade phase angle.

The signing of the imaginary component is such that a negative value would indicate a pressure which if integrated along the blade chord would lead to a translational instability. This is in contrast to the sign convention used by Whitehead (Reference 1). In Reference 1 Whitehead states that the existence of all negative imaginary portions of the lift coefficient indicates no bending instabilities for the range of the analysis.

Examining Figures 46 through 49, it can be seen that for a limited range of interblade phase angles negative imaginary parts of the coefficients occur. At the 8% meanline location, Figure 46, only the 1.5 expansion ratio results remain positive, while data from the other three expansion ratios have negative values in the 0 deg to +45 deg interblade phase angle range. This is seen to be true also at the 57.7% meanline station results presented in Figure 47. In Figure 48, which presents data from the 71.2% meanline location, only

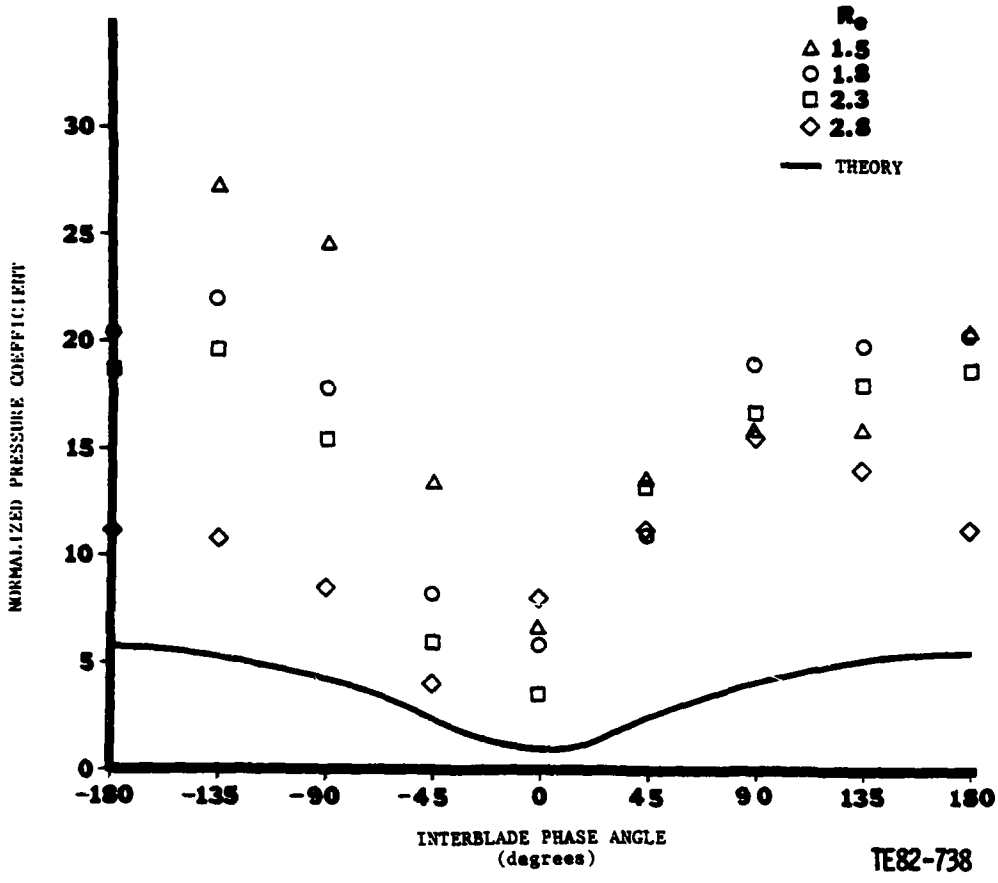

Figure 38. Normalized pressure coefficients as a function of interblade phase angle at 8% meanline station.

the 1.8 expansion ratio results indicate all positive values for the imaginary component. At the 88.5% meanline position, Figure 49 indicates that the imaginary components at all expansion ratios have a range of negative imaginary components.

The existence of these negative regions of the imaginary components of the pressure coefficient points out the possibility of an instability in the translational mode for this airfoil section at the reduced frequency tested. Additionally, Figures 46 through 49 indicate that the aerodynamic damping in the translational mode is greatly affected by interblade phase angle. The maximum damping occurs in the near 180 deg interblade phase angle region.

In summary of the data, comparisons between the analytical and experimental results have been presented for four values of expansion ratio. Presentations have been made in terms of pressure coefficient magnitude and phase as functions of the meanline position on the airfoil. At constant meanline positions, these same quantities have been examined in terms of trends with interblade phase angles. Discussion has been used to point out noteworthy features of the data.

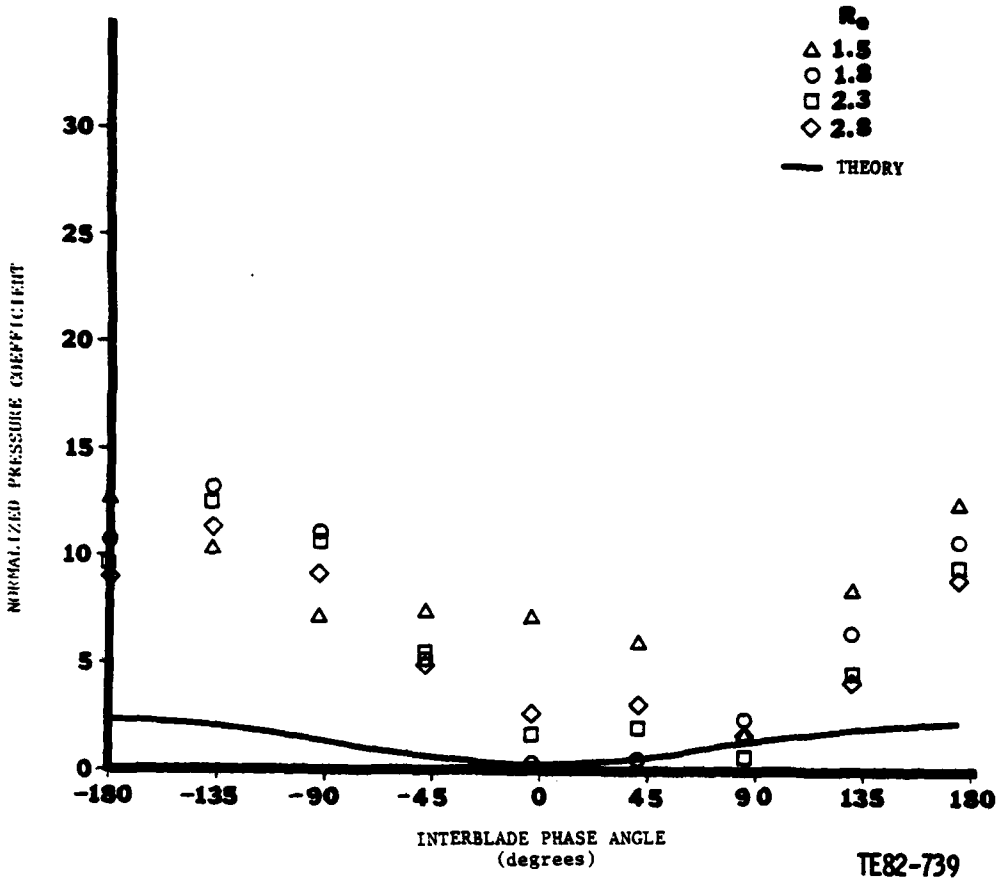

Figure 39. Normalized pressure coefficients as a function of interblade phase angle at 57.7% meanline station.

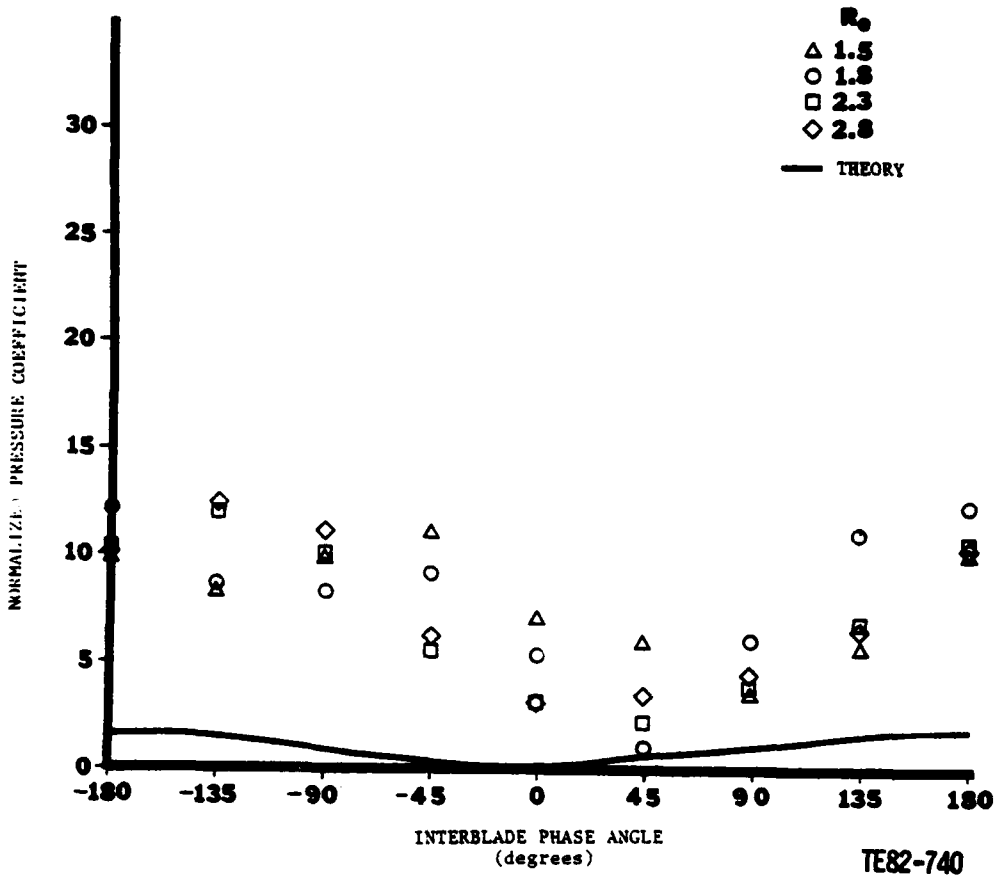

Figure 40. Normalized pressure coefficients as a function of interblade phase angle at 71.2% meanline station.

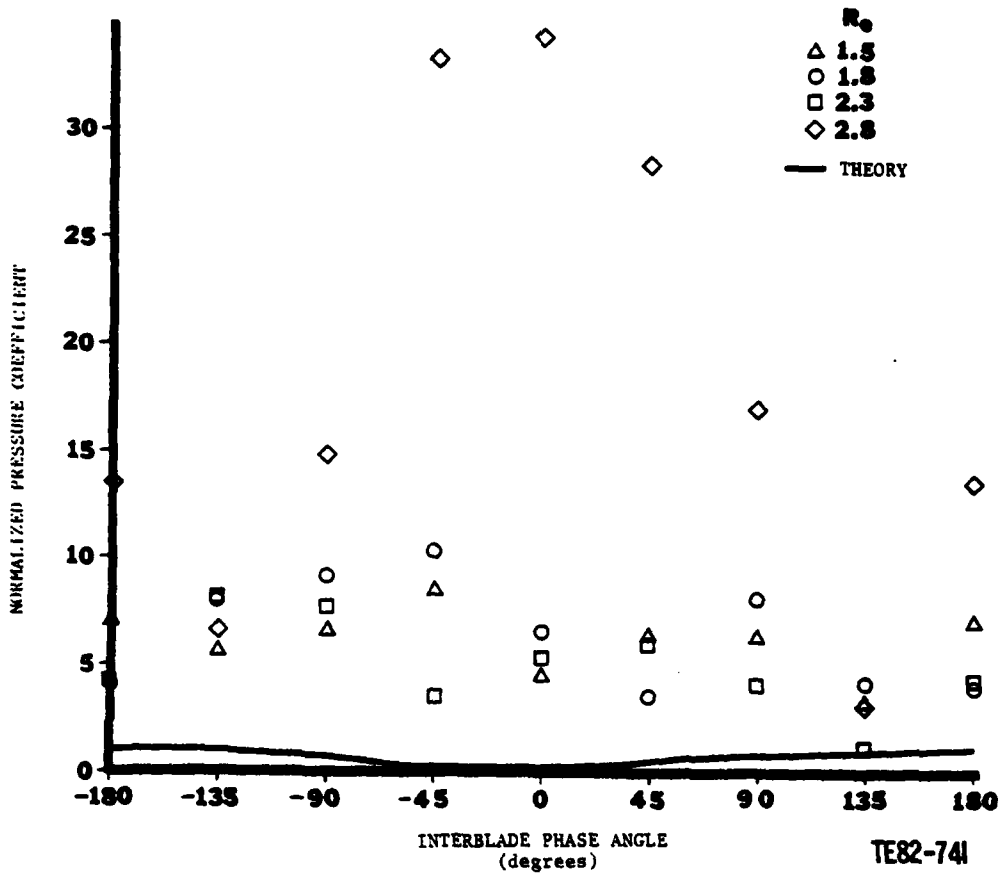

Figure 41. Normalized pressure coefficients as a function of interblade phase angle at 88.5% meanline station.

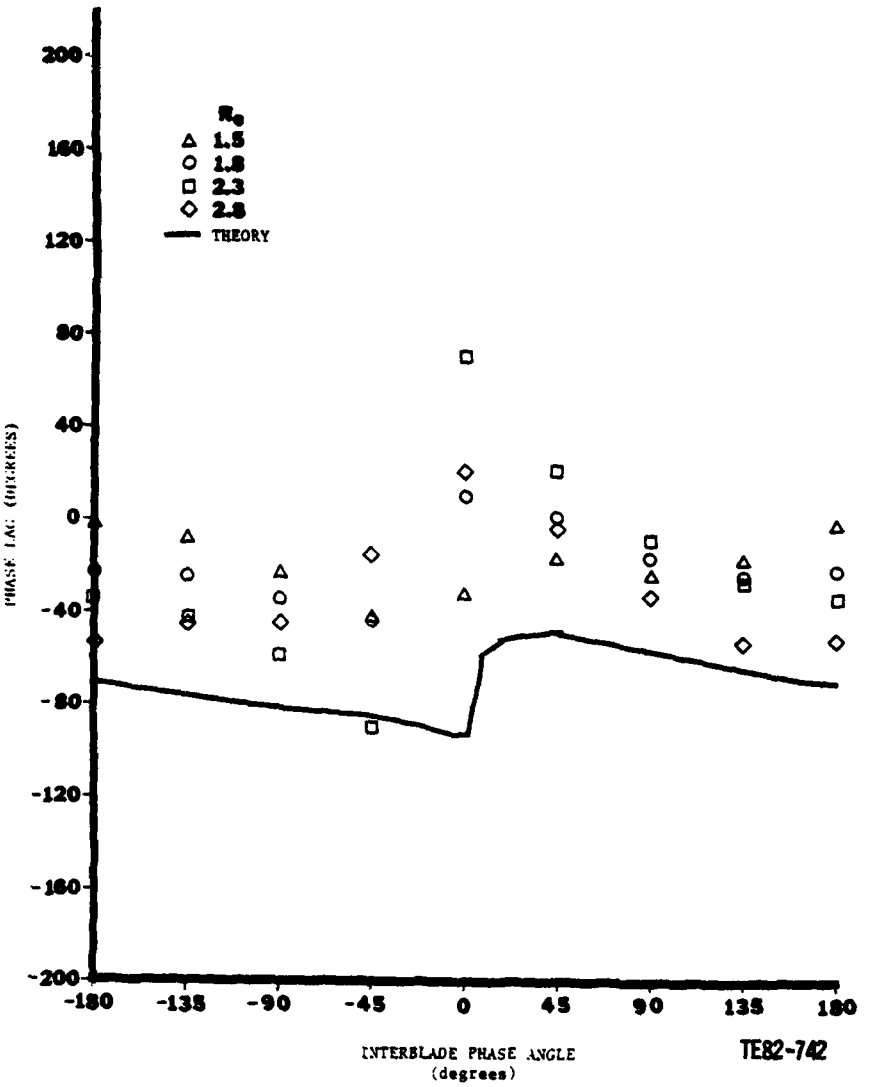

Figure 42. Phase lag as a function of interblade phase angle at 8% meanline station.

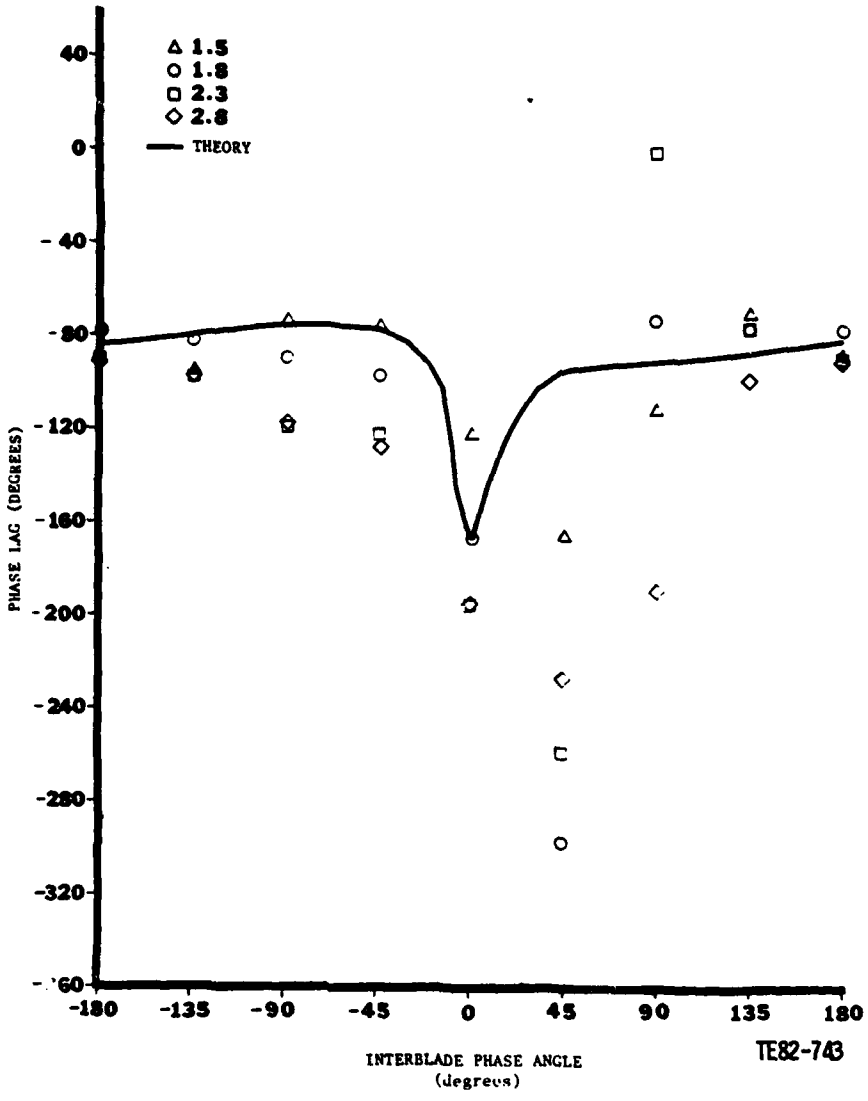

Figure 43. Phase lag as a function of interblade phase angle at 57.7% meanline station.

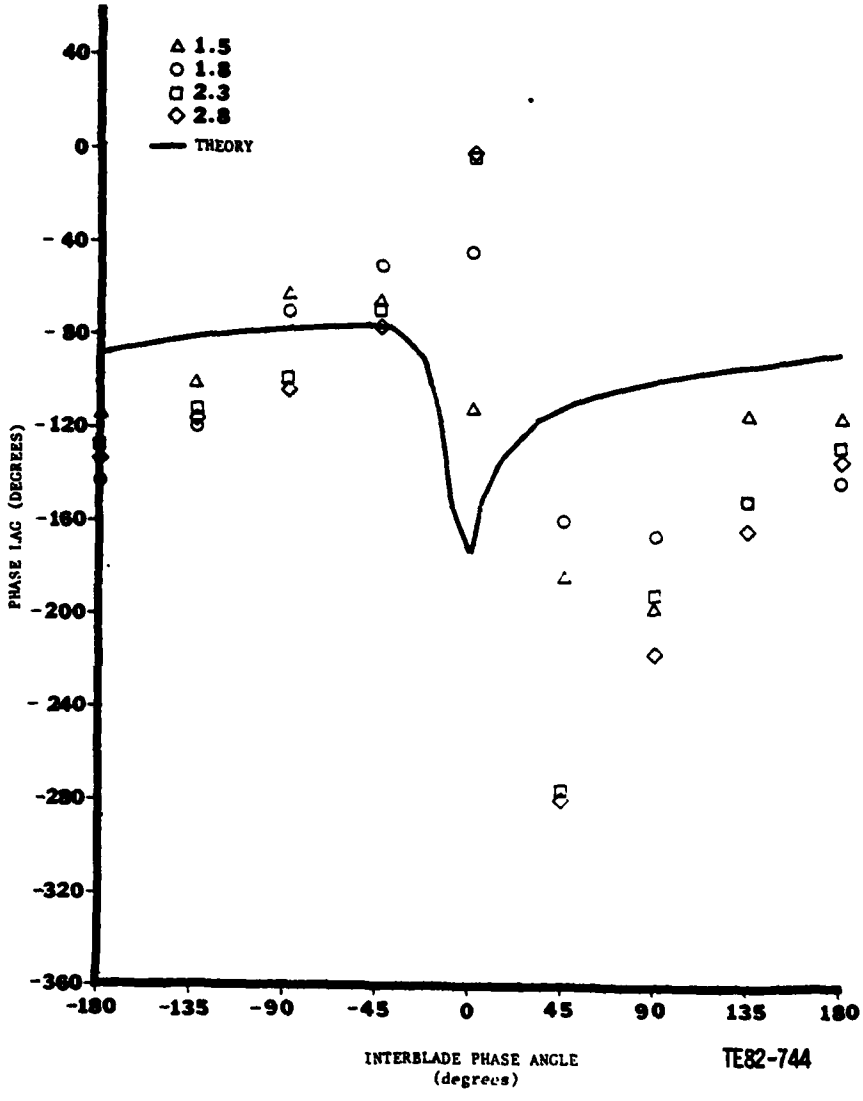

Figure 44. Phase lag as a function of interblade phase angle at 71.2% meanline statin.

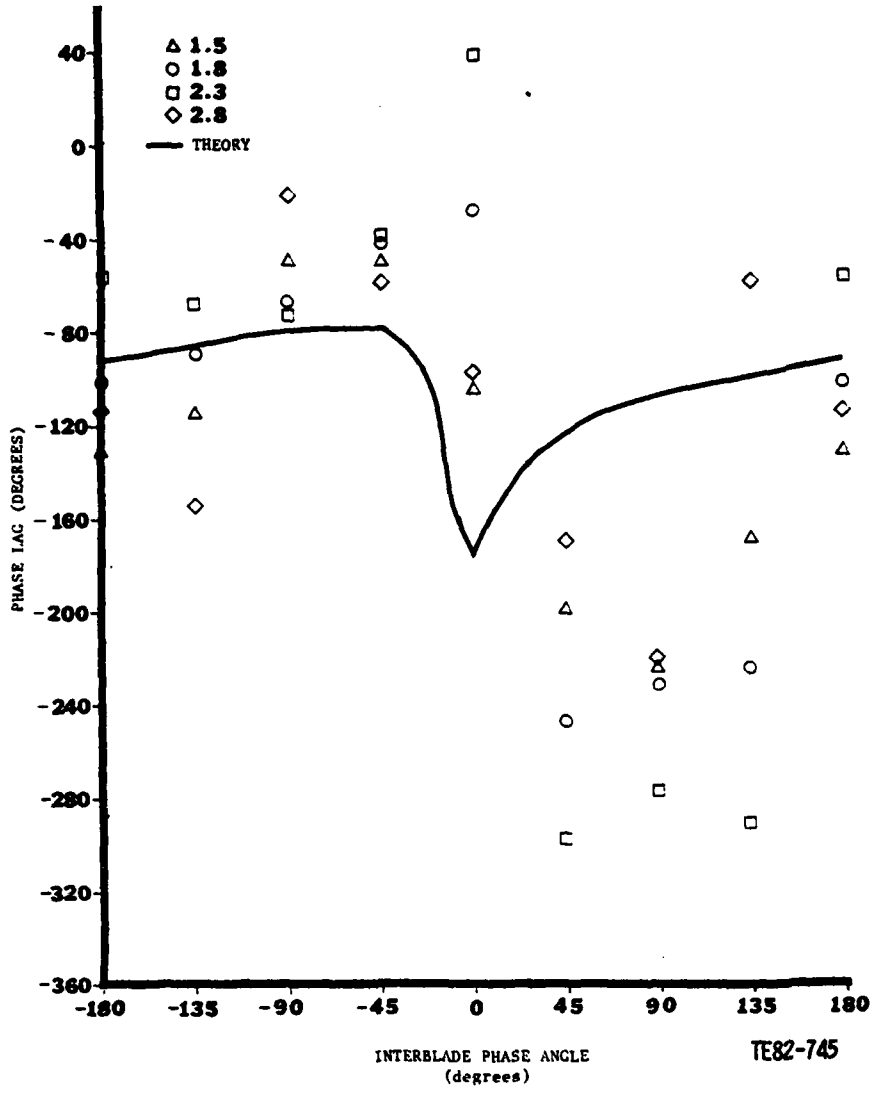

Figure 45. Phase lag as a function of interblade phase angle at 88.5% meanline station.

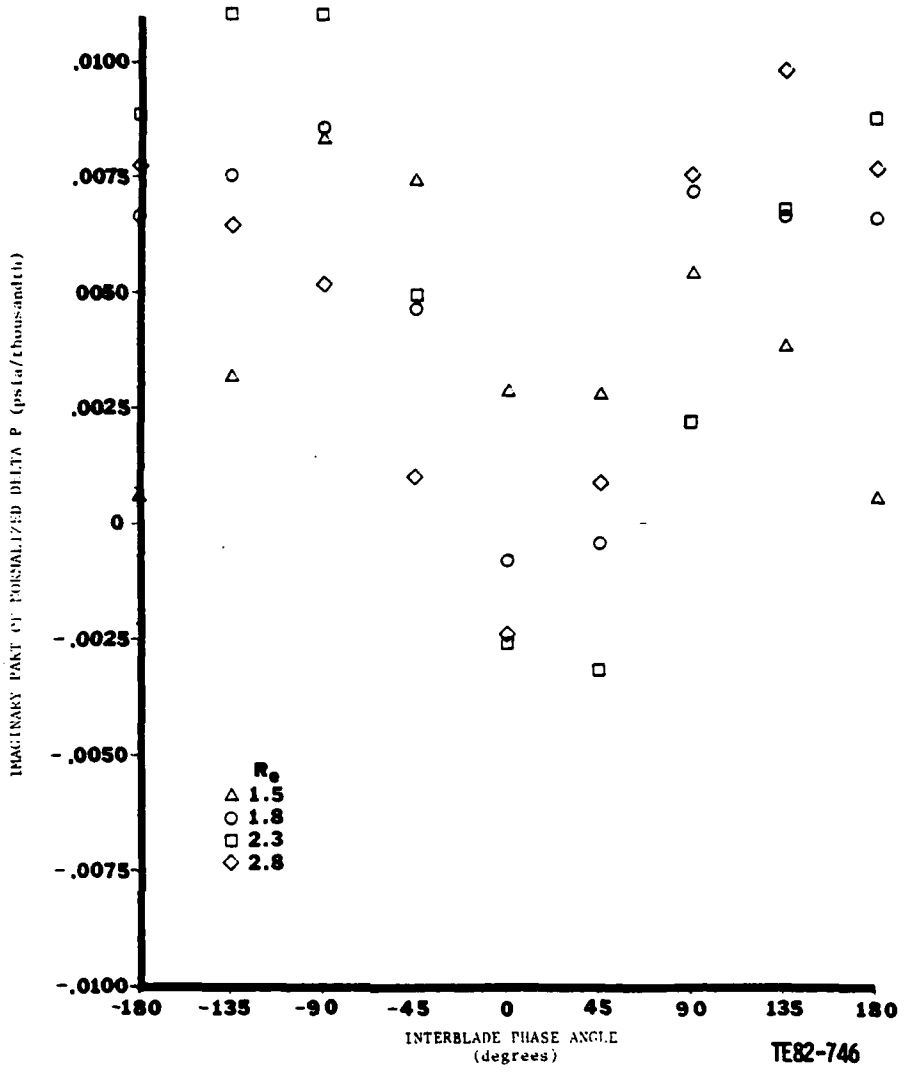

Figure 46. Imaginary part of the pressure difference across the center airfoil at 8% meanline station.

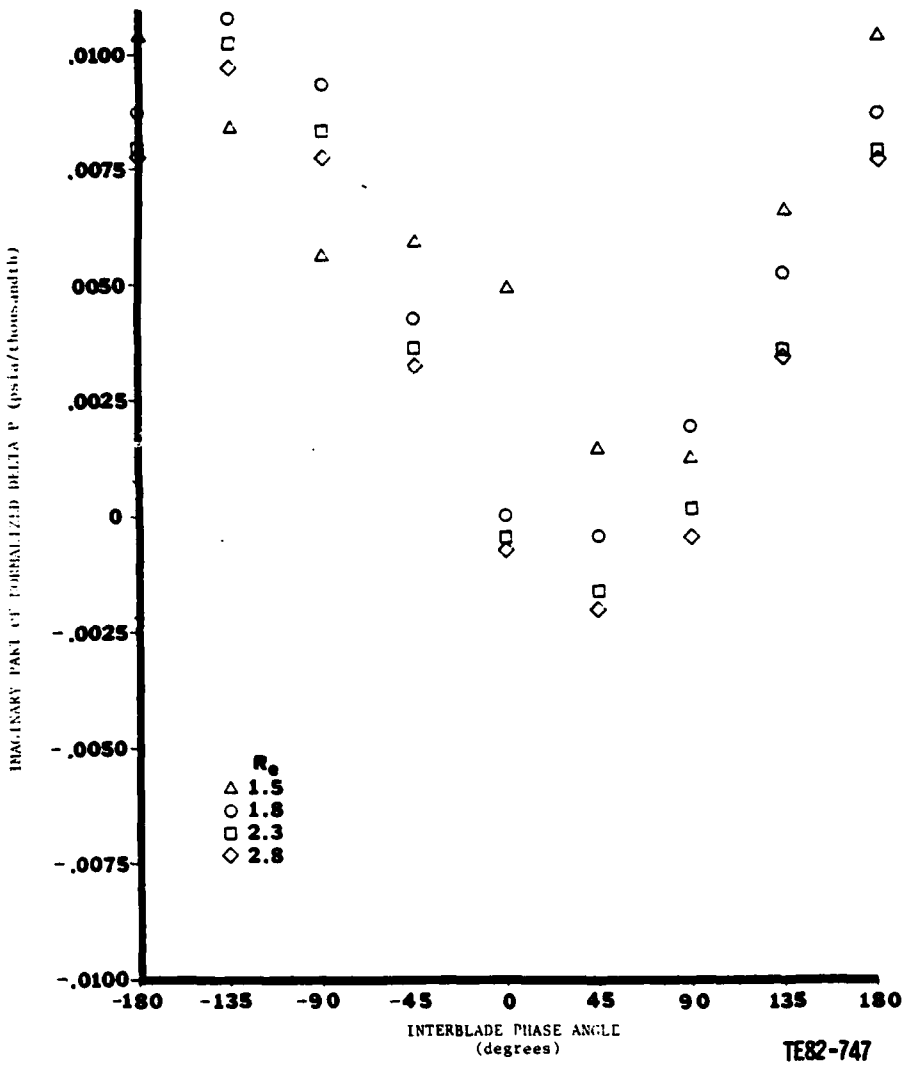

Figure 47. Imaginary part of the pressure difference across the center airfoil at 57.7% meanline station.

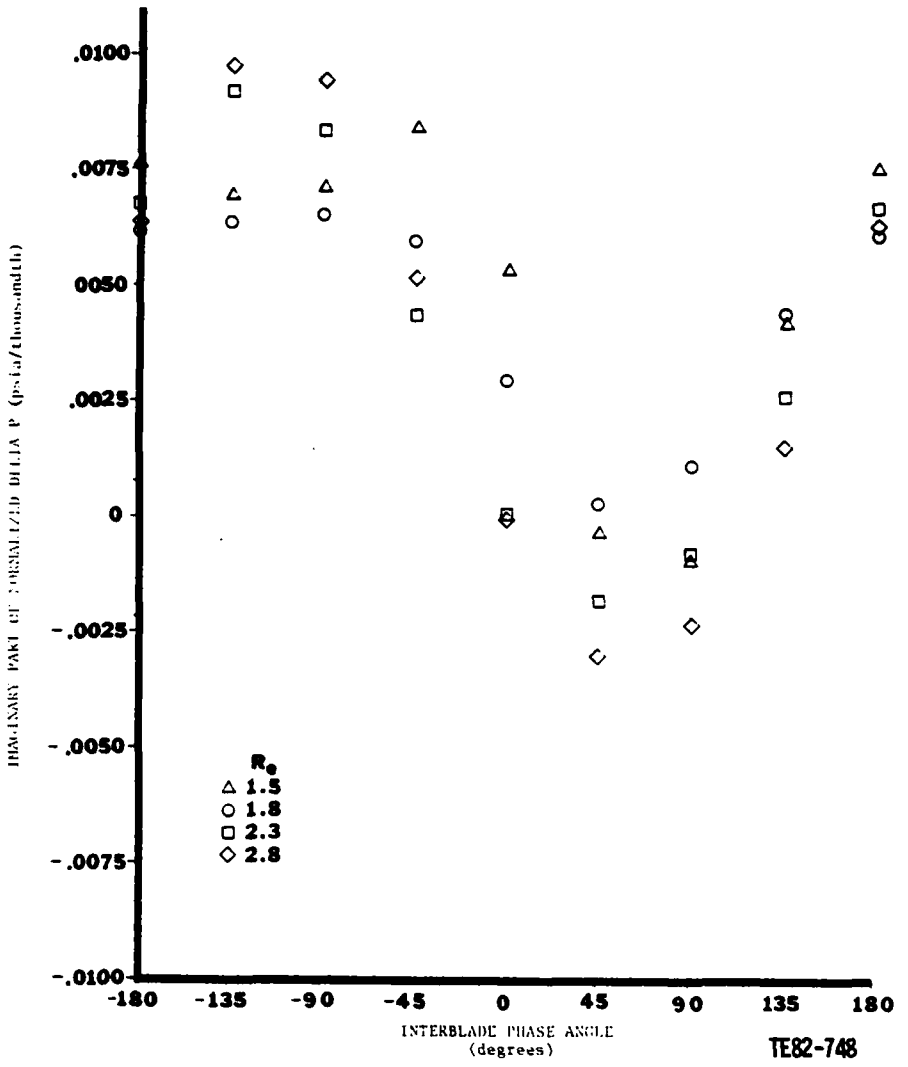

Figure 48. Imaginary part of the pressure difference across the center airfoil at 71.2% meanline station.

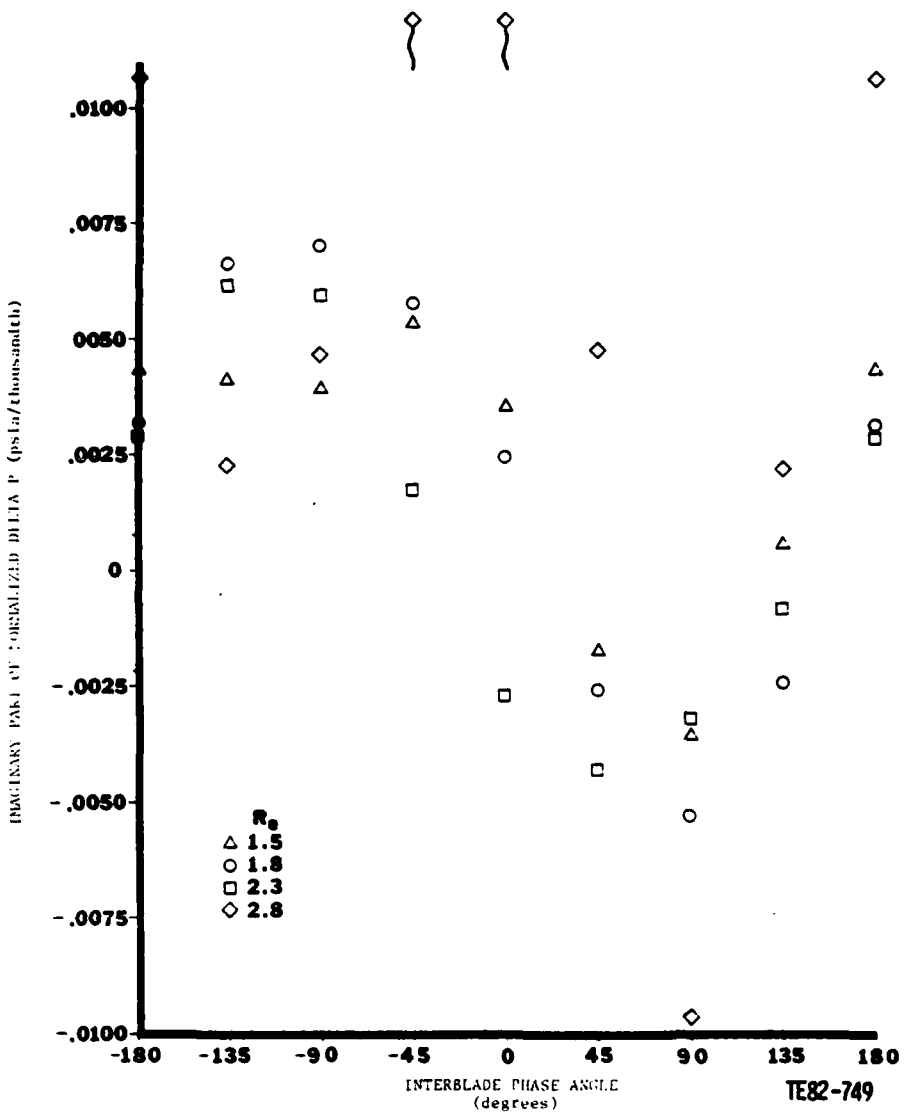

Figure 49. Imaginary part of the pressure difference across the center airfoil at 88.5% meanline station.

III. CONCLUSIONS AND RECOMMENDATIONS

From the experimental program conducted as described in this report, several conclusions became evident. These conclusions are as follows:

1. Predictions from the analytical model by Delaney (Reference 17) compares excellently with measured steady-state pressure distributions on both surfaces of the airfoil in regions where flow is not separated.

2. A separated zone exists in a region of the leading edge pressure surface of the airfoil.

3. Measured pressure coefficient magnitudes are larger than those predicted by a flat-plate, unloaded cascade analysis.

4. Measured phase lags between the pressure differences across the center airfoil and its motion are in fair agreement with the flat-plate model results.

5. Experimental trends of pressure magnitude and phase lag with respect to interblade phase angle indicate that:

   a. Minimum pressures occur in a region from 0 deg to 90 deg interblade phase angle.

   b. Maximum pressures occur in a range from -135 deg to -180 deg interblade phase angle

   c. A severe gradient of phase lag occurs in the 0 deg to +45 deg interblade phase angle range.

   These trends are in agreement with predictions from the analytical model.

6. Experimentally determined imaginary components of the pressure differences across the center airfoil occurring over a range of interblade phase angles indicate that:

   a. A translational instability of the tested cascade could occur (dependent on structural damping) in a range of interblade phase angles from 0 deg to +90 deg.

   b. Maximum aerodynamic damping occurs near 180 deg interblade phase angle.

7. Effects of increasing expansion ratio on measured unsteady pressures are most dominantly noted in trailing edge regions.

These conclusions address the results presented in this report. Implications of these results and conclusions based on them with regard to the overall aeroelasticity problem have not been fully developed. This was done deliberately, so that no bias for the use of the data would be shown. The data are self-standing and complete, the use of the data left to the investigators' own needs.

From the foregoing conclusions, the preparation of this report, and the experience gained in this experimental program, the following recommendations are presented:

1. Develop a transonic unsteady aerodynamic analysis for prediction of time-variant behavior of highly cambered, thick airfoils operating in a loaded cascade. This analysis should include steady flow field effects.

2. Investigate a series of airfoil cascades with airfoils having increasingly less turning in both torsional and translational modes to determine time-variant responses and trends. This would aid in current model development.

3. Develop an experimental investigation to isolate effects of camber and thickness on the time-variant aerodynamics of loaded cascades.

4. Examine data presented in this report and in torsional results (Reference 13) for the same cascade at various twist/bend ratios to determine aerodynamic damping at varying interblade phase angles.

These recommendations encompass the experimental programs supported by NASC which have investigated the time-variant pressures on airfoils oscillating in torsion and translation.

IV. REFERENCES

1. Whitehead, D. S., Force and Moment Coefficients for Vibrating Airfoils in Cascade, Aeronautical Research Council R and M 3254, February 1960.

2. Smith, S. M., Discrete Frequency Sound Generation in Axial Flow Turbomachines, University of Cambridge, Department of Engineering Report CUED/A-Turbo/TR 29, 1971.

3. Caruthers, J. E., "Theoretical Analysis of Unsteady Supersonic Flow Around Harmonically Oscillating Turbofan Cascades," Ph.D. Thesis, Georgia Tech. (Sept. 1976).

4. Brix, C. W., Jr. and Platzer, M. F., "Theoretical Investigation of Supersonic Flow Past Oscillating Cascades with Subsonic Leading Edge Locus," AIAA 12th Aerosp. Sci. Mtg., Washington, D.C. AIAA Paper No. 72-14 (Jan 30-Feb 1, 1974).

5. Goldstein, M. E., Braun, W., and Adamczyk, J. J., "Unsteady Flow in a Supersonic Cascade with Strong In-Passage Shocks," J. Fluid Mech., Trans. ASME, 83, Pt. 3, pp 569-604 (1977).

6. Caruthers, J. E., "Wake Induced Vibration of Axial Components," Aeroelasticity of Turbine Engines, Joint NASA/AF/Navy Symposium, preprint, Oct. 1980.

7. Verdon, J. M. and Caspar, J. R., "Development of an Unsteady Cascade Analysis," Aeroelasticity of Turbine Engines, Joint NASA/AF/Navy Symposium, preprint, October 1980.

8. Williams, M. H. and Dowell, E. H., "Unsteady Aerodynamics in Transonic Cascades," Aeroelasticity of Turbine Engines, Joint NASA/AF/Navy Symposium, preprint, October 1980.

9. Platzer, M. F. and Adamson, T. C., "A Method of Characteristics Approach to Analyze Supersonic Blade Flutter," Aeroelasticity of Turbine Engines, Joint NASA/AF/Navy Symposium, preprint, October 1980.

10. Carta, F. O. and St. Hillaire, A. O., "Effect of Interblade Phase Angle and Incidence Angle on Cascade Pitching Stability," ASME Journal of Engineering for Power, Vol. 102, No. 2, April 1980.

11. Boldman, D. R. and Buggele, A. E., "LeRC Transonic Oscillating Cascade Wind Tunnel," Aeroelasticity of Turbine Engines, Joint NASA/AF/Navy Symposium, preprint, October 1980.

12. Riffel, R. and Rothrock, M. D., "Experimental Determination of Unsteady Blade Aerodynamics in Cascade," Aeroelasticity in Turbine Engines, NASA/AF/Navy Symposium, preprint, October 1980.

13. Jay, R. L., Rothrock, M., Riffel, R., and Sinnet, G., "Time-Variant Aerodynamics for Torsional Motion of Large Turning Airfoils," DDA EDR 10192, Final Report, NASC Contract No. N00019-79-C-0087, January 1980.

14. Jay, R. L. and Bennett, W. A., "The Effects of Solidity, Interblade-Phase Angle, and Reduced Frequency on the Time-Variant Aerodynamic Response of a Compressor Stator," EDR 10339, June 1980.

15. Szechenyi, E., Loiseau, H., and MaQuennehan, B., "Study of Aeroelastic Instabilities of Compressors in a Straight Cascade Wind Tunnel," FTD-ID(RS)T-00063-80, January 1980.

16. Platzer, M. F., "Unsteady Flows in Turbomachines--A Review of Recent Developments," AGARD-CP-227, September 1977.

17. Delaney, R. A., "Time Marching Analysis of Steady Transonic Flow in Turbomachinery Cascades Using the Hopscotch Method," ASME Paper No. 82-GT-152, will be presented in London at the 27th International Gas Turbine Conference, April 18-22, 1982.

APPENDIX

TIME-VARIANT DATA

APPENDIX A

In this Appendix, the pressure magnitudes and phase lags as referenced to center airfoil motion are presented as discussed under "Time Variant Testing".

NORMALIZED SURFACE PRESSURE AMPLITUDES
1.5 TOTAL TO STATIC EXPANSION RATIO
180. DEGREES INTERBLADE PHASE ANGLE
+ PRESSURE SURFACE
□ SUCTION SURFACE

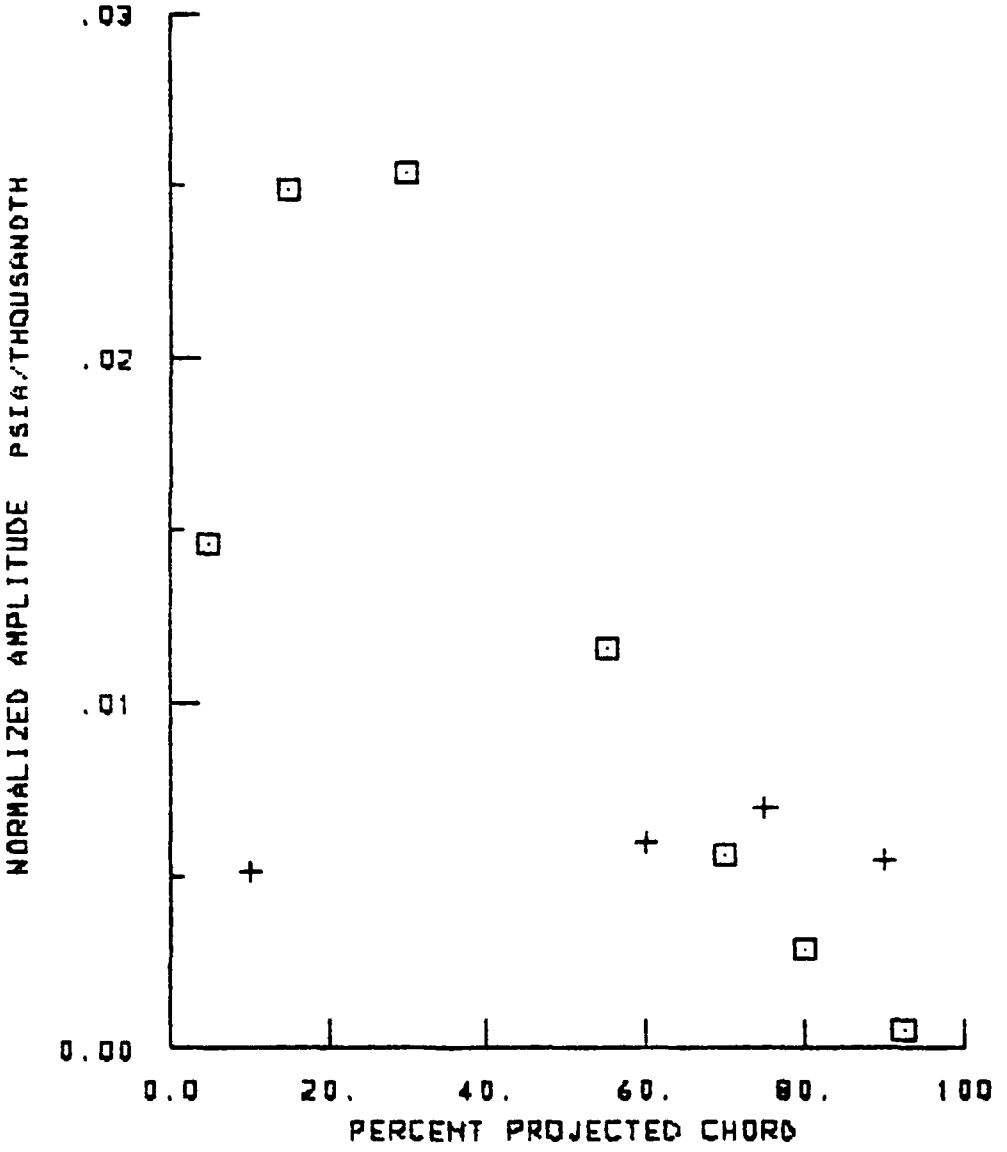

1 FEB., 1982

SURFACE PRESSURE PHASE LAGS
1.5 TOTAL TO STATIC EXPANSION RATIO
180. DEGREES INTERBLADE PHASE ANGLE
+ PRESSURE SURFACE
□ SUCTION SURFACE

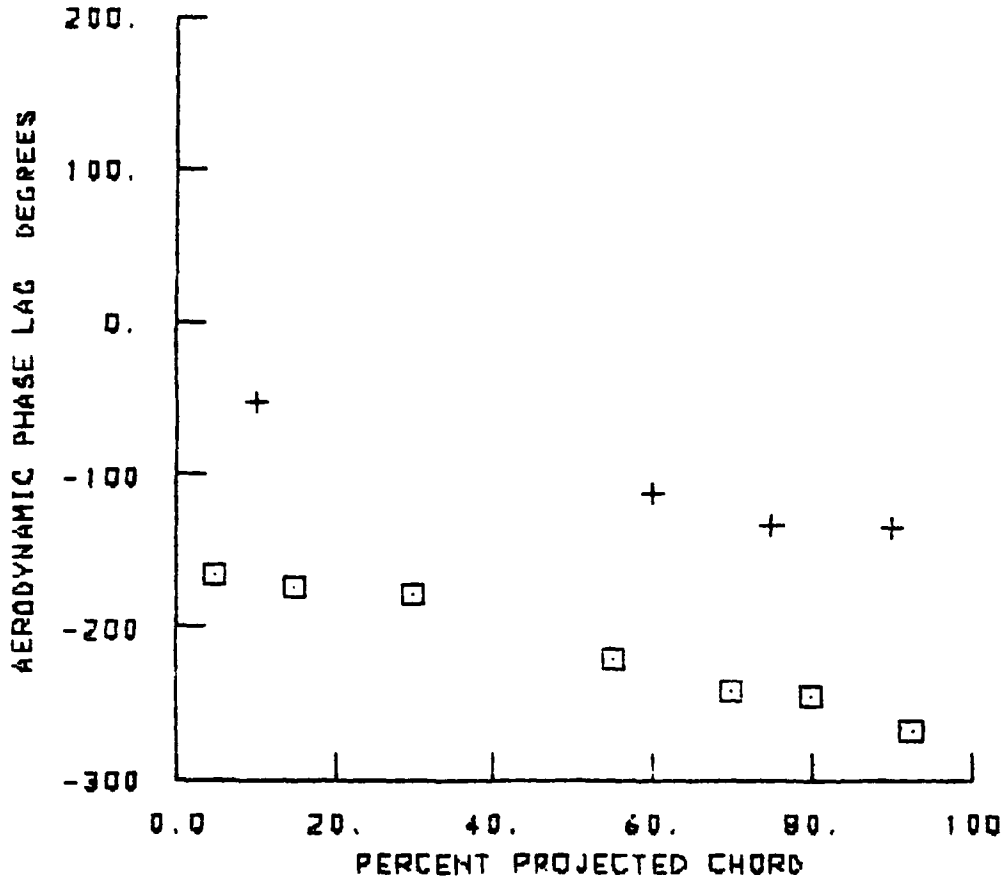

1 FEB., 1982

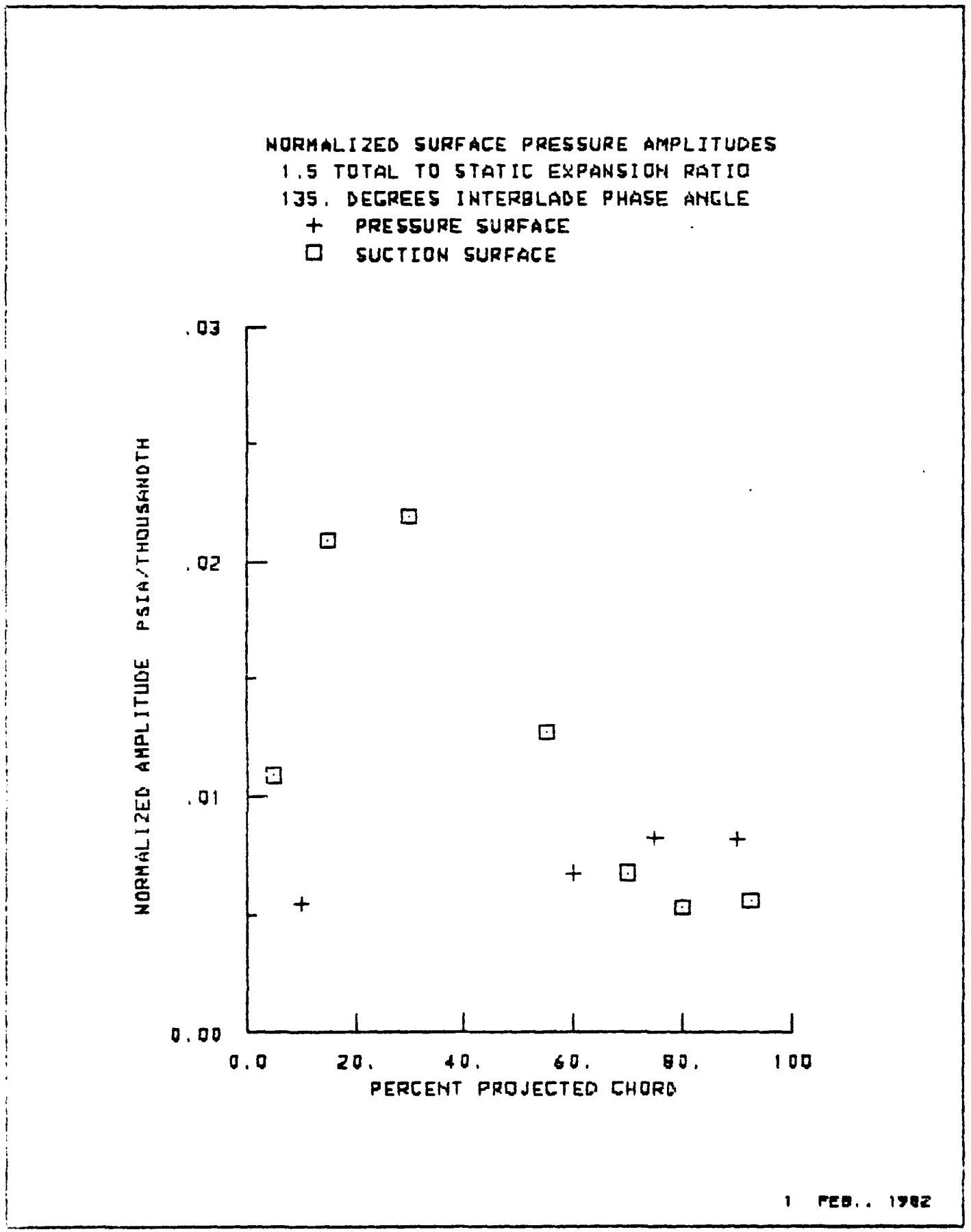
NORMALIZED SURFACE PRESSURE AMPLITUDES
1.5 TOTAL TO STATIC EXPANSION RATIO
135. DEGREES INTERBLADE PHASE ANGLE
+ PRESSURE SURFACE
□ SUCTION SURFACE
NORMALIZED AMPLITUDE PSIA/THOUSANDTH
.03
.02
.01
0.00
0.0
20.
40.
60.
80.
100
PERCENT PROJECTED CHORD
1 FEB., 1982

SURFACE PRESSURE PHASE LAGS
1.5 TOTAL TO STATIC EXPANSION RATIO
135. DEGREES INTERBLADE PHASE ANGLE
+ PRESSURE SURFACE
□ SUCTION SURFACE

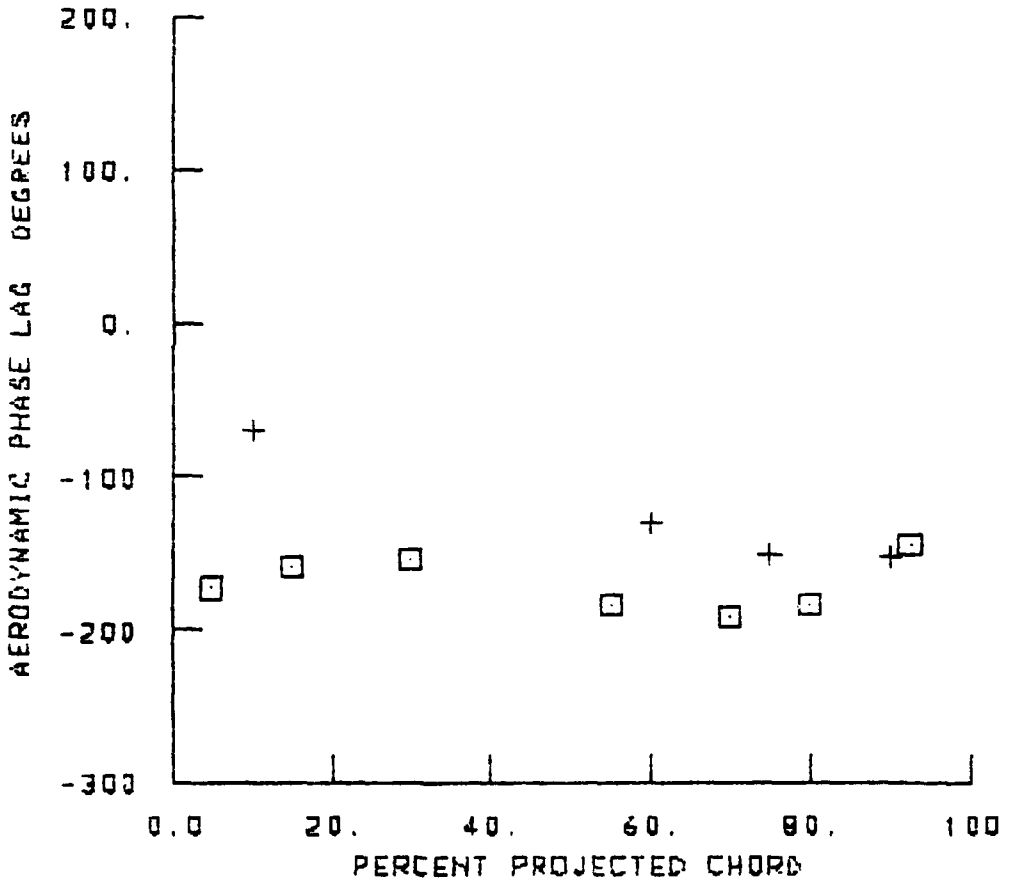

1 FEB., 1982

NORMALIZED SURFACE PRESSURE AMPLITUDES
1.5 TOTAL TO STATIC EXPANSION RATIO
90. DEGREES INTERBLADE PHASE ANGLE
+ PRESSURE SURFACE
□ SUCTION SURFACE

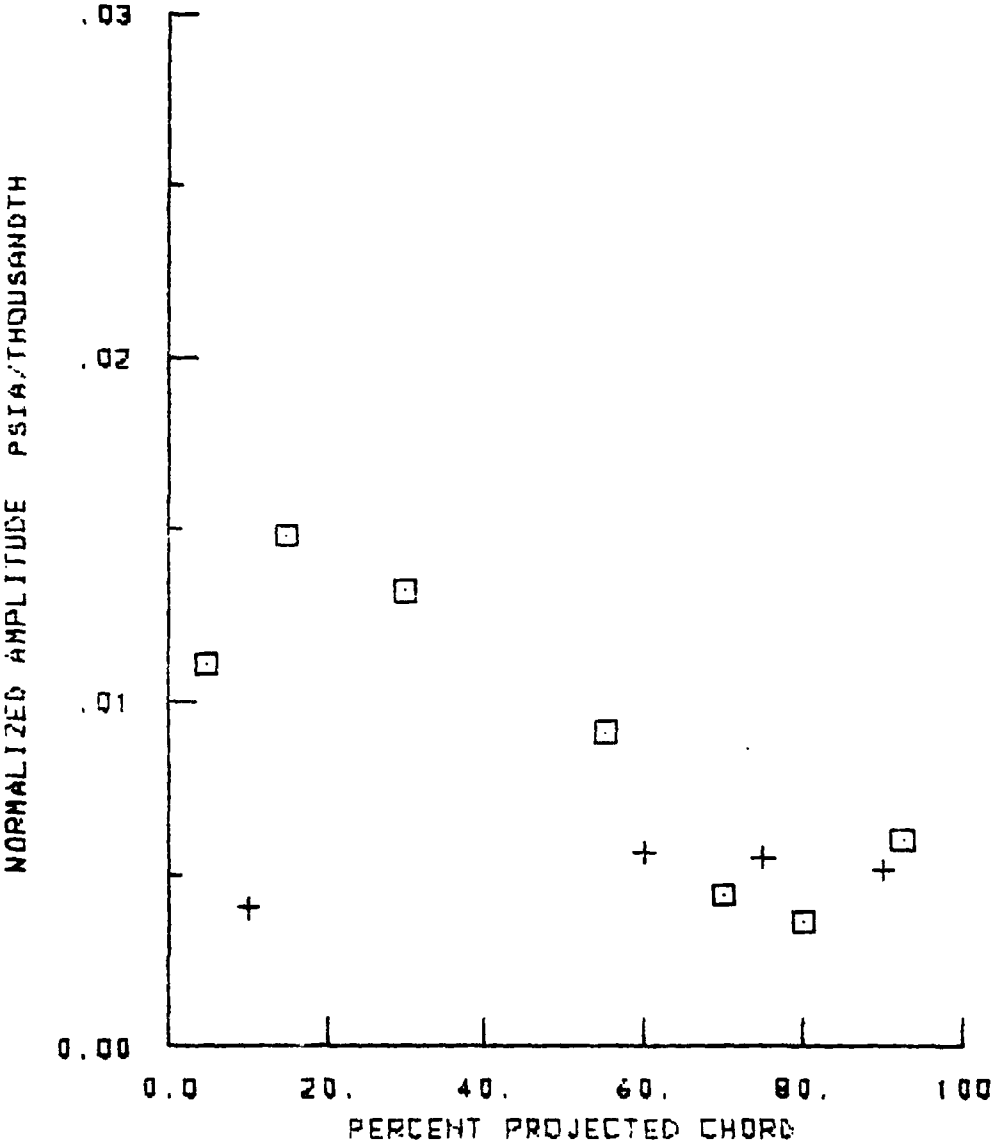

1 FEB., 1962

SURFACE PRESSURE PHASE LAGS
1.5 TOTAL TO STATIC EXPANSION RATIO
90. DEGREES INTERBLADE PHASE ANGLE
+ PRESSURE SURFACE
□ SUCTION SURFACE

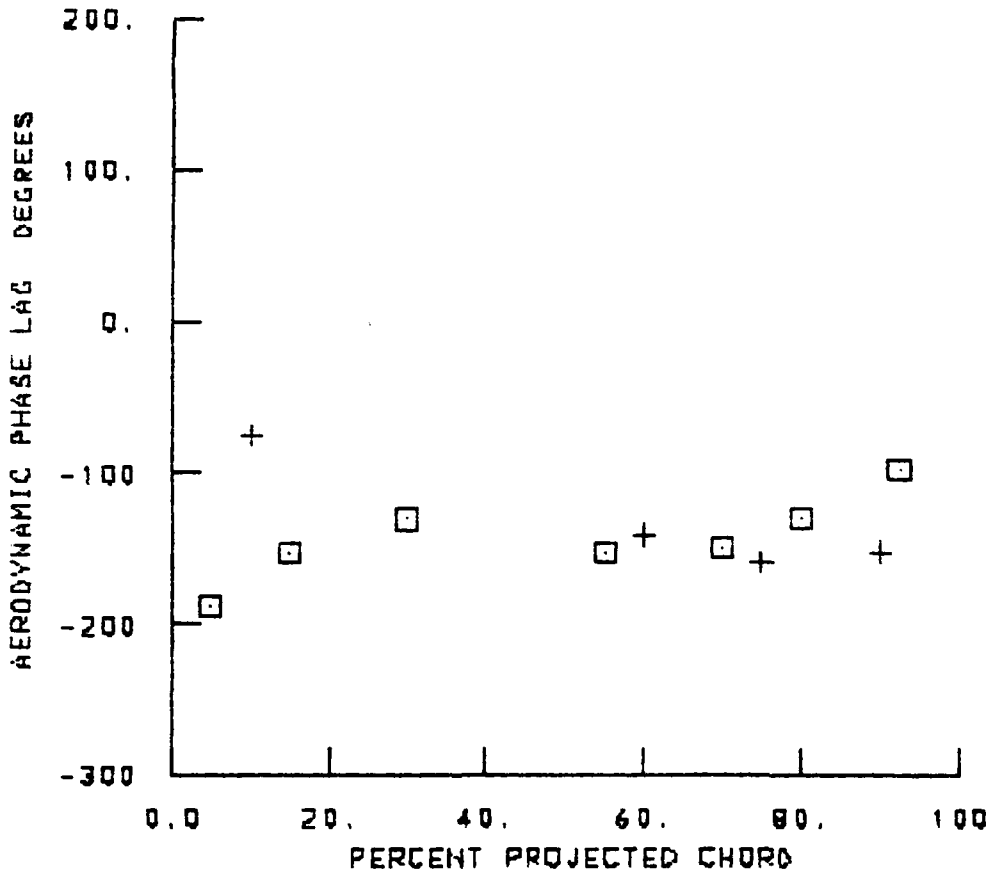

1 FEB., 1982

NORMALIZED SURFACE PRESSURE AMPLITUDES
1.5 TOTAL TO STATIC EXPANSION RATIO
45. DEGREES INTERBLADE PHASE ANGLE
+ PRESSURE SURFACE
□ SUCTION SURFACE

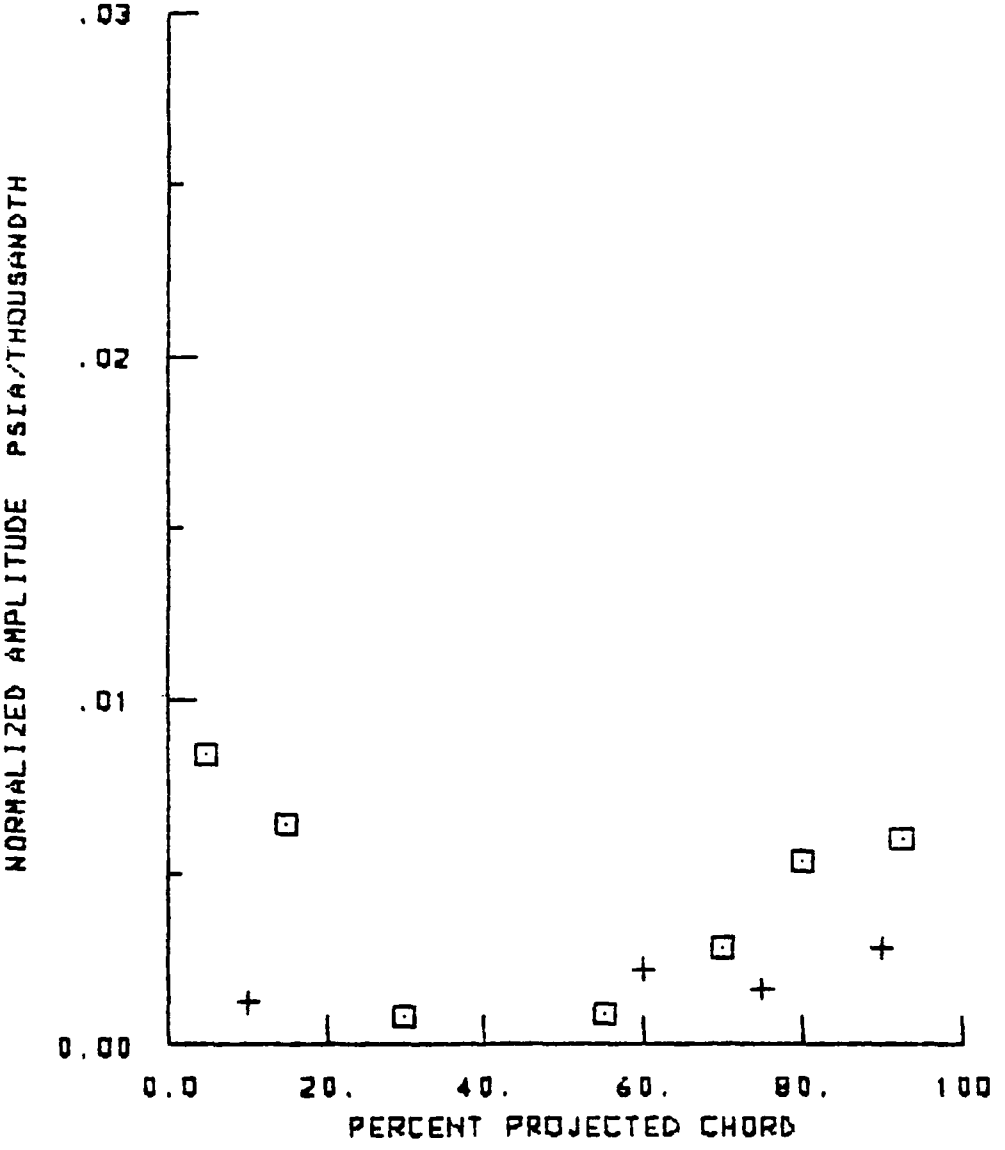

1 FEB., 1982

SURFACE PRESSURE PHASE LAGS
1.5 TOTAL TO STATIC EXPANSION RATIO
45. DEGREES INTERBLADE PHASE ANGLE
+ PRESSURE SURFACE
□ SUCTION SURFACE

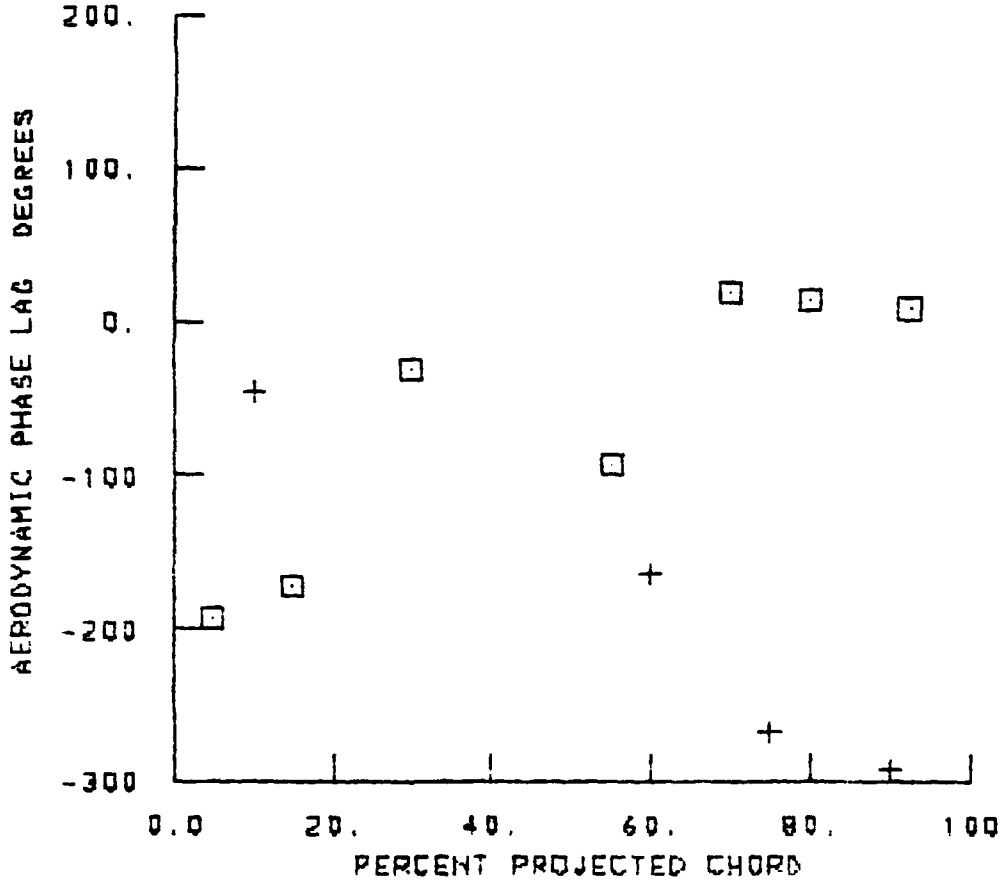

1 FEB., 1982

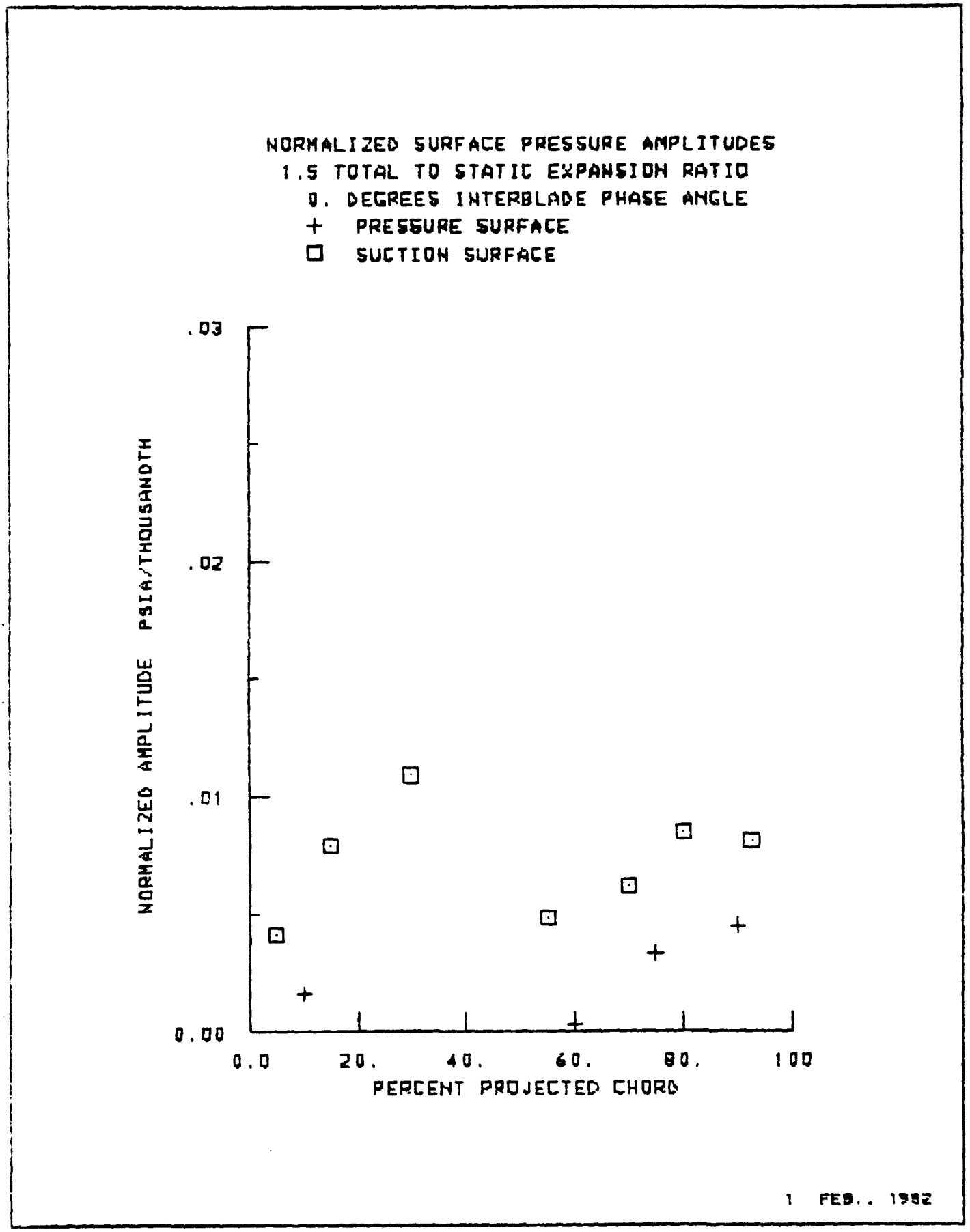
NORMALIZED SURFACE PRESSURE AMPLITUDES
1.5 TOTAL TO STATIC EXPANSION RATIO
0. DEGREES INTERBLADE PHASE ANGLE
+ PRESSURE SURFACE
□ SUCTION SURFACE
.03
.02
.01
0.00
NORMALIZED AMPLITUDE PSIA/THOUSANDTH
0.0
20.
40.
60.
80.
100
PERCENT PROJECTED CHORD
1 FEB., 1982

SURFACE PRESSURE PHASE LAGS
1.5 TOTAL TO STATIC EXPANSION RATIO
0. DEGREES INTERBLADE PHASE ANGLE
+ PRESSURE SURFACE
□ SUCTION SURFACE

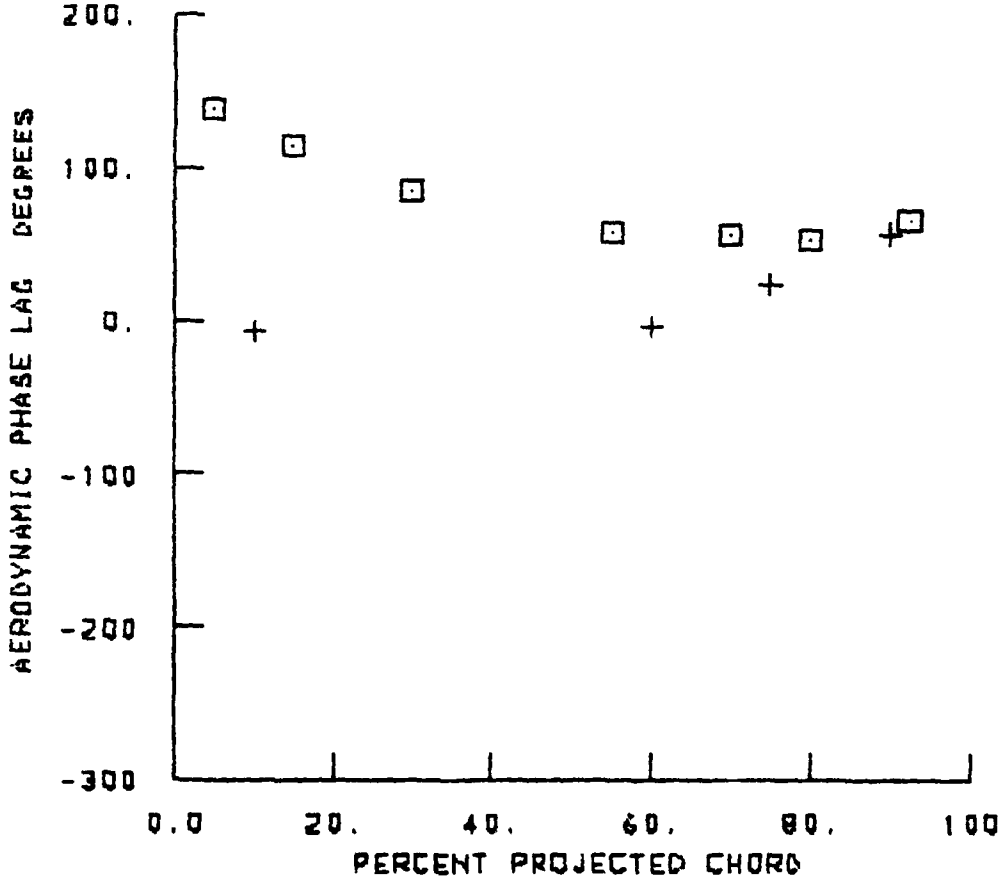

1 FEB., 1982

NORMALIZED SURFACE PRESSURE AMPLITUDES
1.5 TOTAL TO STATIC EXPANSION RATIO
-45. DEGREES INTERBLADE PHASE ANGLE
+ PRESSURE SURFACE
□ SUCTION SURFACE

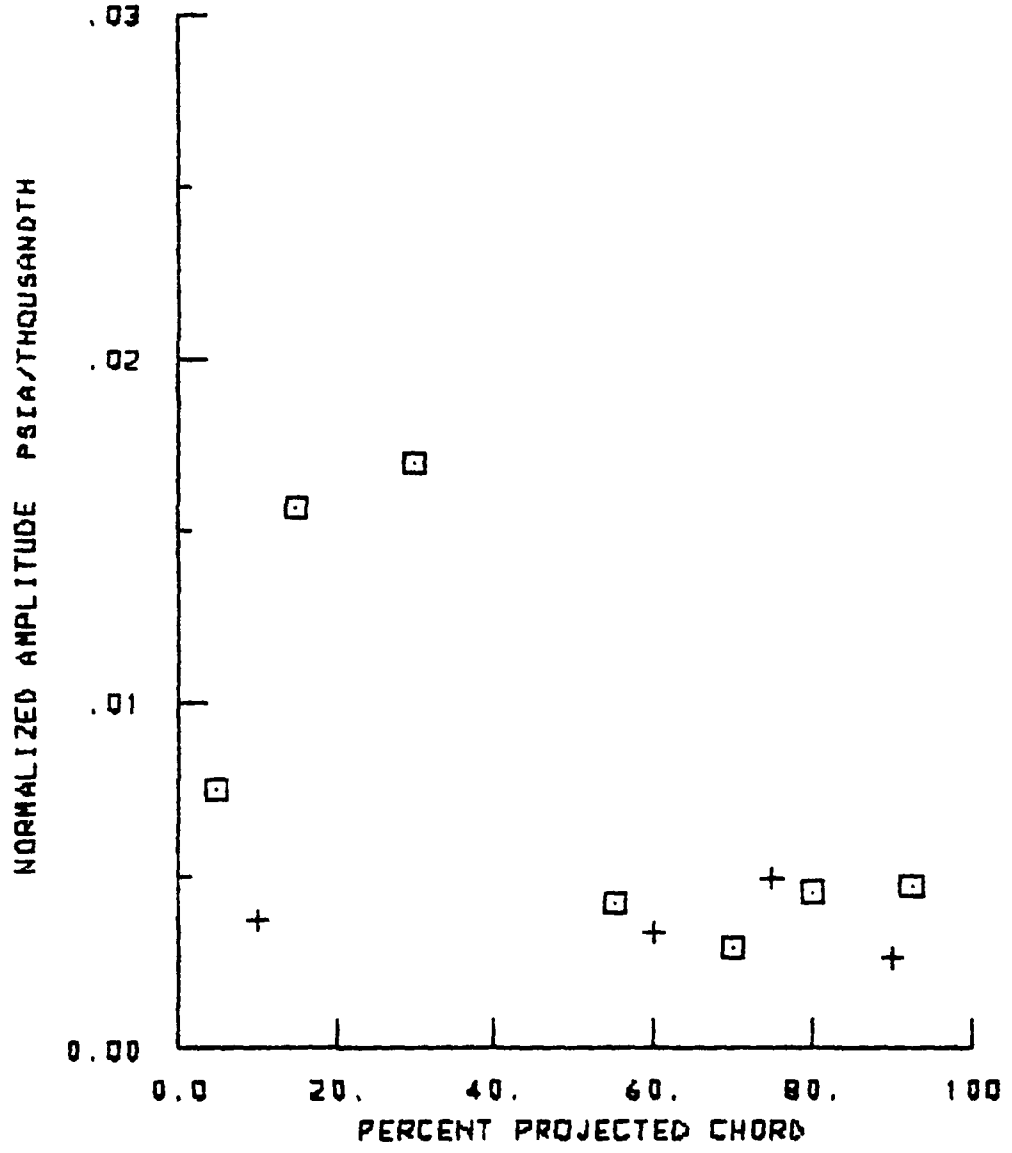

1 FEB., 1982

SURFACE PRESSURE PHASE LAGS
1.5 TOTAL TO STATIC EXPANSION RATIO
-45. DEGREES INTERBLADE PHASE ANGLE
\+ PRESSURE SURFACE
□ SUCTION SURFACE

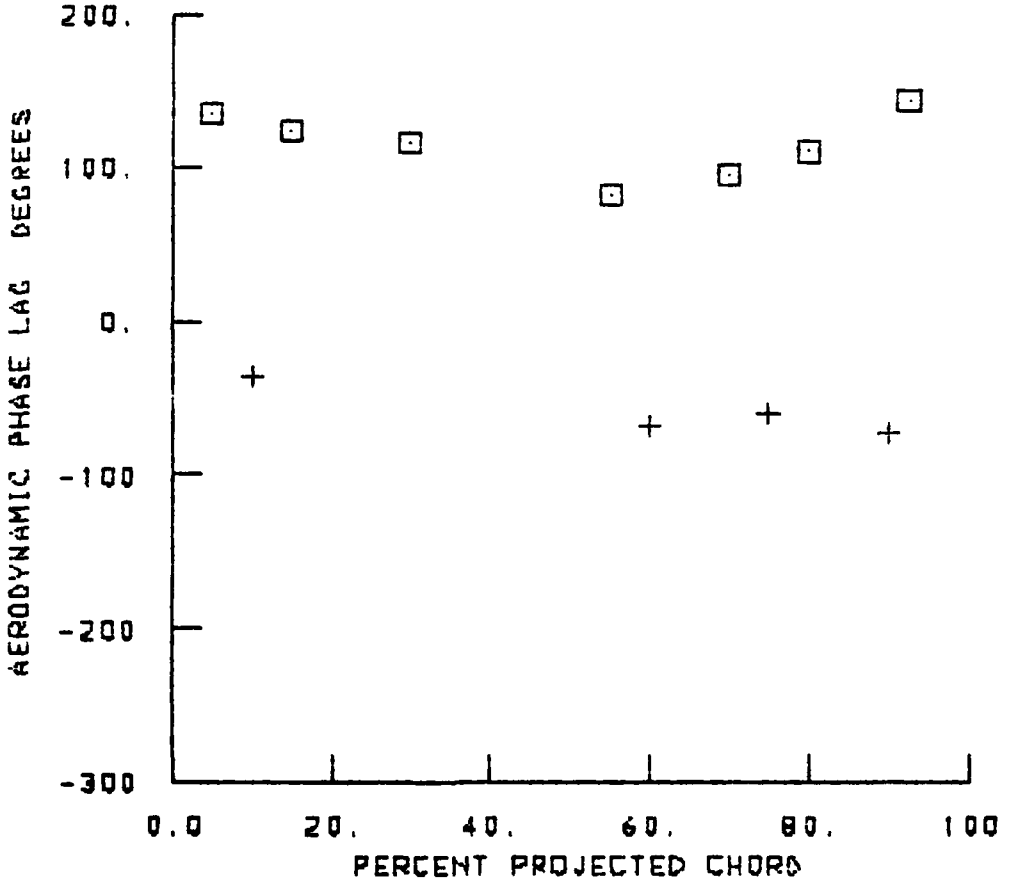

1 FEB., 1982

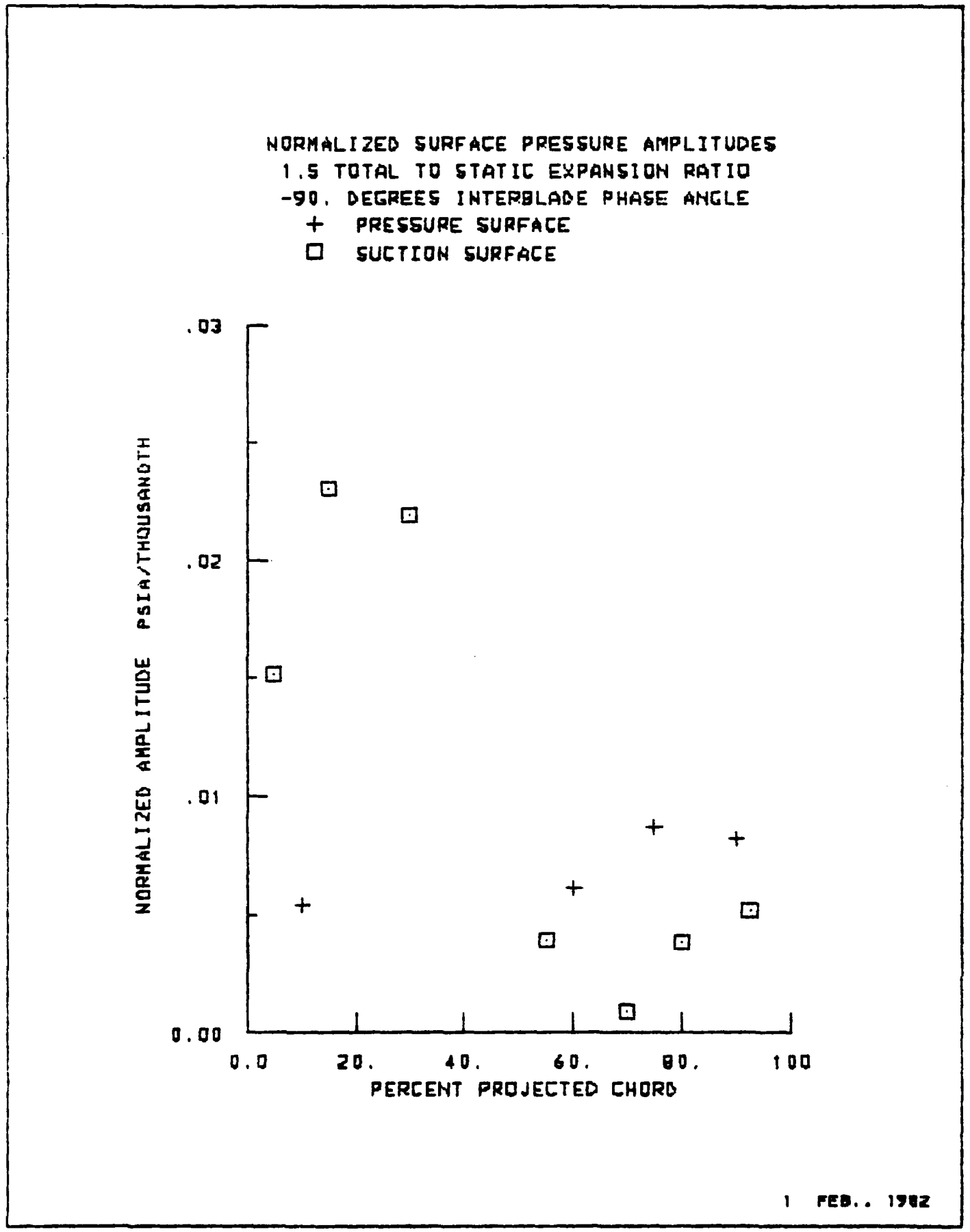
NORMALIZED SURFACE PRESSURE AMPLITUDES
1.5 TOTAL TO STATIC EXPANSION RATIO
-90. DEGREES INTERBLADE PHASE ANGLE
+ PRESSURE SURFACE
□ SUCTION SURFACE
NORMALIZED AMPLITUDE PSIA/THOUSANDTH
.03
.02
.01
0.00
0.0
20.
40.
60.
80.
100
PERCENT PROJECTED CHORD
1 FEB., 1982

SURFACE PRESSURE PHASE LAGS
1.5 TOTAL TO STATIC EXPANSION RATIO
-90. DEGREES INTERBLADE PHASE ANGLE
+ PRESSURE SURFACE
□ SUCTION SURFACE

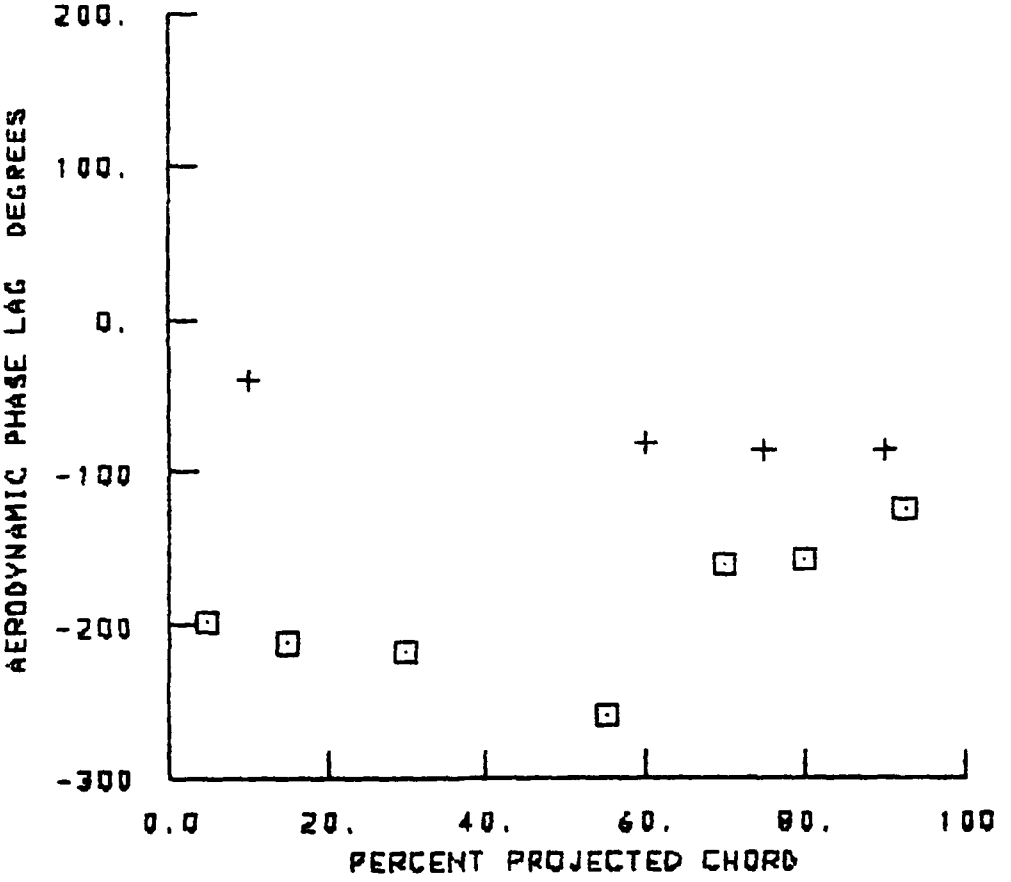

1 FEB., 1982

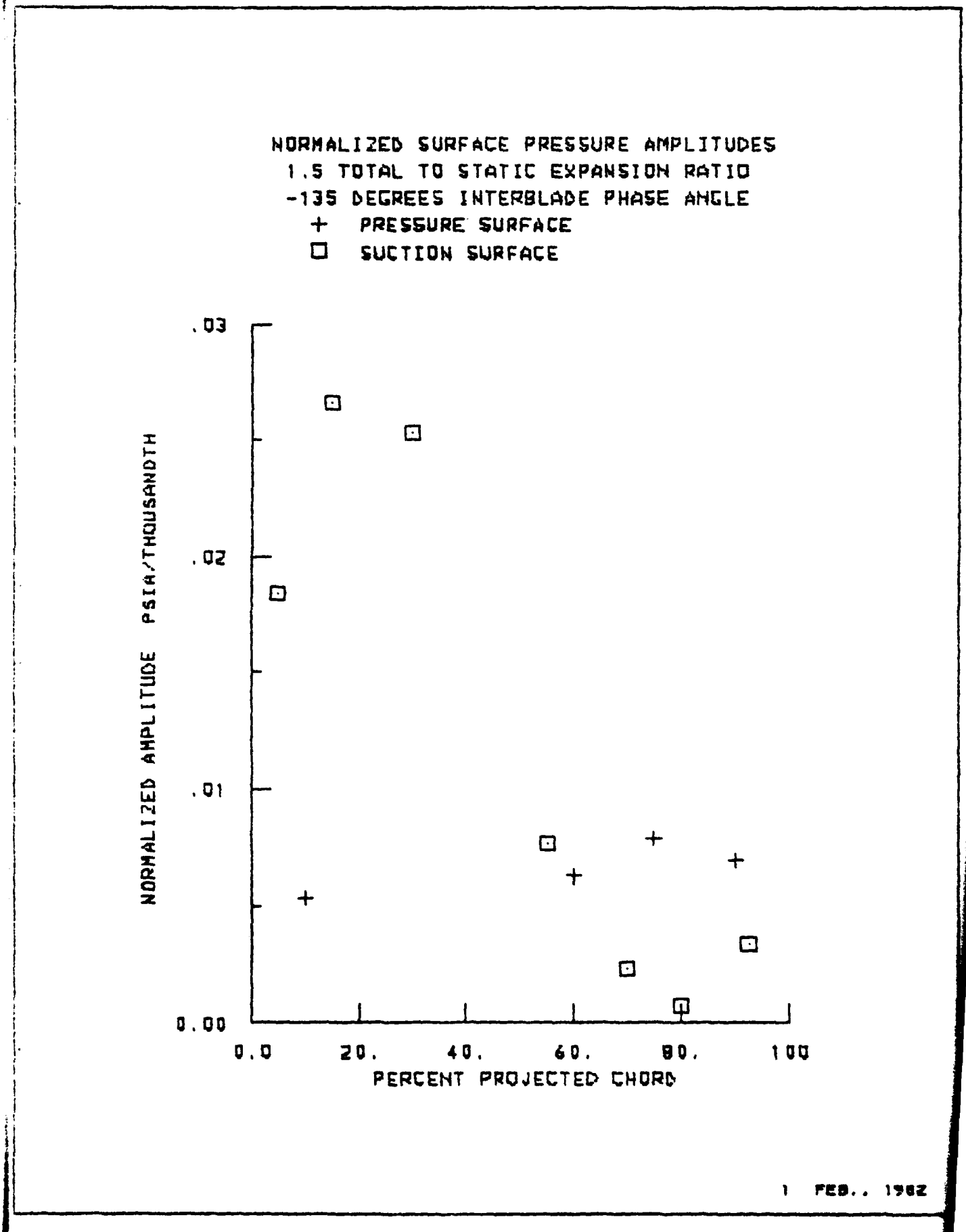
NORMALIZED SURFACE PRESSURE AMPLITUDES
1.5 TOTAL TO STATIC EXPANSION RATIO
-135 DEGREES INTERBLADE PHASE ANGLE
+ PRESSURE SURFACE
□ SUCTION SURFACE
NORMALIZED AMPLITUDE PSIA/THOUSANDTH
.03
.02
.01
0.00
0.0
20.
40.
60.
80.
100
PERCENT PROJECTED CHORD
1 FEB., 1982

SURFACE PRESSURE PHASE LAGS
1.5 TOTAL TO STATIC EXPANSION RATIO
-135 DEGREES INTERBLADE PHASE ANGLE
+ PRESSURE SURFACE
□ SUCTION SURFACE

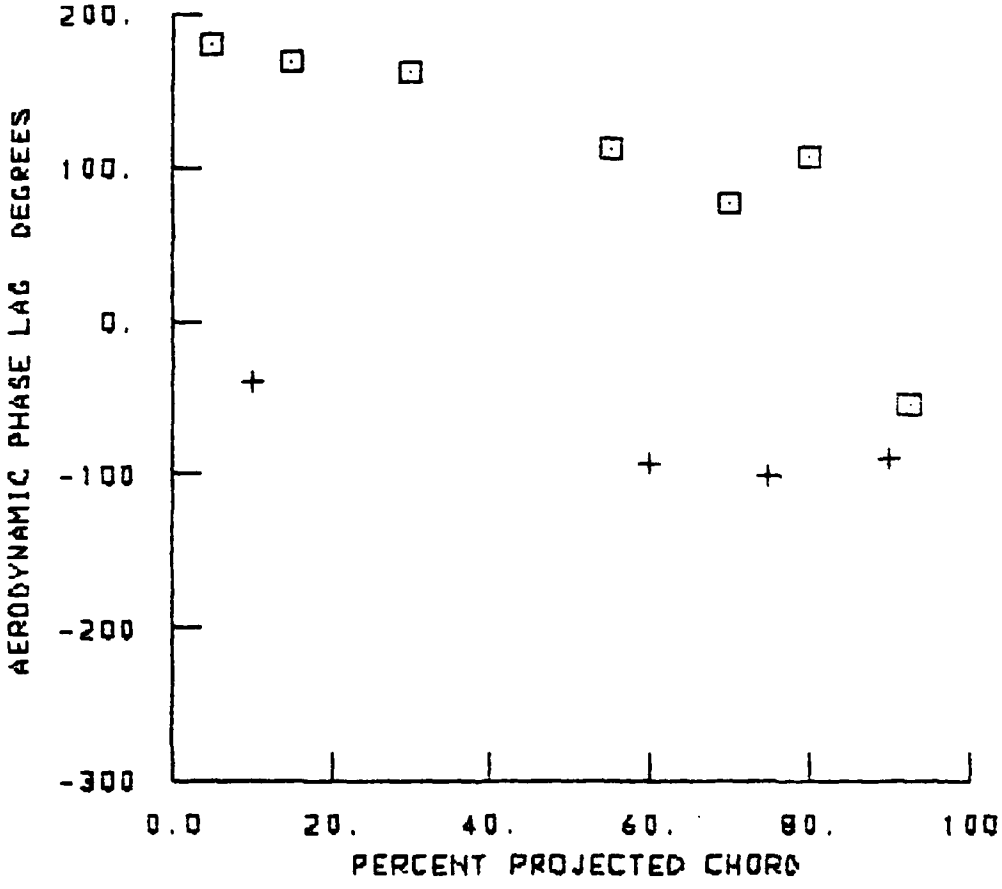

1 FEB., 1982

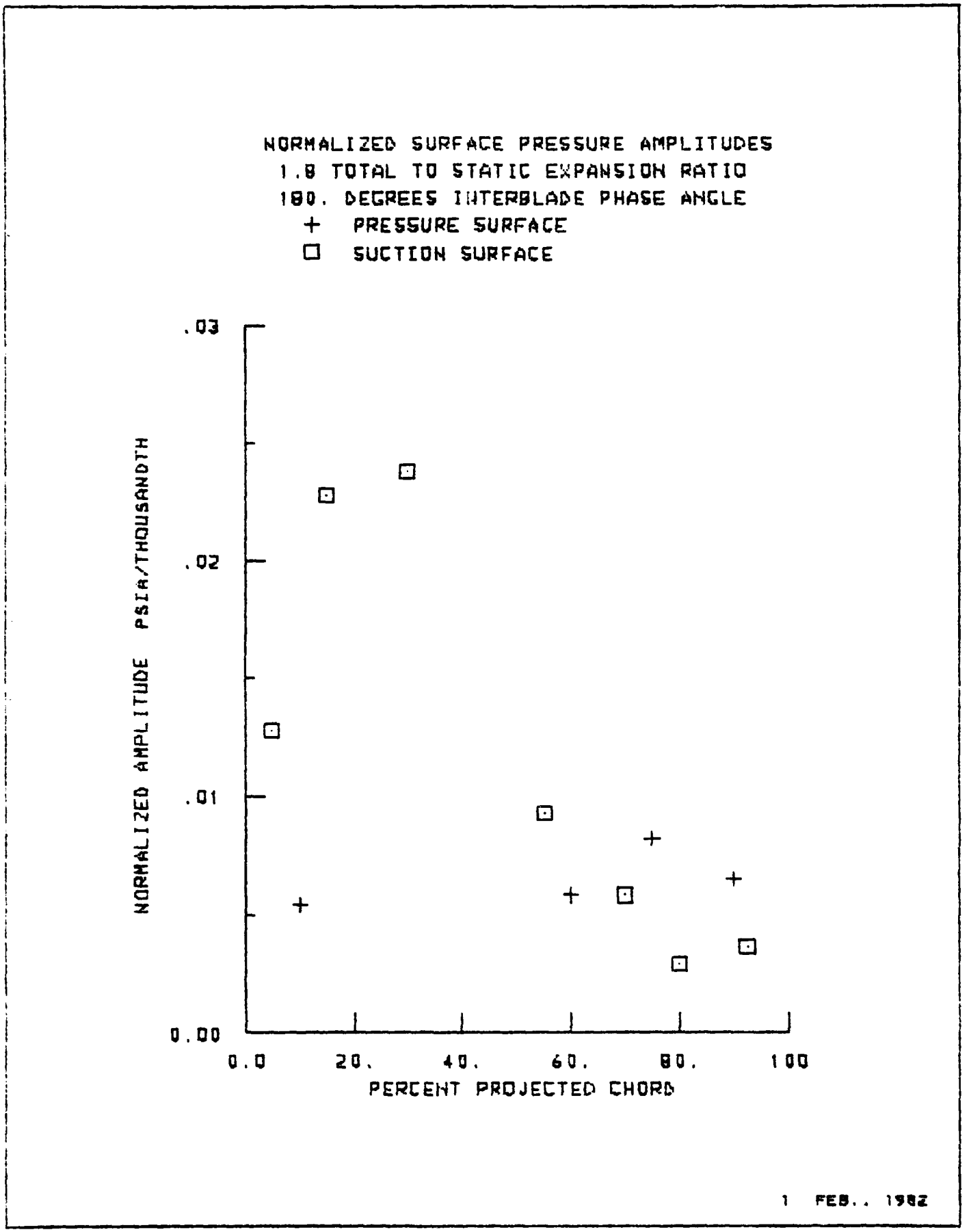
NORMALIZED SURFACE PRESSURE AMPLITUDES
1.8 TOTAL TO STATIC EXPANSION RATIO
180. DEGREES INTERBLADE PHASE ANGLE
+ PRESSURE SURFACE
□ SUCTION SURFACE
.03
.02
.01
0.00
NORMALIZED AMPLITUDE PSIA/THOUSANDTH
0.0
20.
40.
60.
80.
100
PERCENT PROJECTED CHORD
1 FEB., 1982

SURFACE PRESSURE PHASE LAGS
1.8 TOTAL TO STATIC EXPANSION RATIO
180. DEGREES INTERBLADE PHASE ANGLE
+ PRESSURE SURFACE
□ SUCTION SURFACE

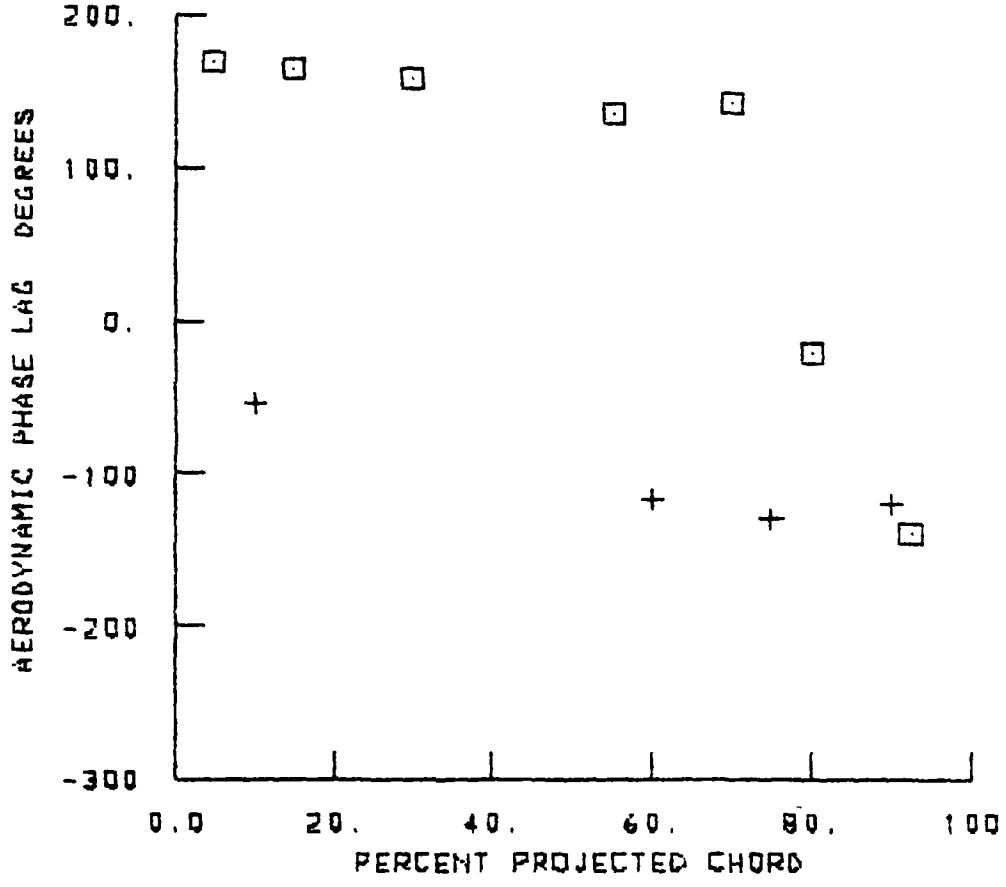

1 FEB., 1982

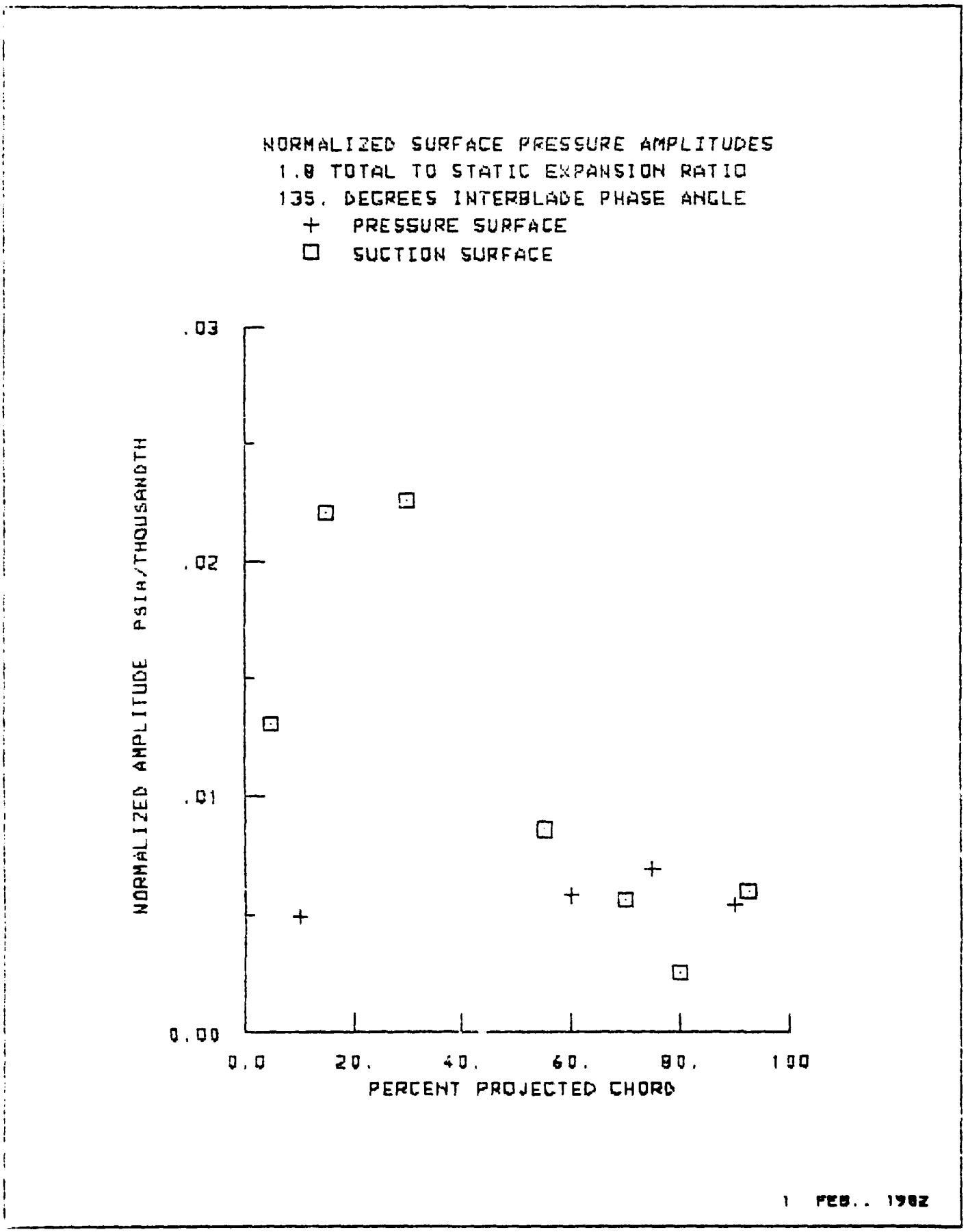
NORMALIZED SURFACE PRESSURE AMPLITUDES
1.0 TOTAL TO STATIC EXPANSION RATIO
135. DEGREES INTERBLADE PHASE ANGLE
+ PRESSURE SURFACE
□ SUCTION SURFACE
.03
.02
.01
0.00
NORMALIZED AMPLITUDE PSIA/THOUSANDTH
0.0
20.
40.
60.
80.
100
PERCENT PROJECTED CHORD
1 FEB., 1982

SURFACE PRESSURE PHASE LAGS
1.8 TOTAL TO STATIC EXPANSION RATIO
135. DEGREES INTERBLADE PHASE ANGLE
+ PRESSURE SURFACE
□ SUCTION SURFACE

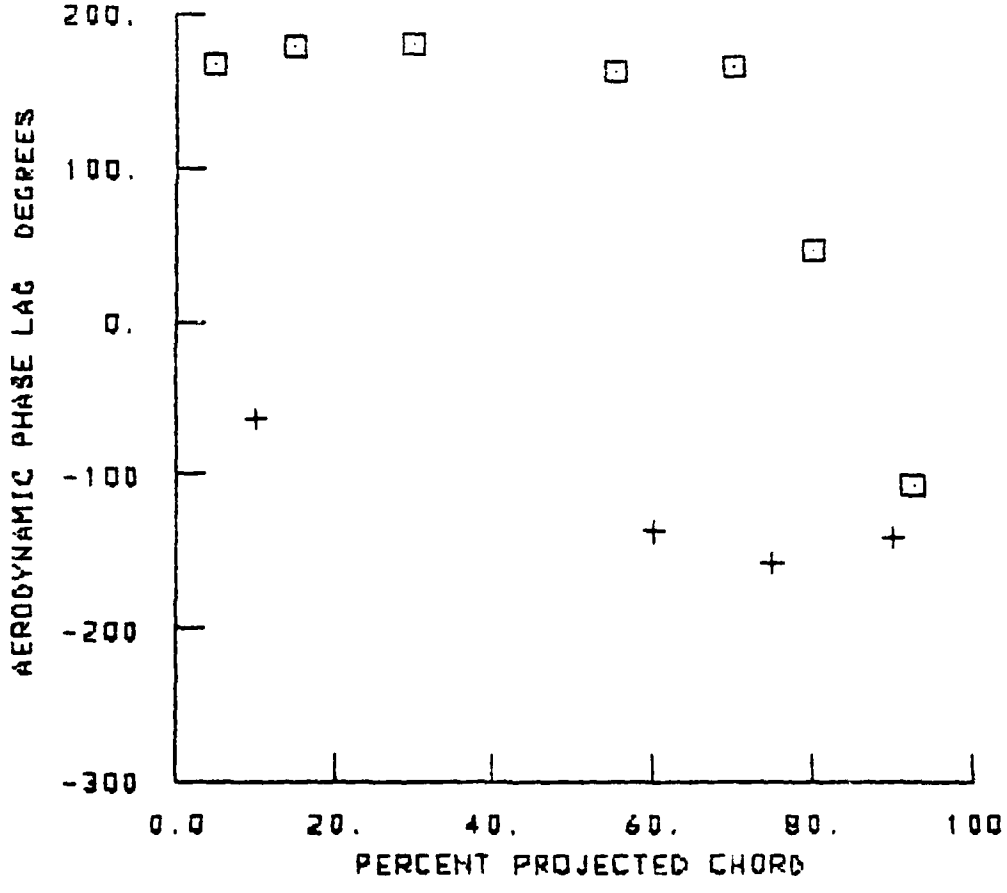

1 FEB., 1982

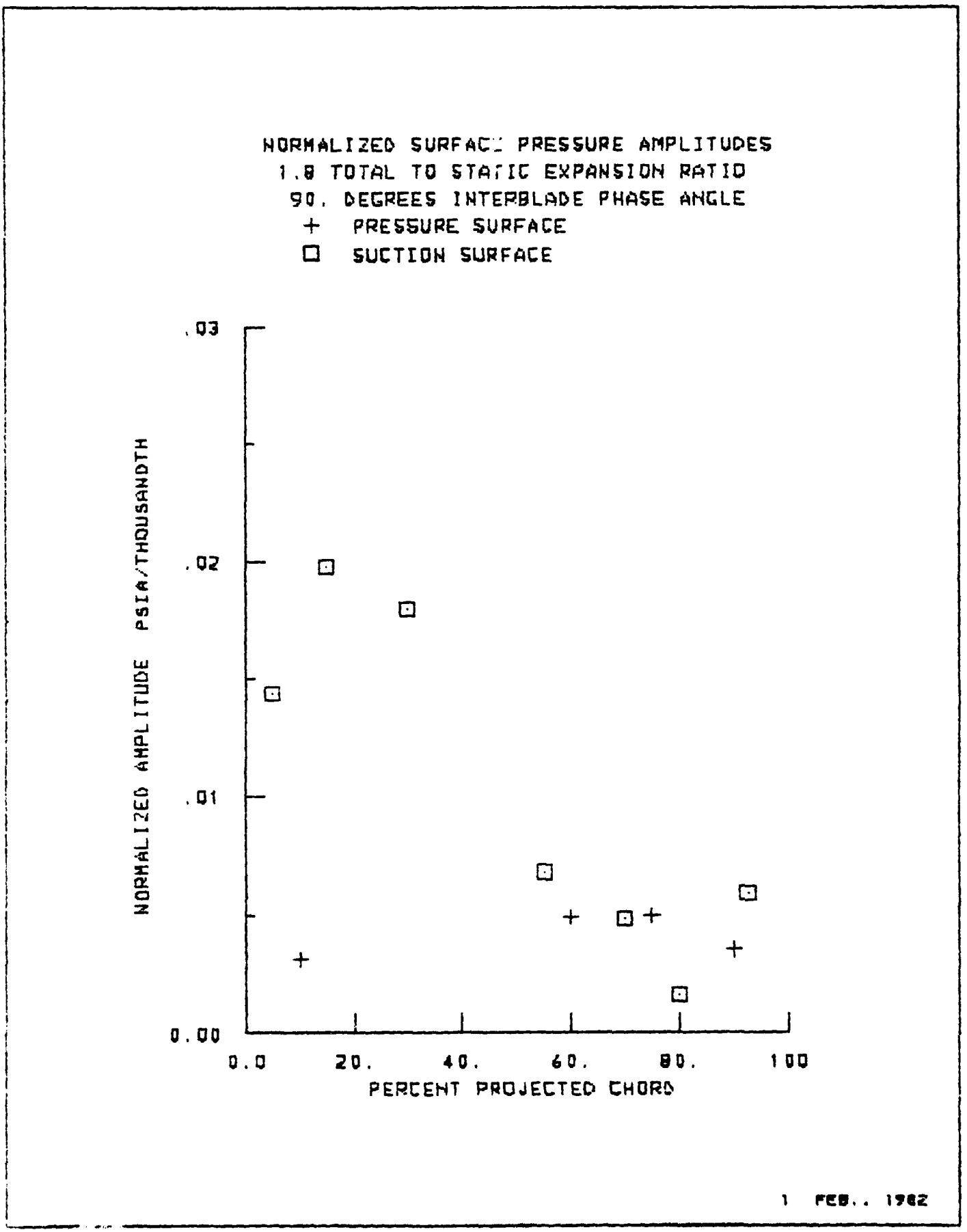
NORMALIZED SURFACE PRESSURE AMPLITUDES
1.8 TOTAL TO STATIC EXPANSION RATIO
90. DEGREES INTERBLADE PHASE ANGLE
+ PRESSURE SURFACE
□ SUCTION SURFACE
.03
.02
.01
0.00
NORMALIZED AMPLITUDE PSIA/THOUSANDTH
0.0
20.
40.
60.
80.
100
PERCENT PROJECTED CHORD
1 FEB., 1982

SURFACE PRESSURE PHASE LAGS
1.8 TOTAL TO STATIC EXPANSION RATIO
90. DEGREES INTERBLADE PHASE ANGLE
+ PRESSURE SURFACE
□ SUCTION SURFACE

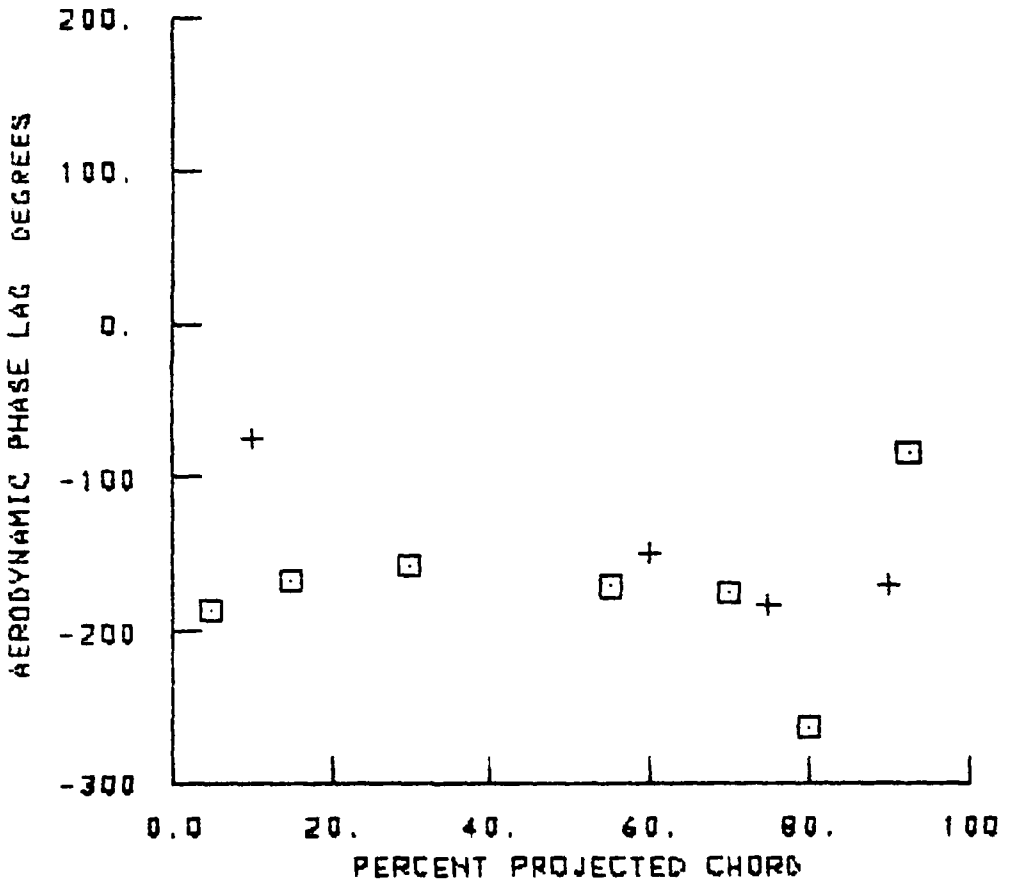

1 FEB., 1982

NORMALIZED SURFACE PRESSURE AMPLITUDES
1.8 TOTAL TO STATIC EXPANSION RATIO
45. DEGREES INTERBLADE PHASE ANGLE
\+ PRESSURE SURFACE
□ SUCTION SURFACE

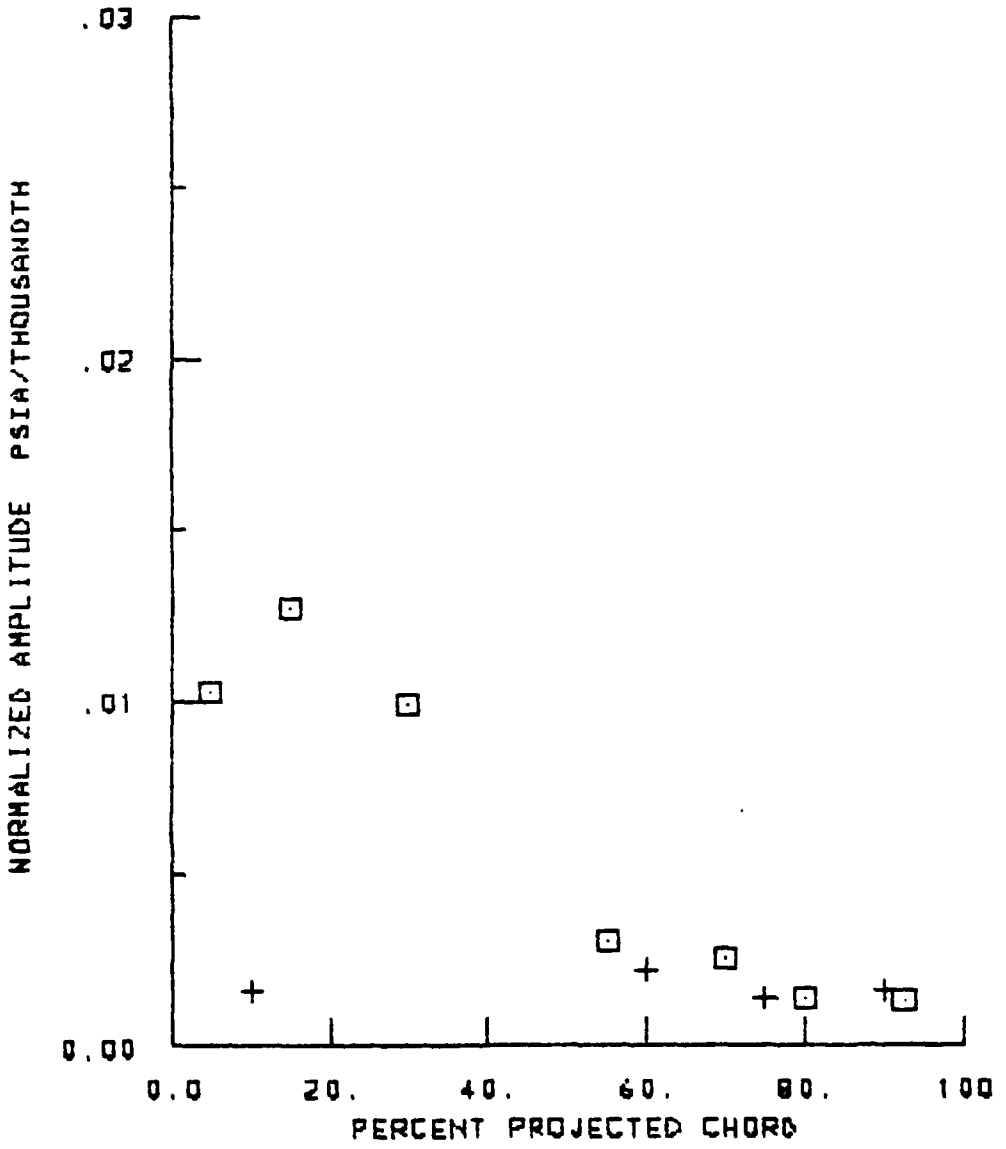

1 FEB., 1982

SURFACE PRESSURE PHASE LAGS
1.8 TOTAL TO STATIC EXPANSION RATIO
45. DEGREES INTERBLADE PHASE ANGLE
\+ PRESSURE SURFACE
□ SUCTION SURFACE

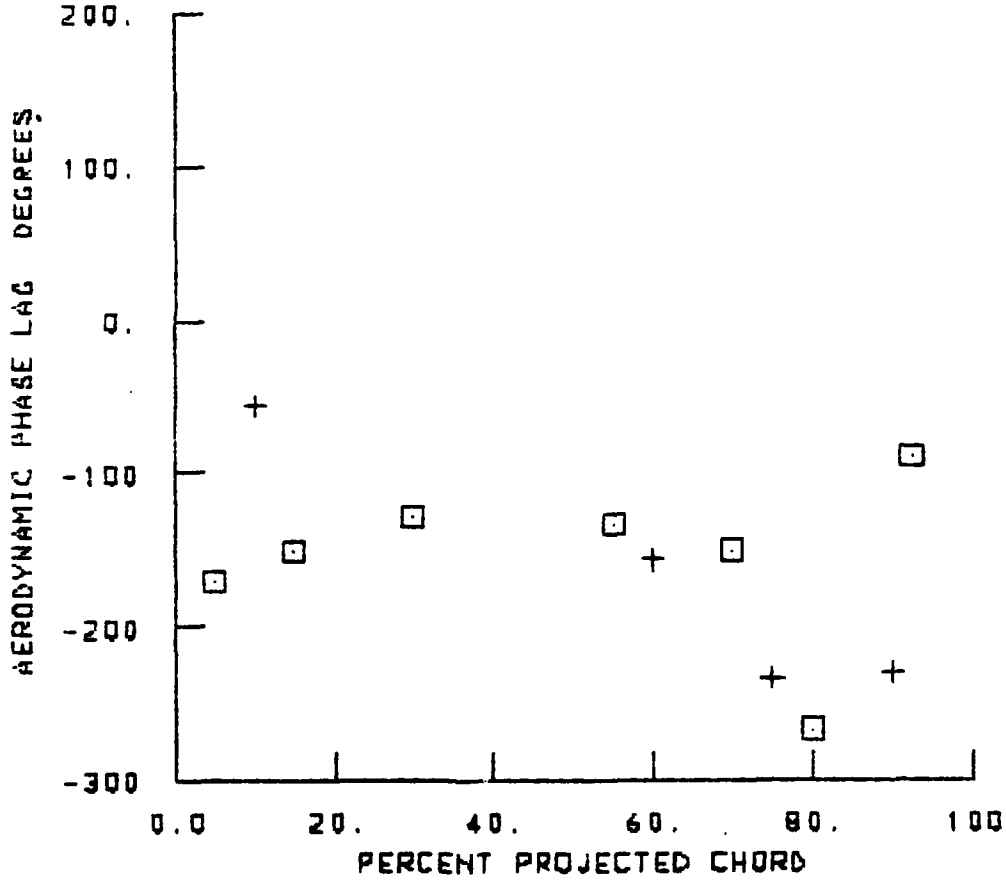

1 FEB., 1982

1.8 TOTAL TO STATIC EXPANSION RATIO
0. DEGREES INTERBLADE PHASE ANGLE
\+ PRESSURE SURFACE
□ SUCTION SURFACE

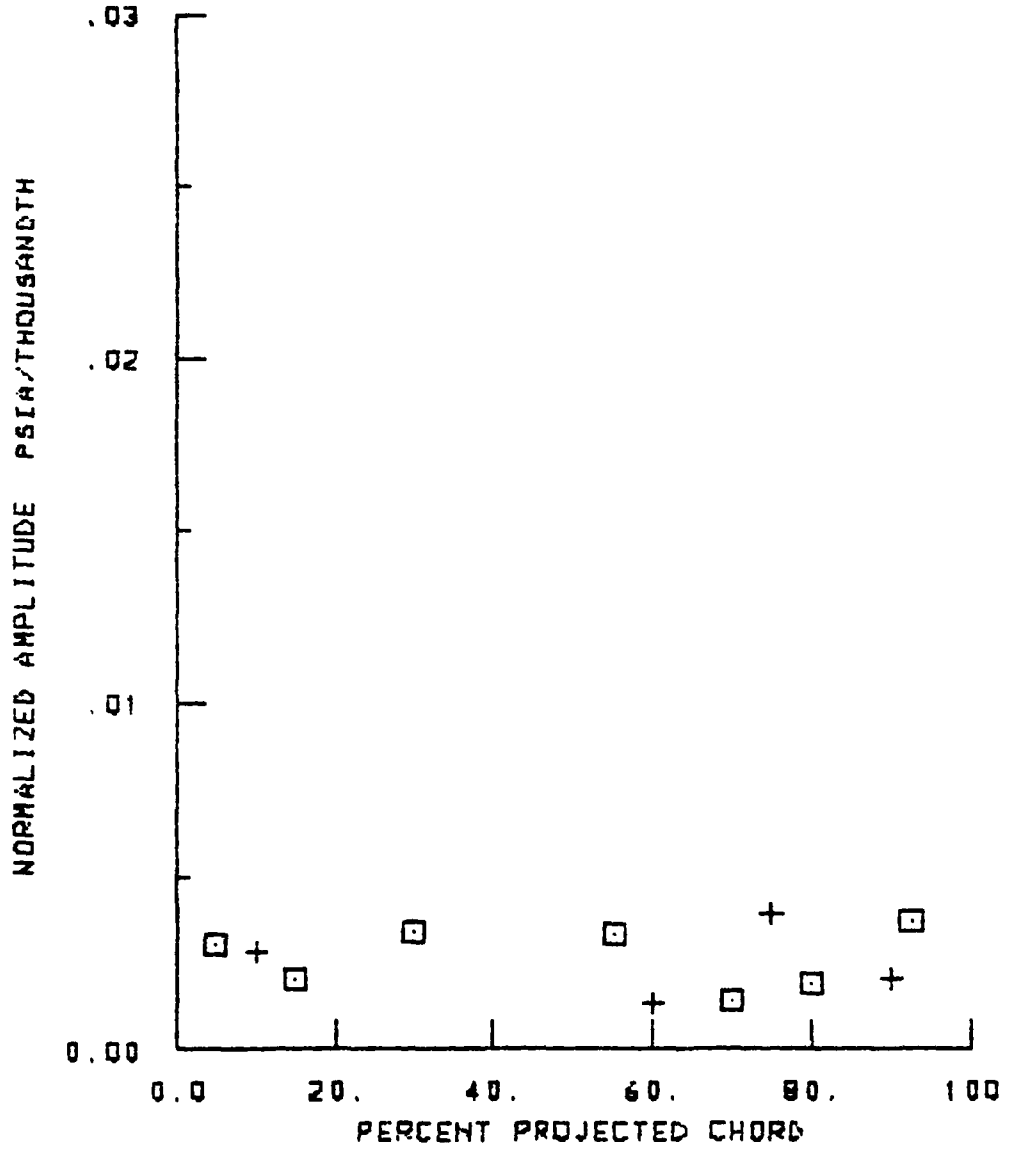

1 FEB., 1982

SURFACE PRESSURE PHASE LAGS
1.8 TOTAL TO STATIC EXPANSION RATIO
0. DEGREES INTERBLADE PHASE ANGLE
\+ PRESSURE SURFACE
□ SUCTION SURFACE

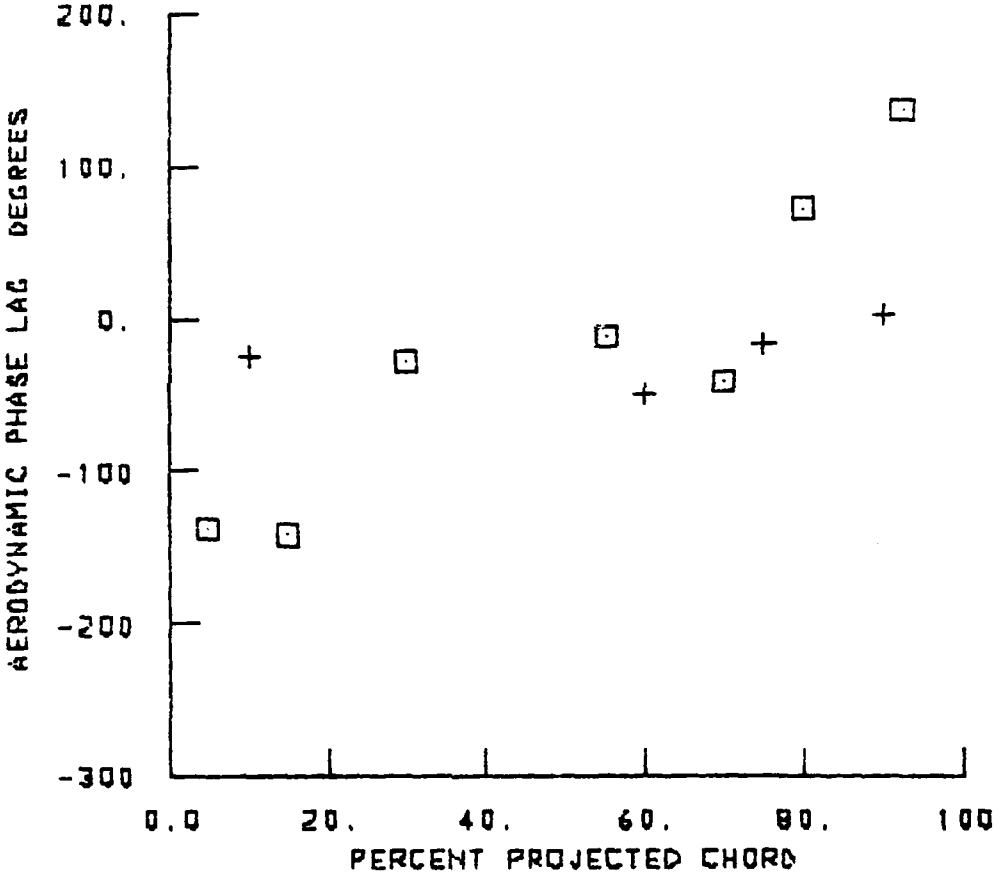

1 FEB., 1982

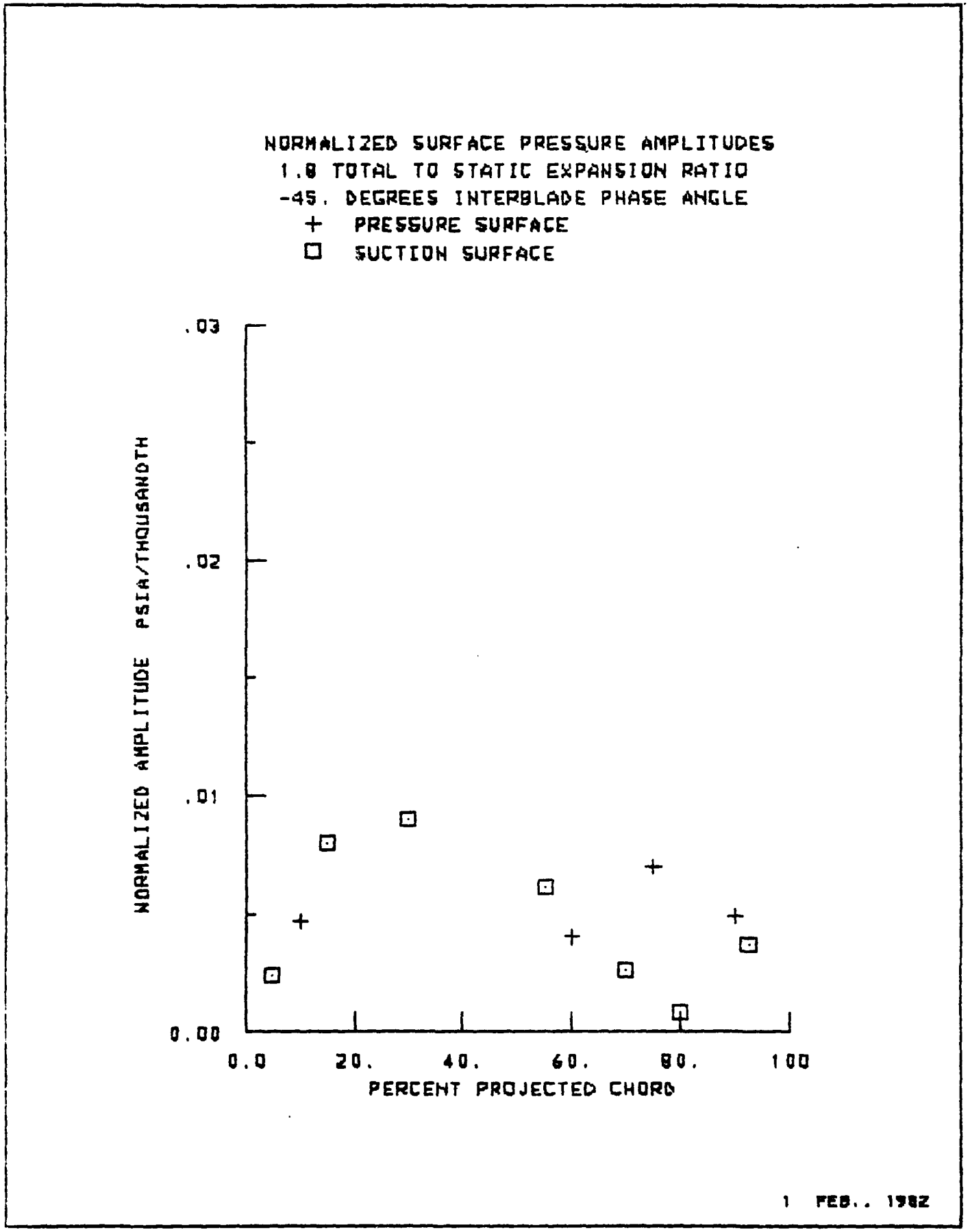
NORMALIZED SURFACE PRESSURE AMPLITUDES
1.8 TOTAL TO STATIC EXPANSION RATIO
-45. DEGREES INTERBLADE PHASE ANGLE
+ PRESSURE SURFACE
□ SUCTION SURFACE
.03
.02
.01
0.00
NORMALIZED AMPLITUDE PSIA/THOUSANDTH
0.0
20.
40.
60.
80.
100
PERCENT PROJECTED CHORD
1 FEB., 1982

SURFACE PRESSURE PHASE LAGS
1.8 TOTAL TO STATIC EXPANSION RATIO
-45. DEGREES INTERBLADE PHASE ANGLE
+ PRESSURE SURFACE
□ SUCTION SURFACE

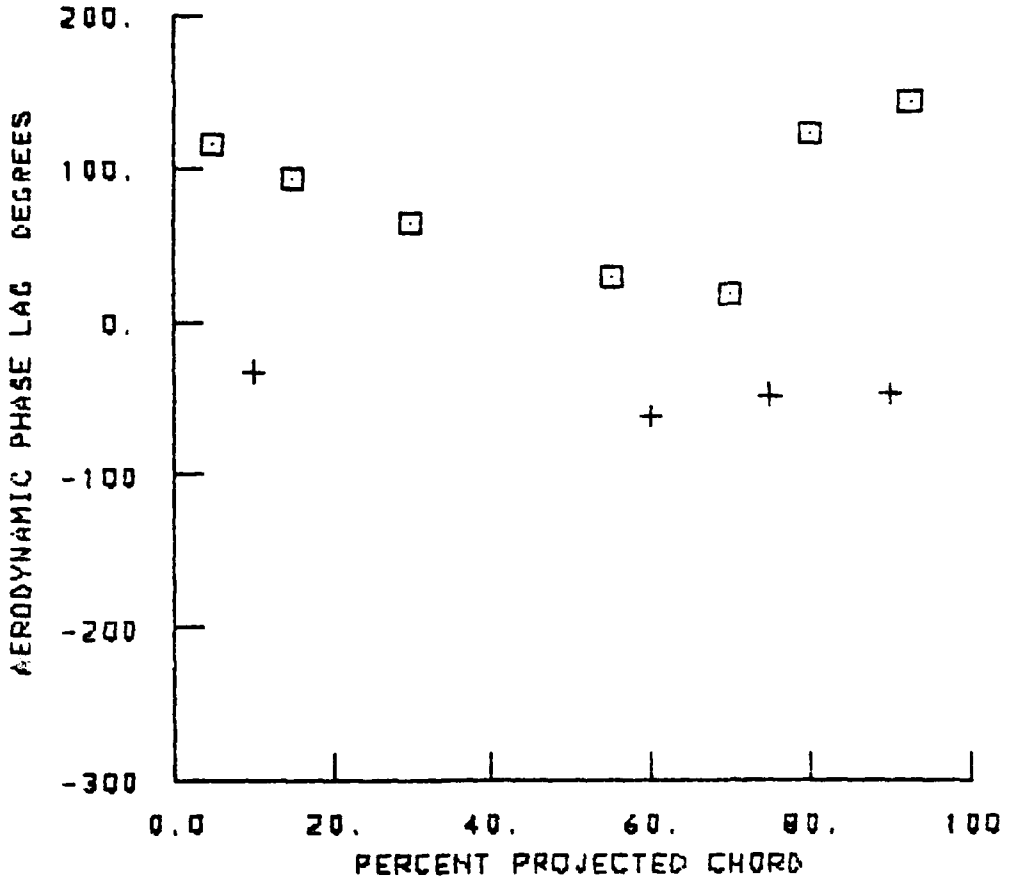

1 FEB., 1982

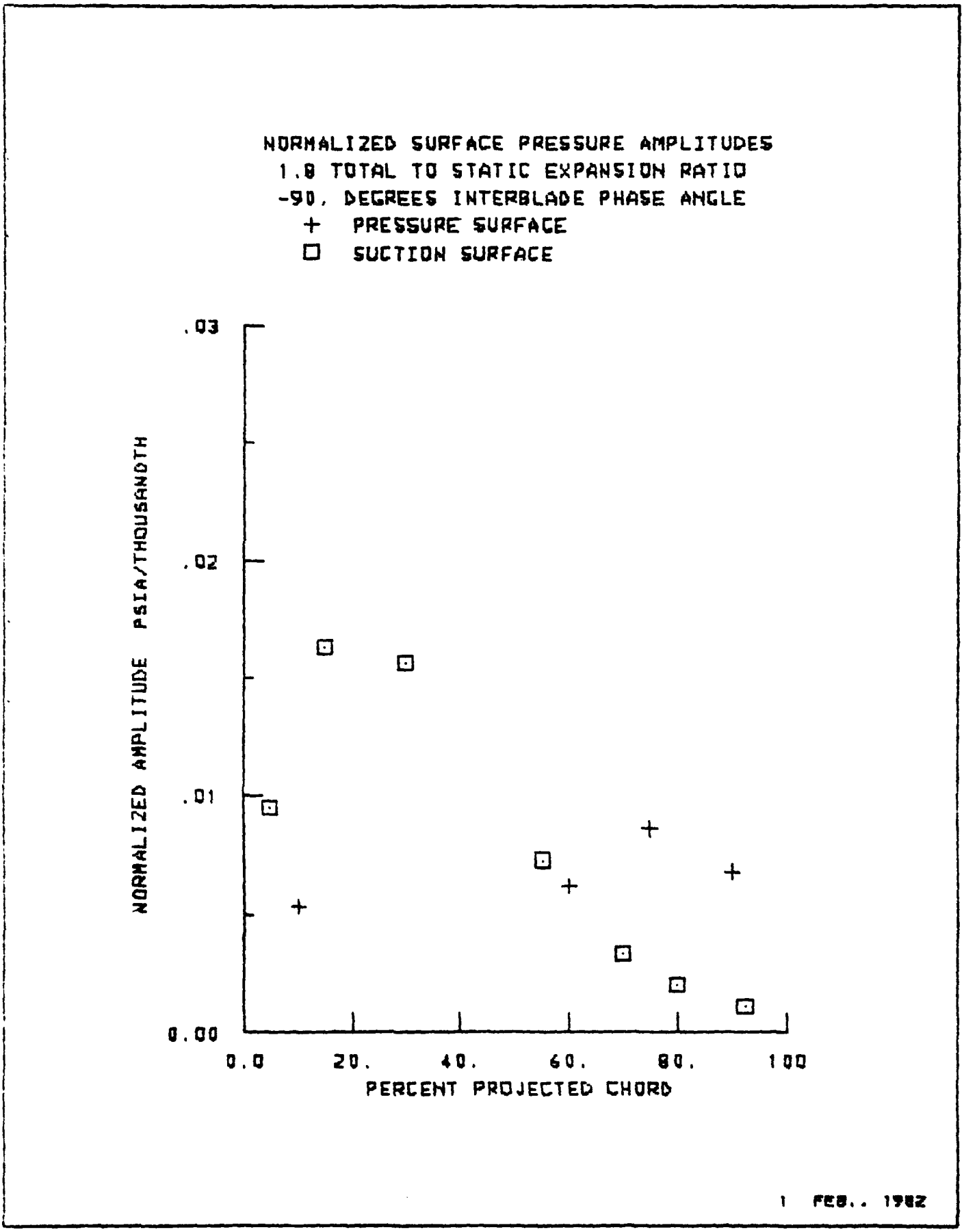
NORMALIZED SURFACE PRESSURE AMPLITUDES
1.8 TOTAL TO STATIC EXPANSION RATIO
-90. DEGREES INTERBLADE PHASE ANGLE
+ PRESSURE SURFACE
□ SUCTION SURFACE
NORMALIZED AMPLITUDE PSIA/THOUSANDTH
.03
.02
.01
0.00
0.0
20.
40.
60.
80.
100
PERCENT PROJECTED CHORD
1 FEB., 1982

SURFACE PRESSURE PHASE LAGS
1.8 TOTAL TO STATIC EXPANSION RATIO
-90. DEGREES INTERBLADE PHASE ANGLE
+ PRESSURE SURFACE
□ SUCTION SURFACE

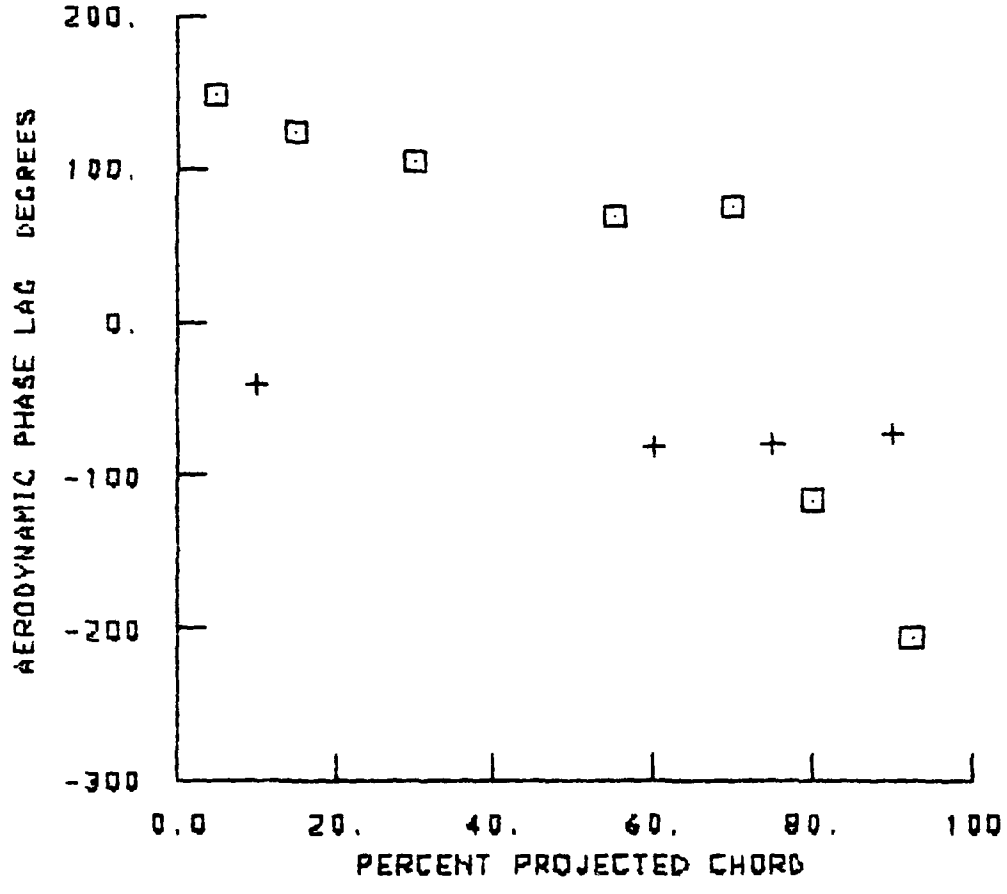

1 FEB., 1982

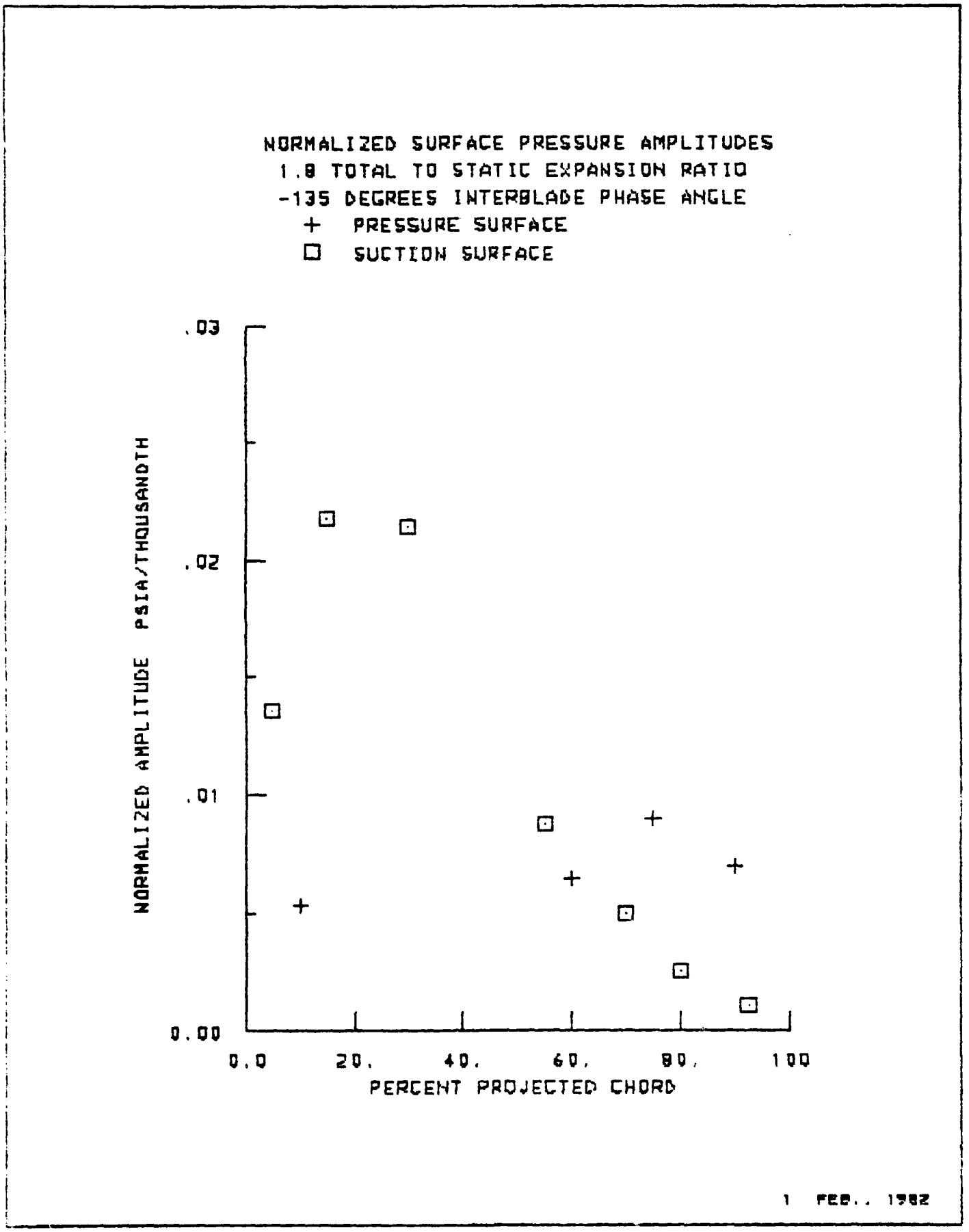
NORMALIZED SURFACE PRESSURE AMPLITUDES
1.8 TOTAL TO STATIC EXPANSION RATIO
-135 DEGREES INTERBLADE PHASE ANGLE
+ PRESSURE SURFACE
□ SUCTION SURFACE
.03
.02
.01
0.00
NORMALIZED AMPLITUDE PSIA/THOUSANDTH
0.0
20.
40.
60.
80.
100
PERCENT PROJECTED CHORD
1 FEB., 1982

SURFACE PRESSURE PHASE LAGS
1.8 TOTAL TO STATIC EXPANSION RATIO
-135 DEGREES INTERBLADE PHASE ANGLE
\+ PRESSURE SURFACE
□ SUCTION SURFACE

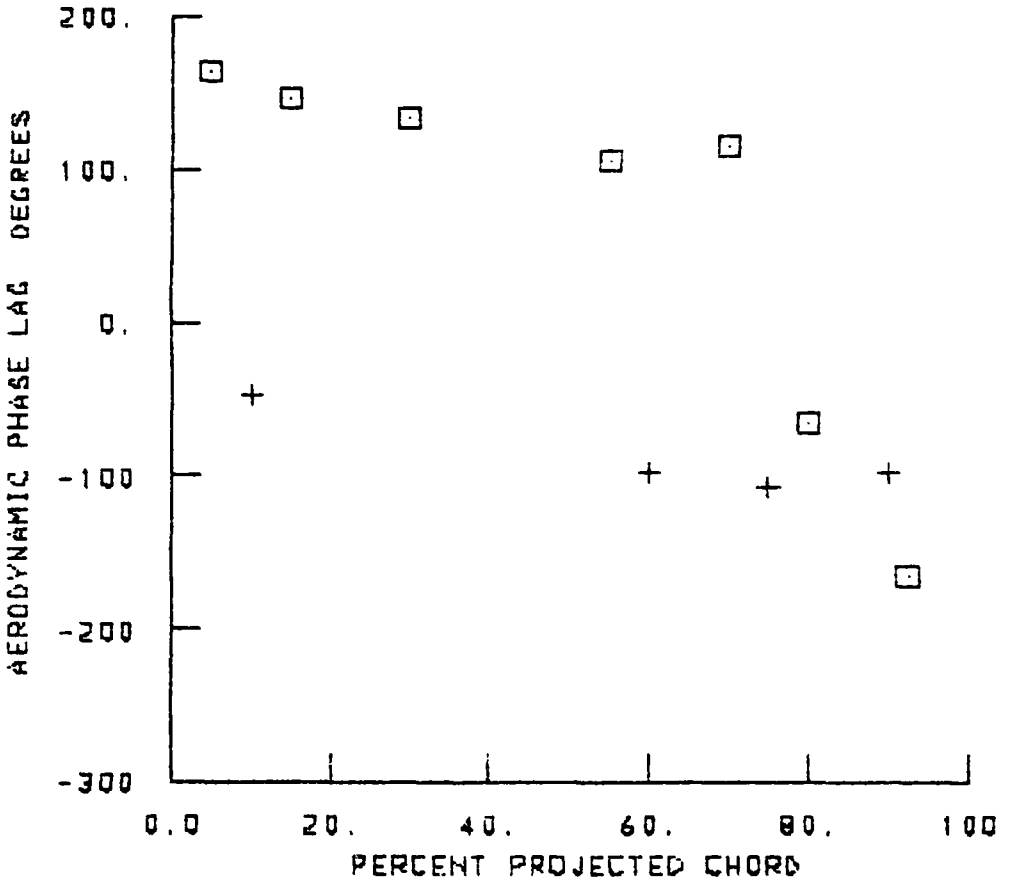

1 FEB., 1982

AD-A118 884 GENERAL MOTORS CORP INDIANAPOLIS IN DETROIT DIESEL A--ETC F/G 21/5
TIME-VARIANT AERODYNAMICS FOR TRANSLATIONAL MOTION OF LARGE-TUR--ETC(U)
FEB 82 R L JAY, M J GRITTON, M D ROTHROCK N00019-80-C-0430

UNCLASSIFIED NL

2 - 2

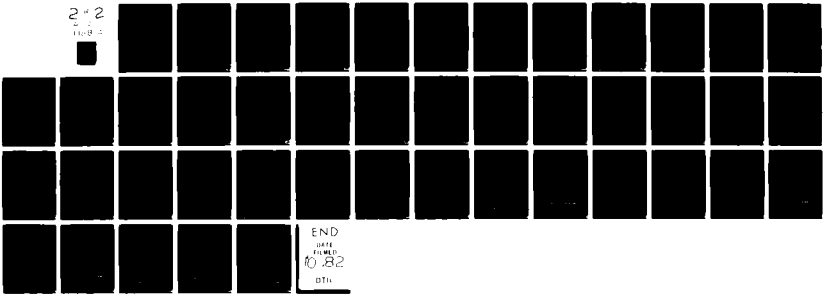

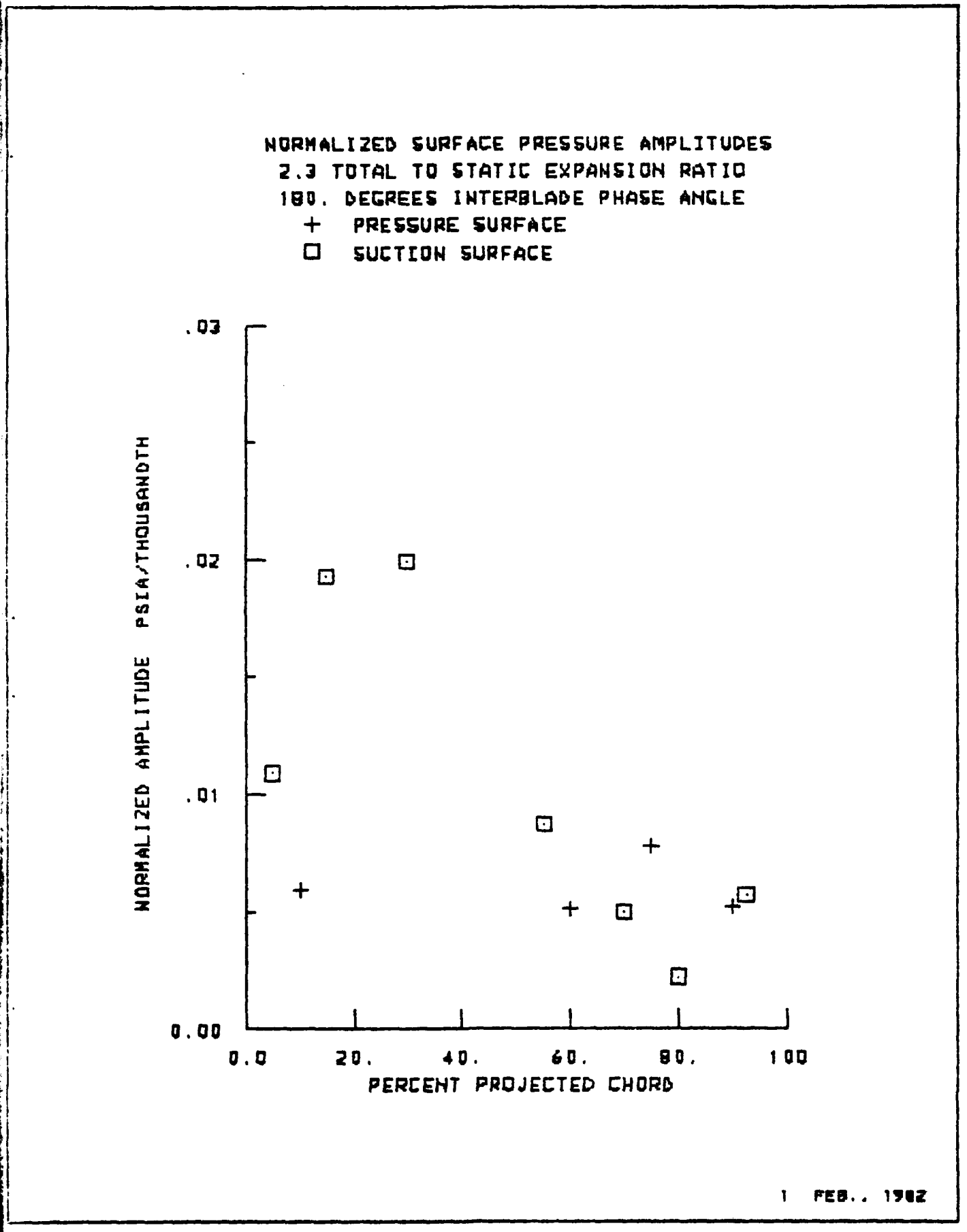
NORMALIZED SURFACE PRESSURE AMPLITUDES
2.3 TOTAL TO STATIC EXPANSION RATIO
180. DEGREES INTERBLADE PHASE ANGLE
+ PRESSURE SURFACE
□ SUCTION SURFACE
.03
.02
.01
0.00
NORMALIZED AMPLITUDE PSIA/THOUSANDTH
0.0
20.
40.
60.
80.
100
PERCENT PROJECTED CHORD
1 FEB., 1982

SURFACE PRESSURE PHASE LAGS
2.3 TOTAL TO STATIC EXPANSION RATIO
180. DEGREES INTERBLADE PHASE ANGLE
+ PRESSURE SURFACE
□ SUCTION SURFACE

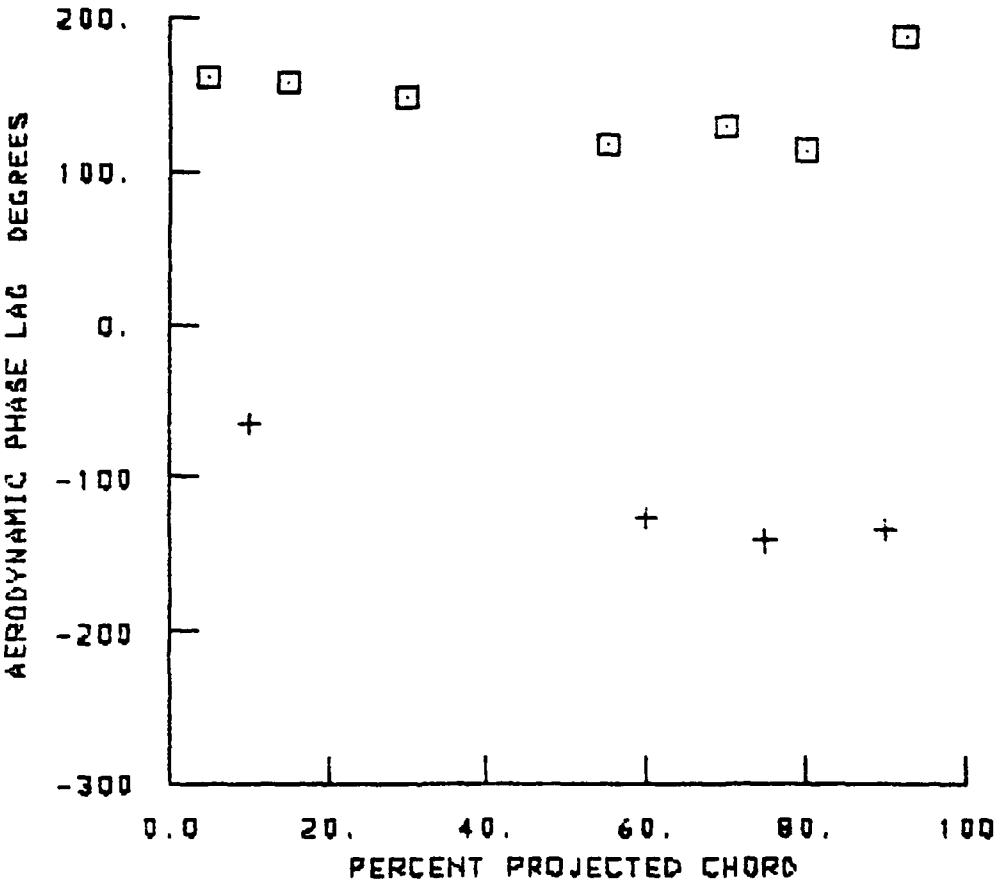

1 FEB., 1982

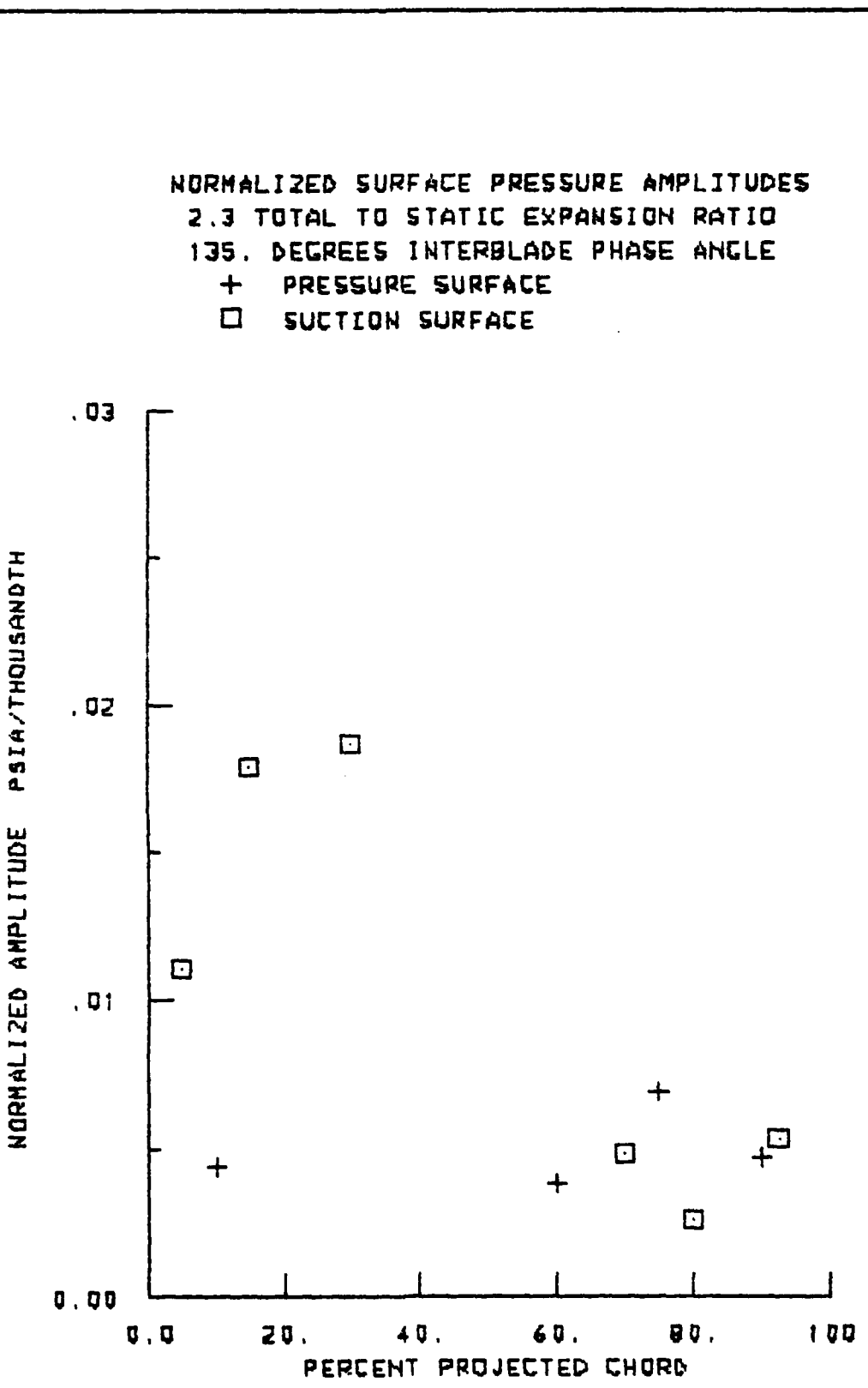
NORMALIZED SURFACE PRESSURE AMPLITUDES
2.3 TOTAL TO STATIC EXPANSION RATIO
135. DEGREES INTERBLADE PHASE ANGLE
+ PRESSURE SURFACE
□ SUCTION SURFACE
.03
.02
.01
0.00
NORMALIZED AMPLITUDE PSIA/THOUSANDTH
0.0
20.
40.
60.
80.
100
PERCENT PROJECTED CHORD
1 FEB., 1982

SURFACE PRESSURE PHASE LAGS
2.3 TOTAL TO STATIC EXPANSION RATIO
135. DEGREES INTERBLADE PHASE ANGLE
+ PRESSURE SURFACE
□ SUCTION SURFACE

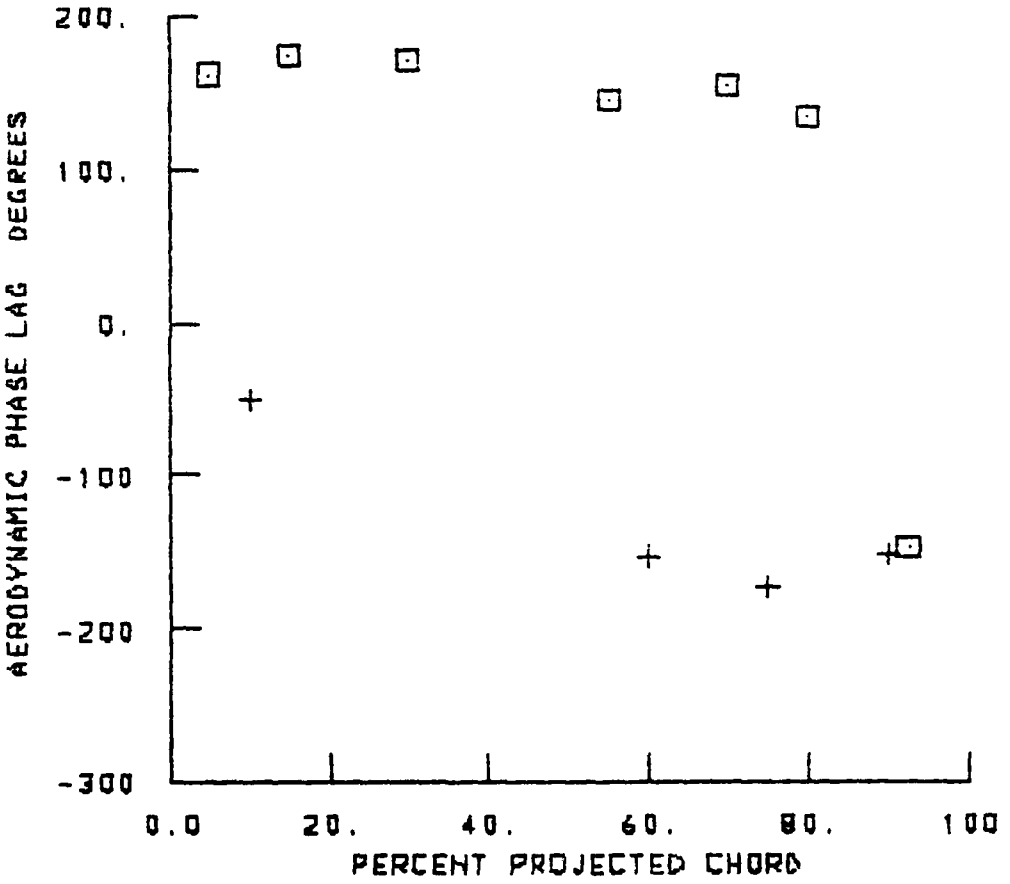

1 FEB., 1982

NORMALIZED SURFACE PRESSURE AMPLITUDES
2.3 TOTAL TO STATIC EXPANSION RATIO
90. DEGREES INTERBLADE PHASE ANGLE
+ PRESSURE SURFACE
□ SUCTION SURFACE

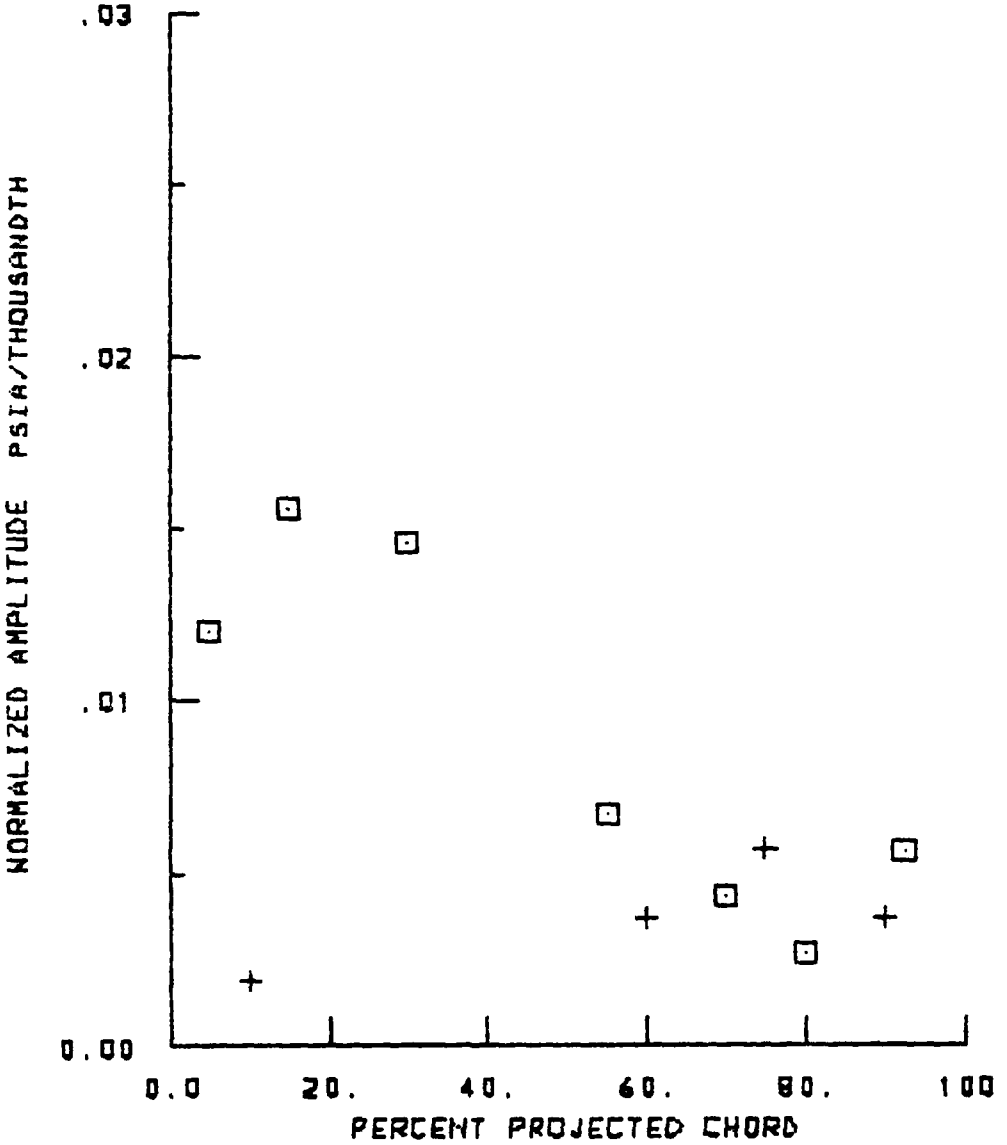

1 FEB., 1982

SURFACE PRESSURE PHASE LAGS
2.3 TOTAL TO STATIC EXPANSION RATIO
90. DEGREES INTERBLADE PHASE ANGLE
+ PRESSURE SURFACE
□ SUCTION SURFACE

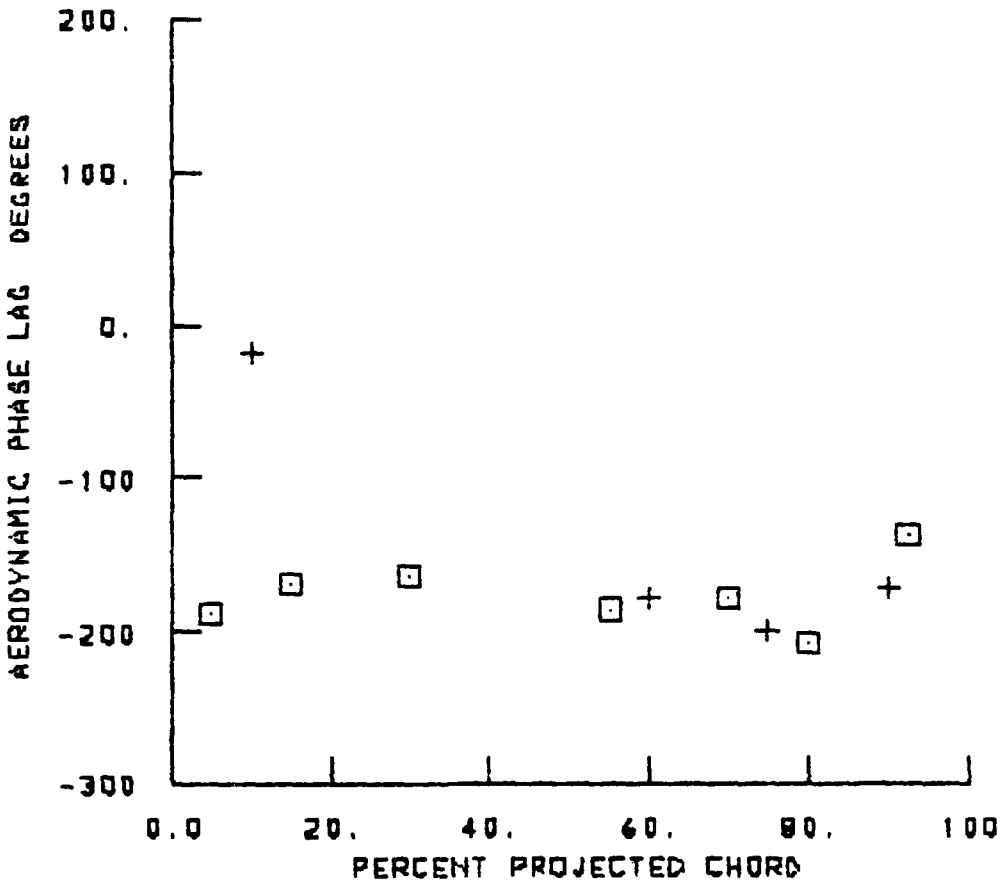

1 FEB., 1982

NORMALIZED SURFACE PPESSURE AMPLITUDES
2.3 TOTAL TO STATIC EXPANSION RATIO
45. DEGREES INTERBLADE PHASE ANGLE
+ PRESSURE SURFACE
□ SUCTION SURFACE

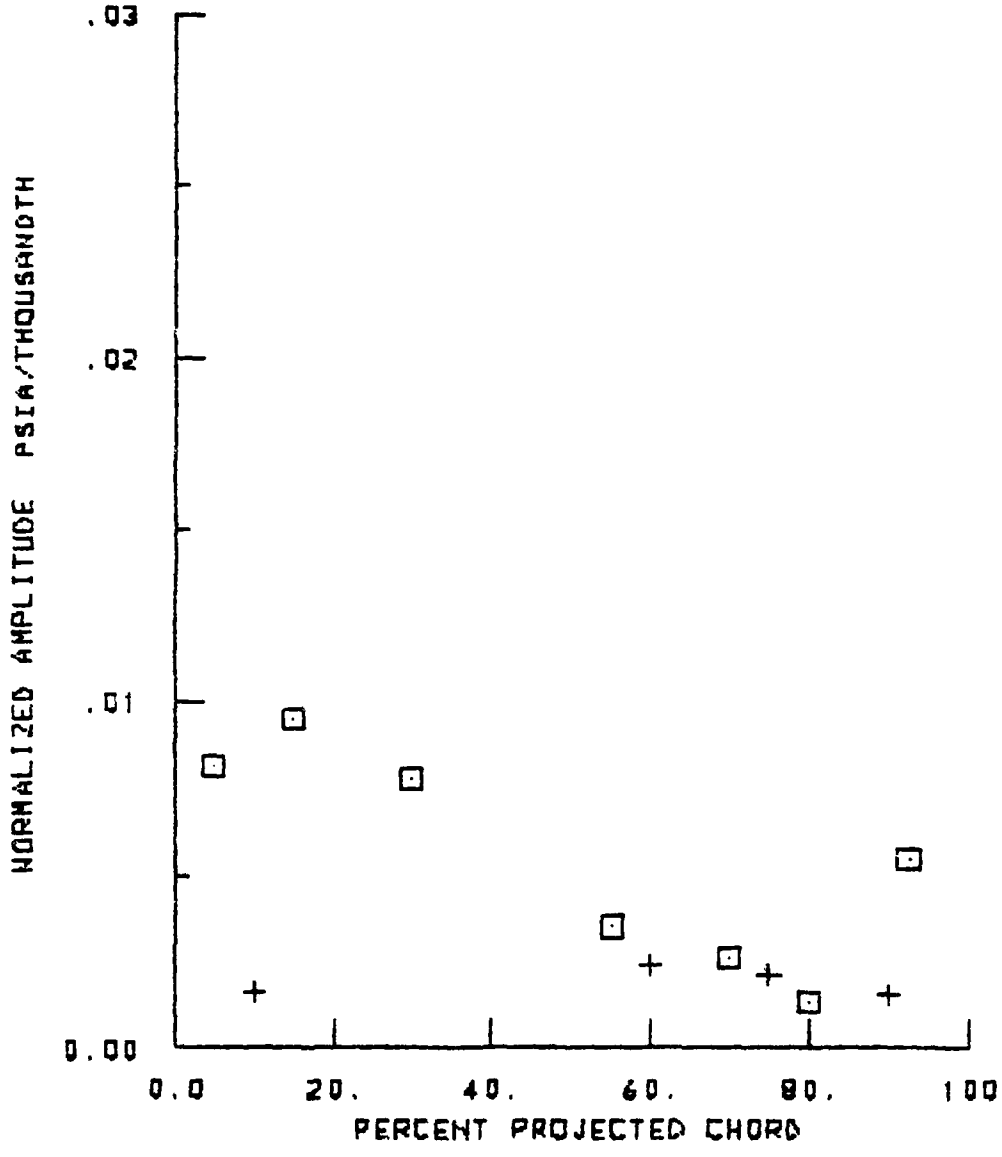

1 FEB., 1982

SURFACE PRESSURE PHASE LAGS
2.3 TOTAL TO STATIC EXPANSION RATIO
45. DEGREES INTERBLADE PHASE ANGLE
+ PRESSURE SURFACE
□ SUCTION SURFACE

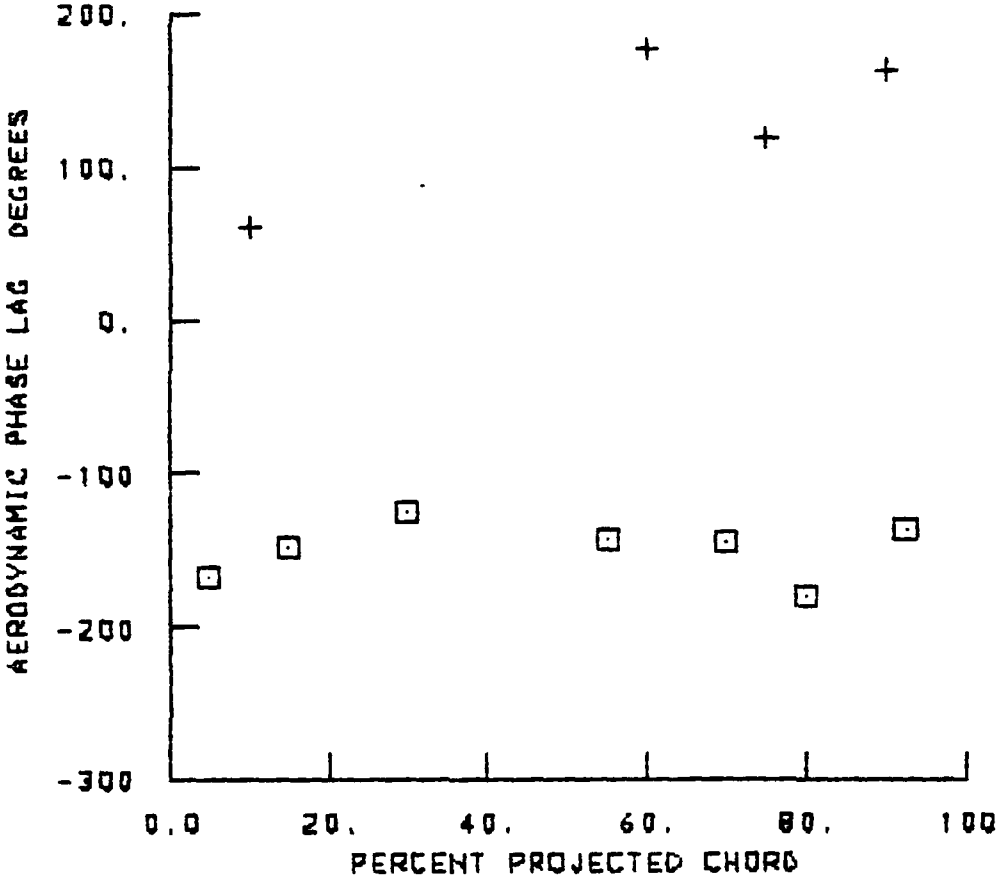

1 FEB., 1982

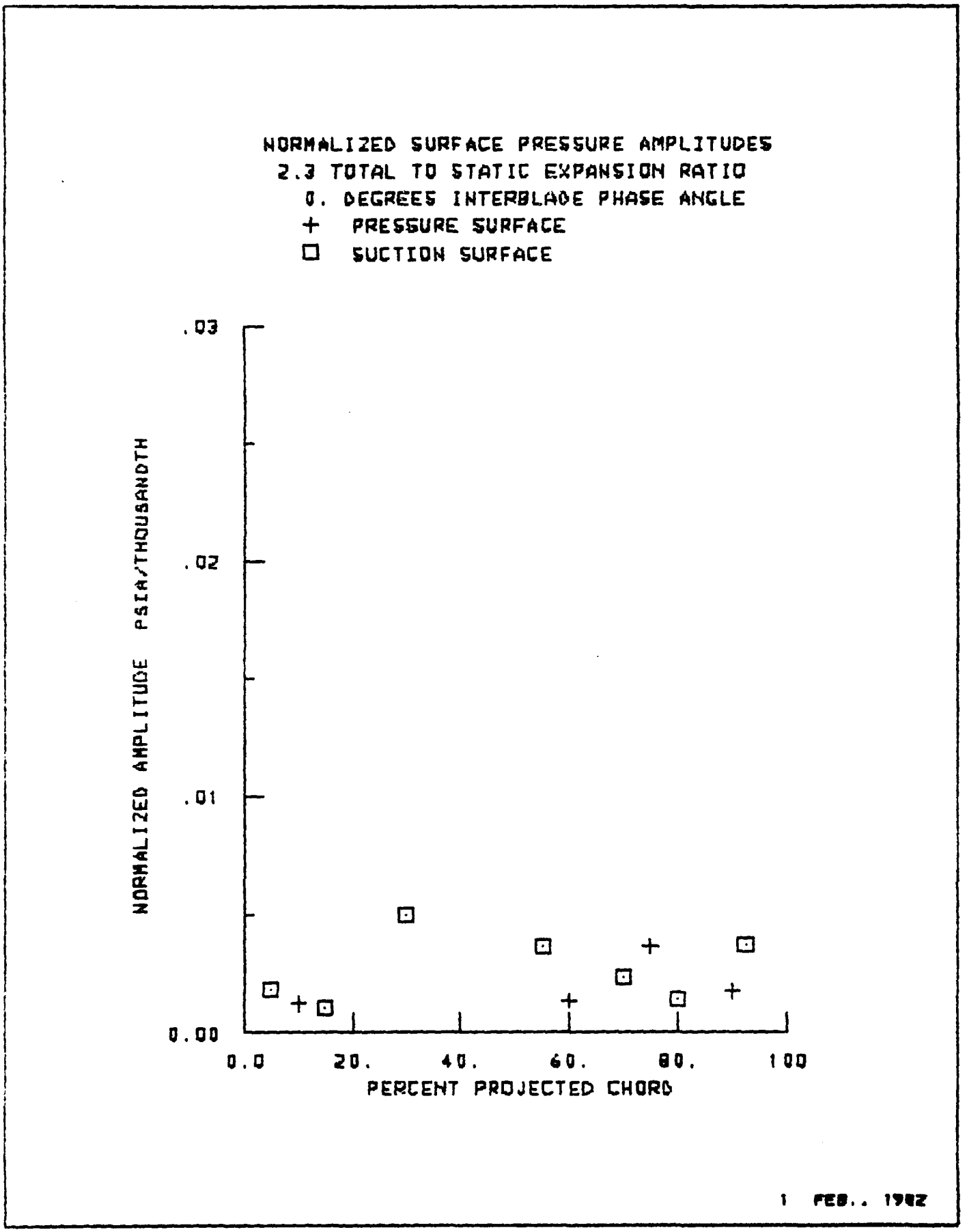
NORMALIZED SURFACE PRESSURE AMPLITUDES
2.3 TOTAL TO STATIC EXPANSION RATIO
0. DEGREES INTERBLADE PHASE ANGLE
+ PRESSURE SURFACE
□ SUCTION SURFACE
.03
.02
.01
0.00
NORMALIZED AMPLITUDE PSIA/THOUSANDTH
0.0
20.
40.
60.
80.
100
PERCENT PROJECTED CHORD
1 FEB., 1982

SURFACE PRESSURE PHASE LAGS
2.3 TOTAL TO STATIC EXPANSION RATIO
0. DEGREES INTERBLADE PHASE ANGLE
\+ PRESSURE SURFACE
□ SUCTION SURFACE

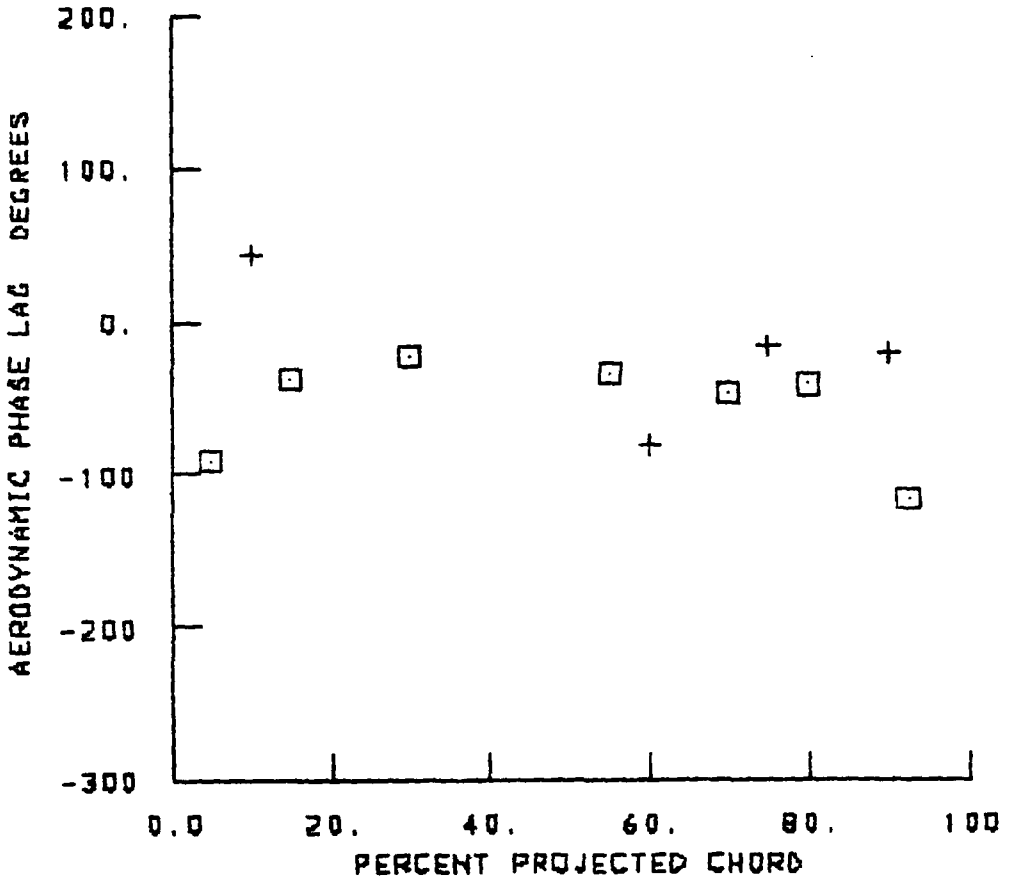

1 FEB., 1982

NORMALIZED SURFACE PRESSURE AMPLITUDES
2.3 TOTAL TO STATIC EXPANSION RATIO
-45. DEGREES INTERBLADE PHASE ANGLE
+ PRESSURE SURFACE
□ SUCTION SURFACE

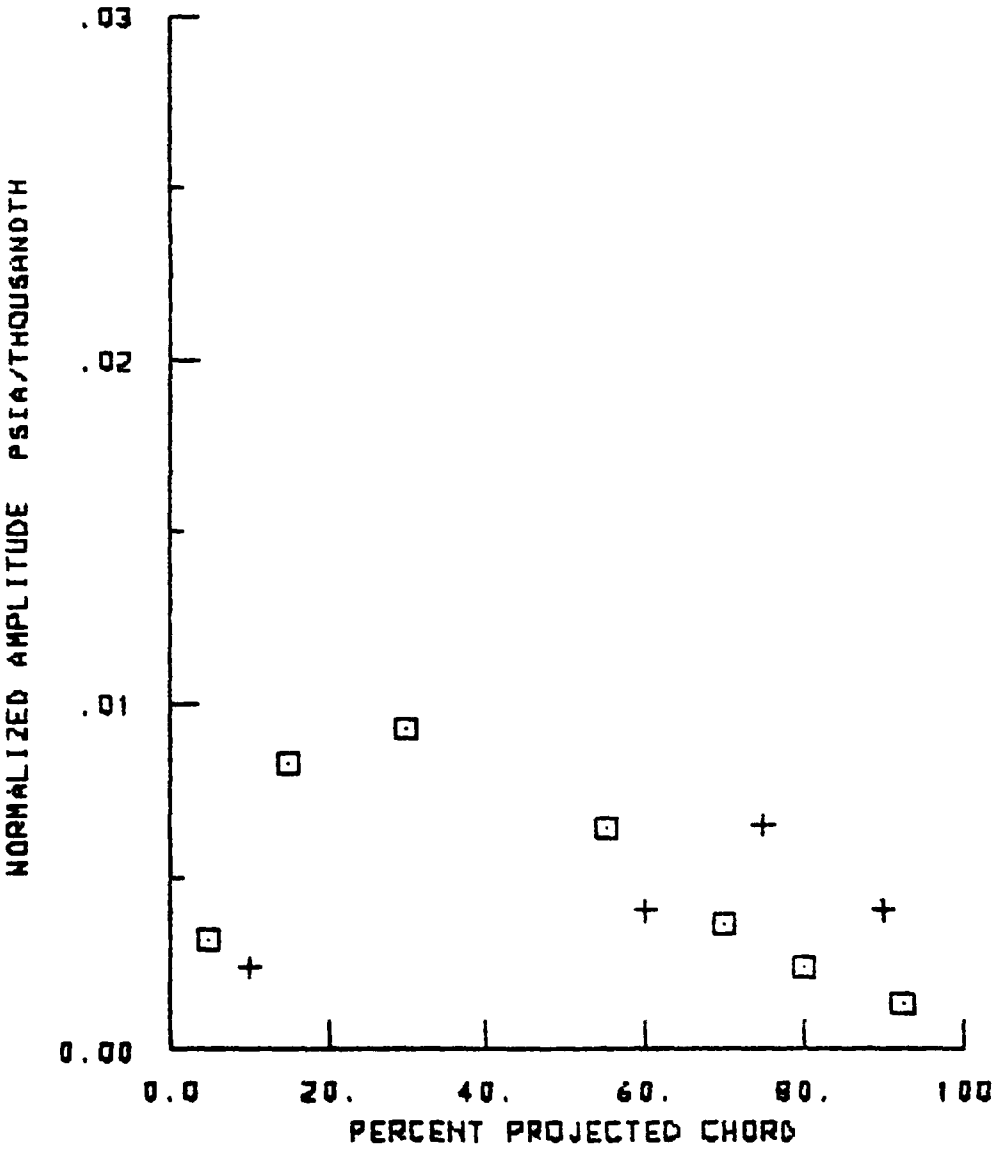

1 FEB., 1982

SURFACE PRESSURE PHASE LAGS
2.3 TOTAL TO STATIC EXPANSION RATIO
-45. DEGREES INTERBLADE PHASE ANGLE
+ PRESSURE SURFACE
□ SUCTION SURFACE

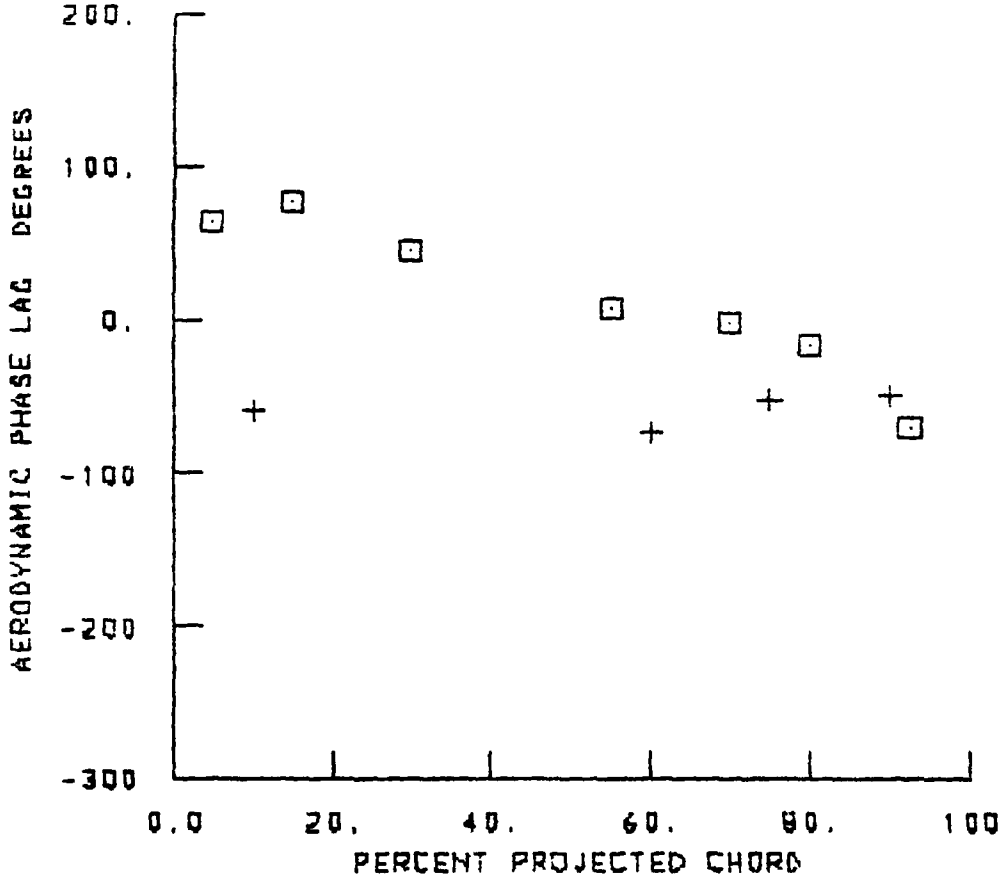

1 FEB., 1982

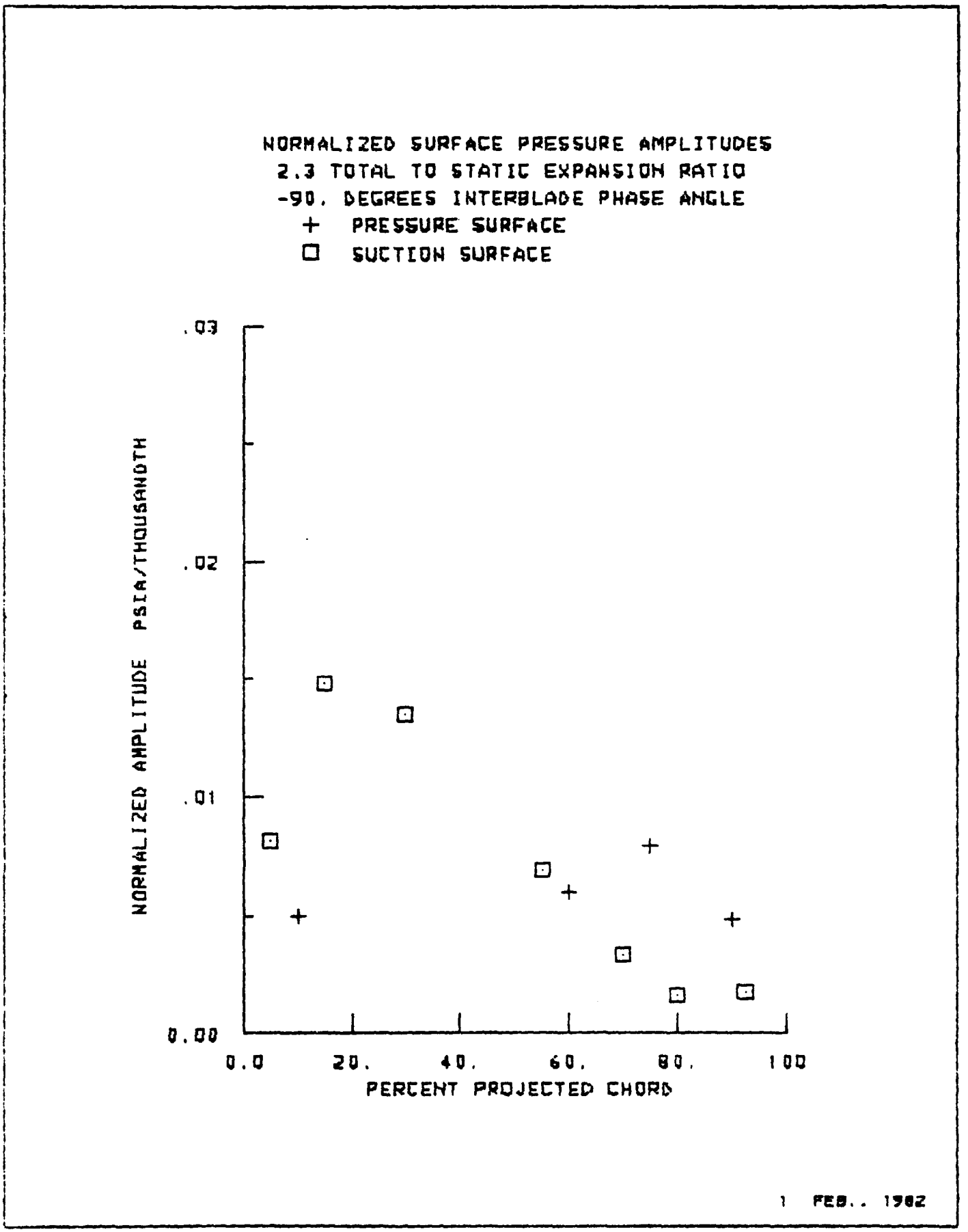
NORMALIZED SURFACE PRESSURE AMPLITUDES
2.3 TOTAL TO STATIC EXPANSION RATIO
-90. DEGREES INTERBLADE PHASE ANGLE
+ PRESSURE SURFACE
□ SUCTION SURFACE
.03
.02
.01
0.00
NORMALIZED AMPLITUDE PSIA/THOUSANDTH
0.0
20.
40.
60.
80.
100
PERCENT PROJECTED CHORD
1 FEB., 1982

SURFACE PRESSURE PHASE LAGS
2.3 TOTAL TO STATIC EXPANSION RATIO
-90. DEGREES INTERBLADE PHASE ANGLE
+ PRESSURE SURFACE
□ SUCTION SURFACE

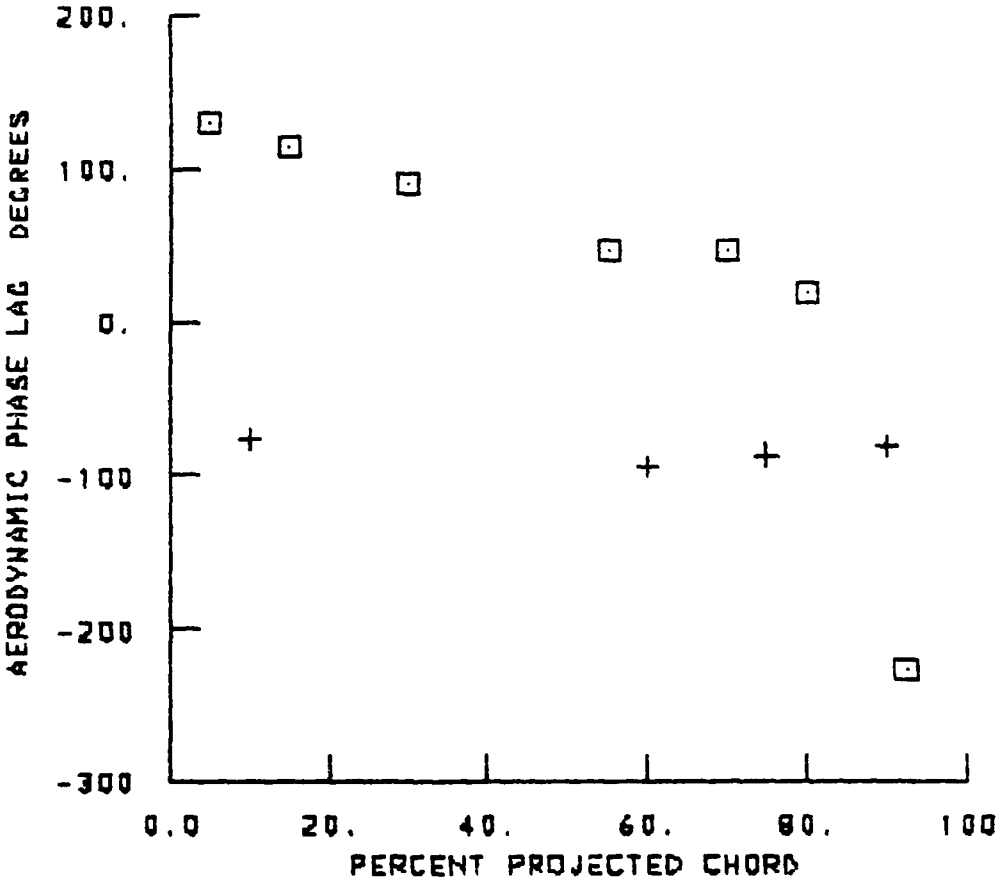

1 FEB., 1982

NORMALIZED SURFACE PRESSURE AMPLITUDES
2.3 TOTAL TO STATIC EXPANSION RATIO
-135 DEGREES INTERBLADE PHASE ANGLE
+ PRESSURE SURFACE
□ SUCTION SURFACE

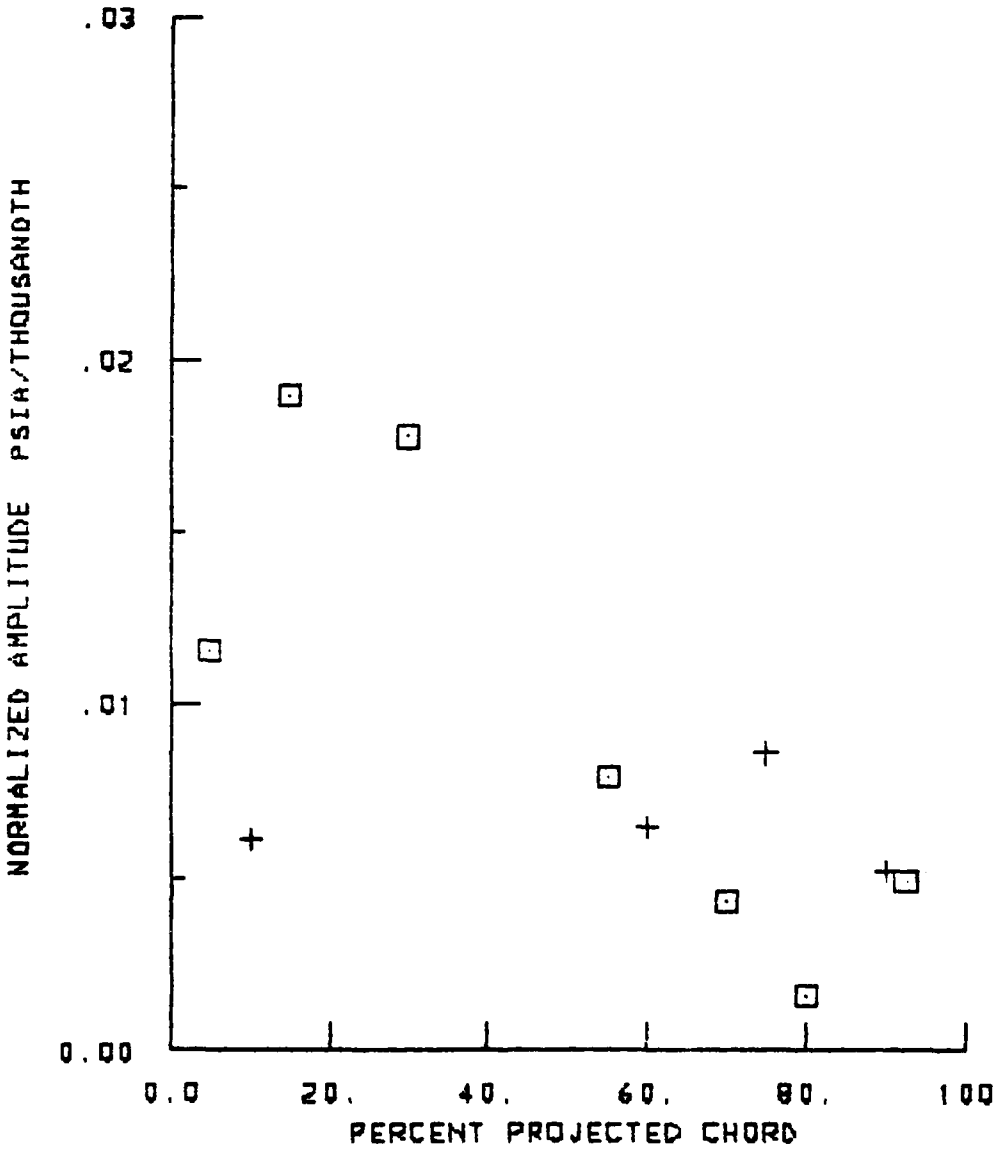

1 FEB., 1982

SURFACE PRESSURE PHASE LAGS
2.3 TOTAL TO STATIC EXPANSION RATIO
-135 DEGREES INTERBLADE PHASE ANGLE
+ PRESSURE SURFACE
□ SUCTION SURFACE

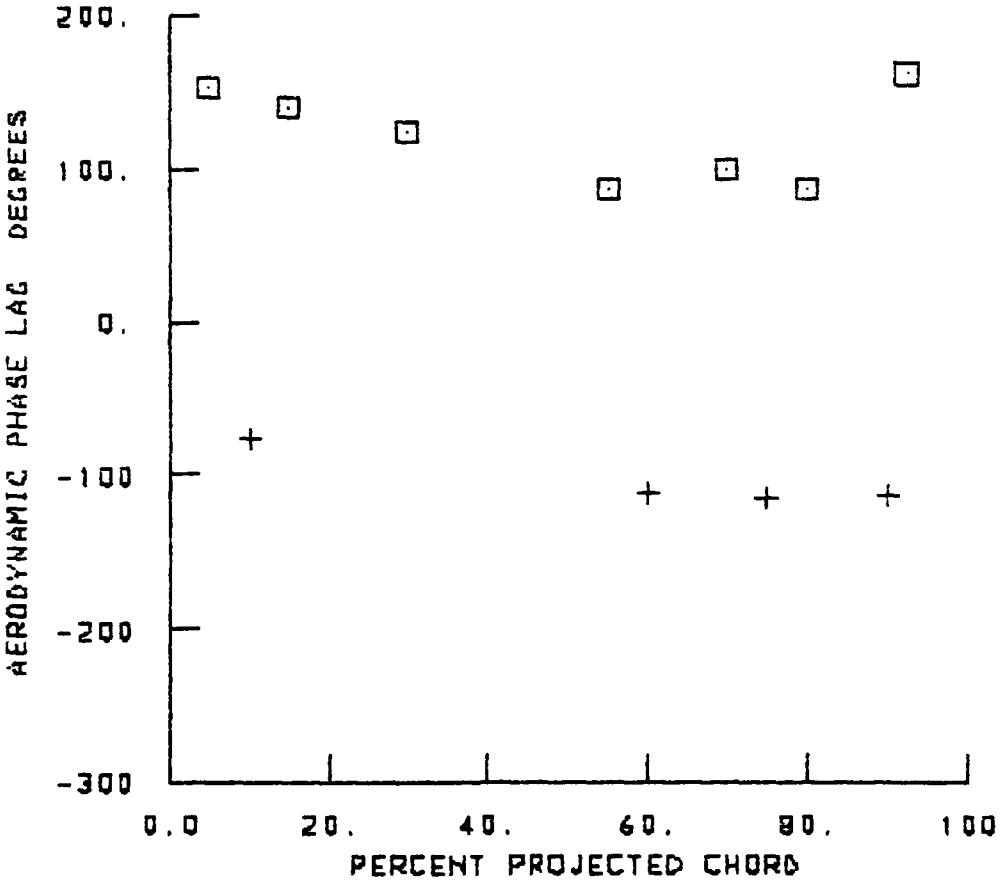

1 FEB., 1982

NORMALIZED SURFACE PRESSURE AMPLITUDES
2.8 TOTAL TO STATIC EXPANSION RATIO
180. DEGREES INTERBLADE PHASE ANGLE
+ PRESSURE SURFACE
□ SUCTION SURFACE

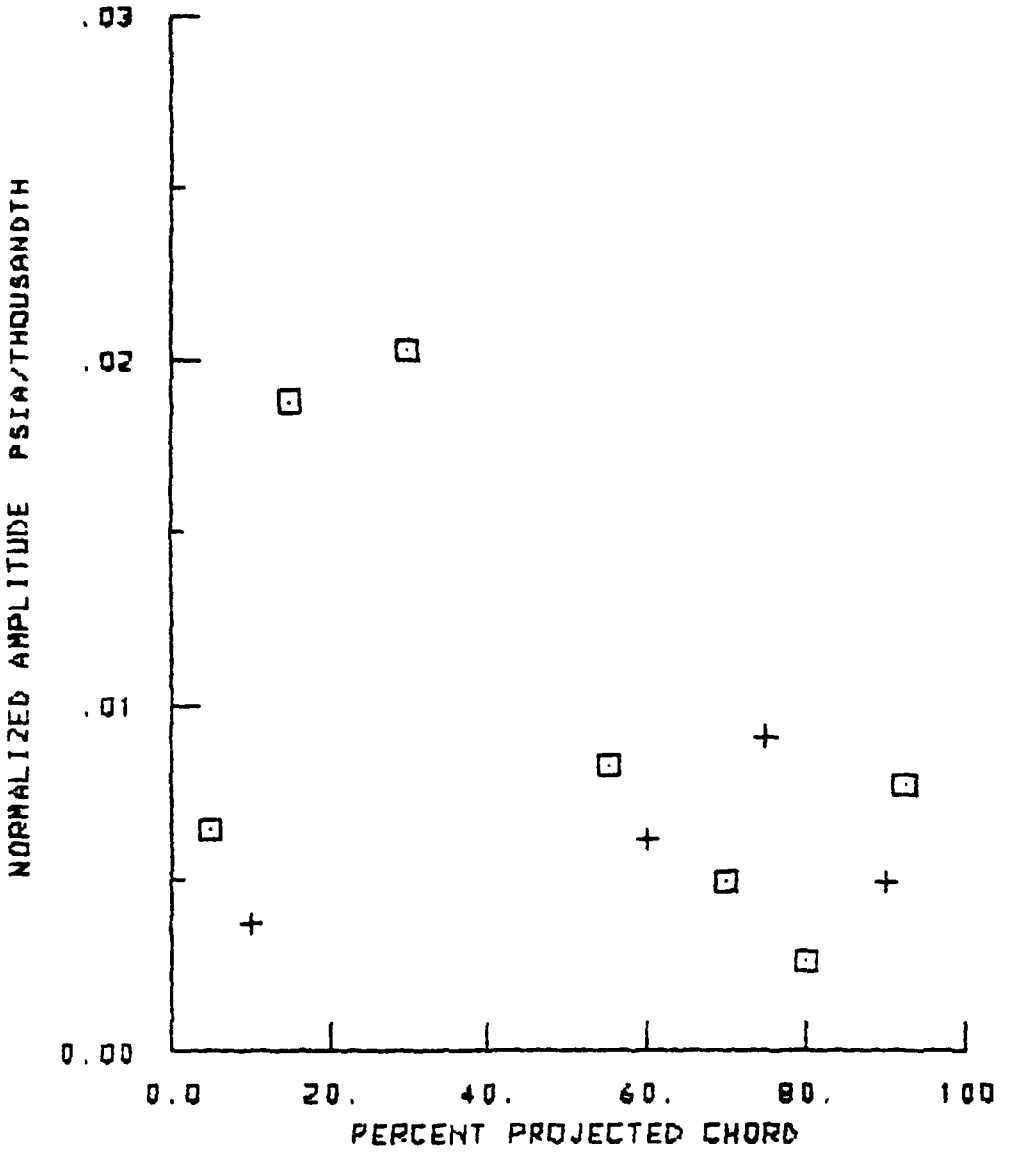

1 FEB., 1982

SURFACE PRESSURE PHASE LAGS
2.8 TOTAL TO STATIC EXPANSION RATIO
180. DEGREES INTERBLADE PHASE ANGLE
+ PRESSURE SURFACE
□ SUCTION SURFACE

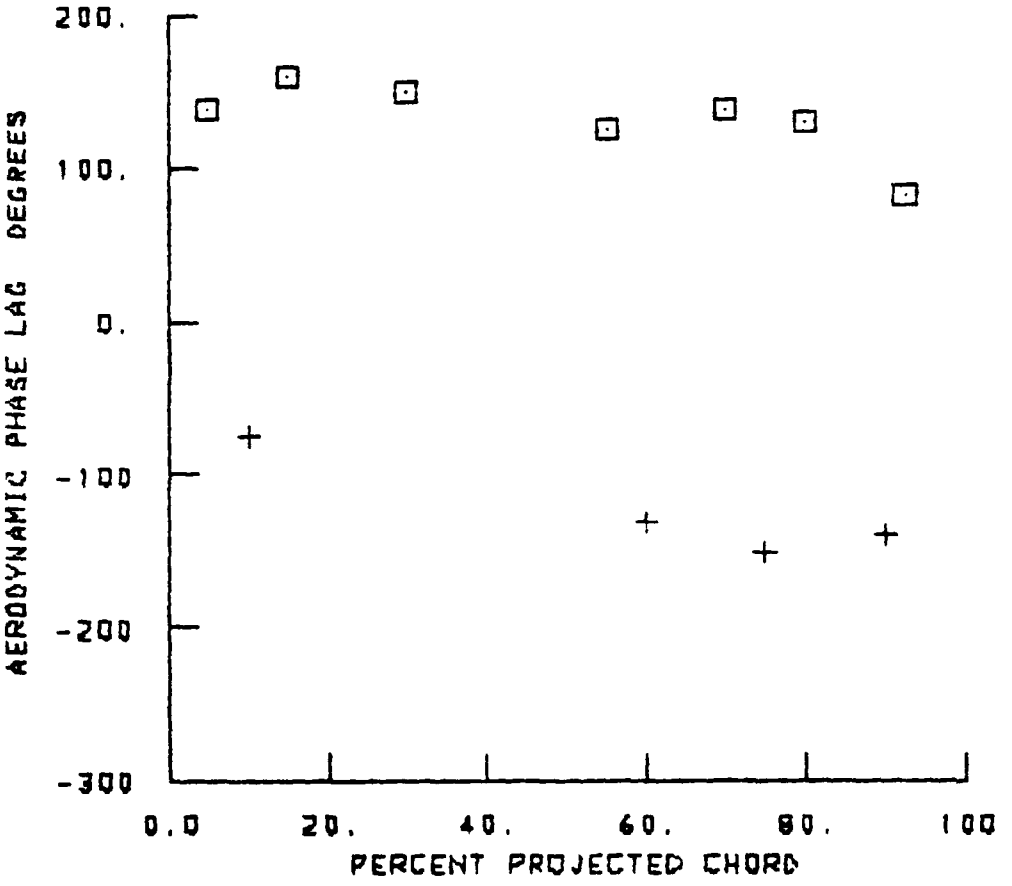

1 FEB., 1982

NORMALIZED SURFACE PRESSURE AMPLITUDES
2.8 TOTAL TO STATIC EXPANSION RATIO
135. DEGREES INTERBLADE PHASE ANGLE
+ PRESSURE SURFACE
□ SUCTION SURFACE

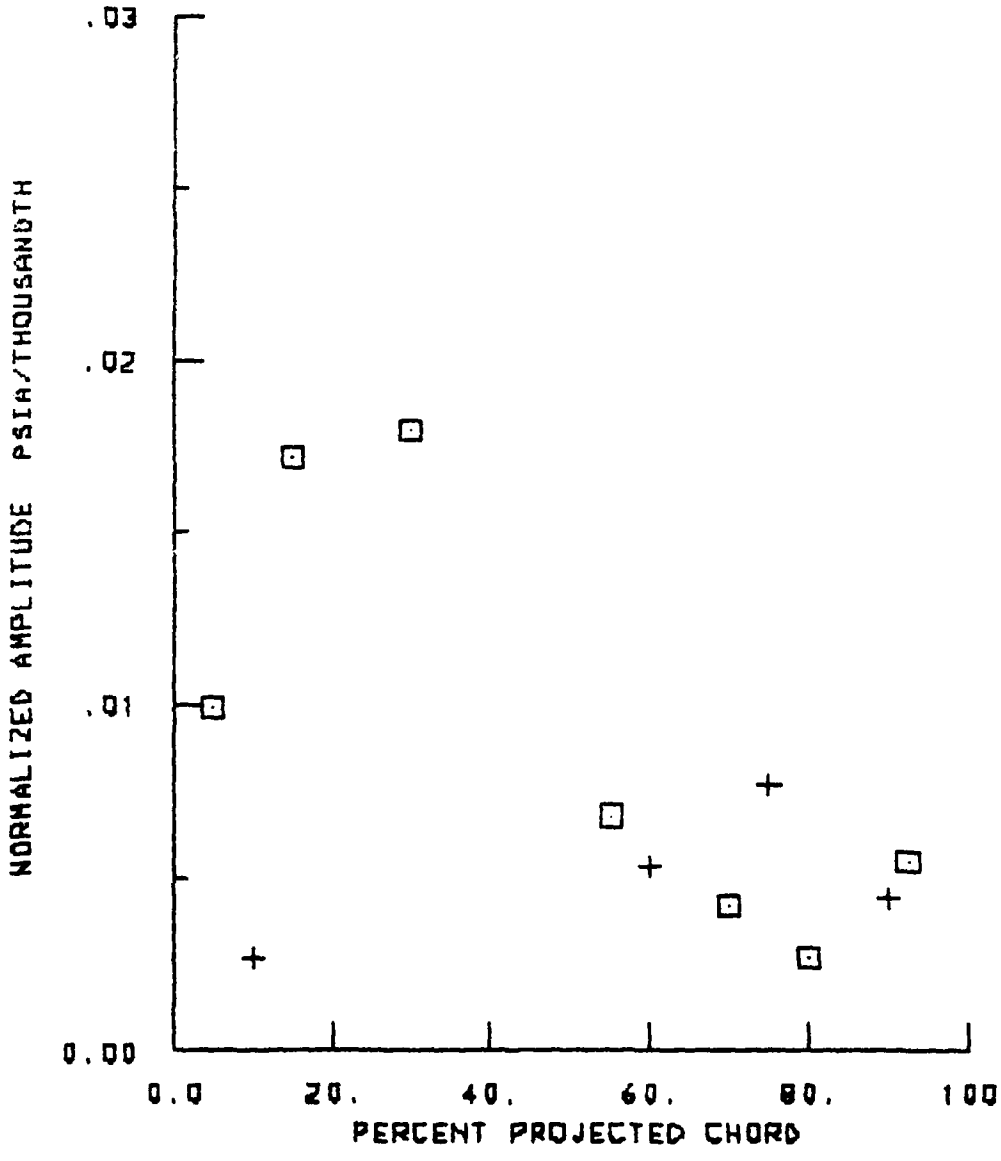

1 FEB., 1982

SURFACE PRESSURE PHASE LAGS
2.0 TOTAL TO STATIC EXPANSION RATIO
135. DEGREES INTERBLADE PHASE ANGLE
+ PRESSURE SURFACE
□ SUCTION SURFACE

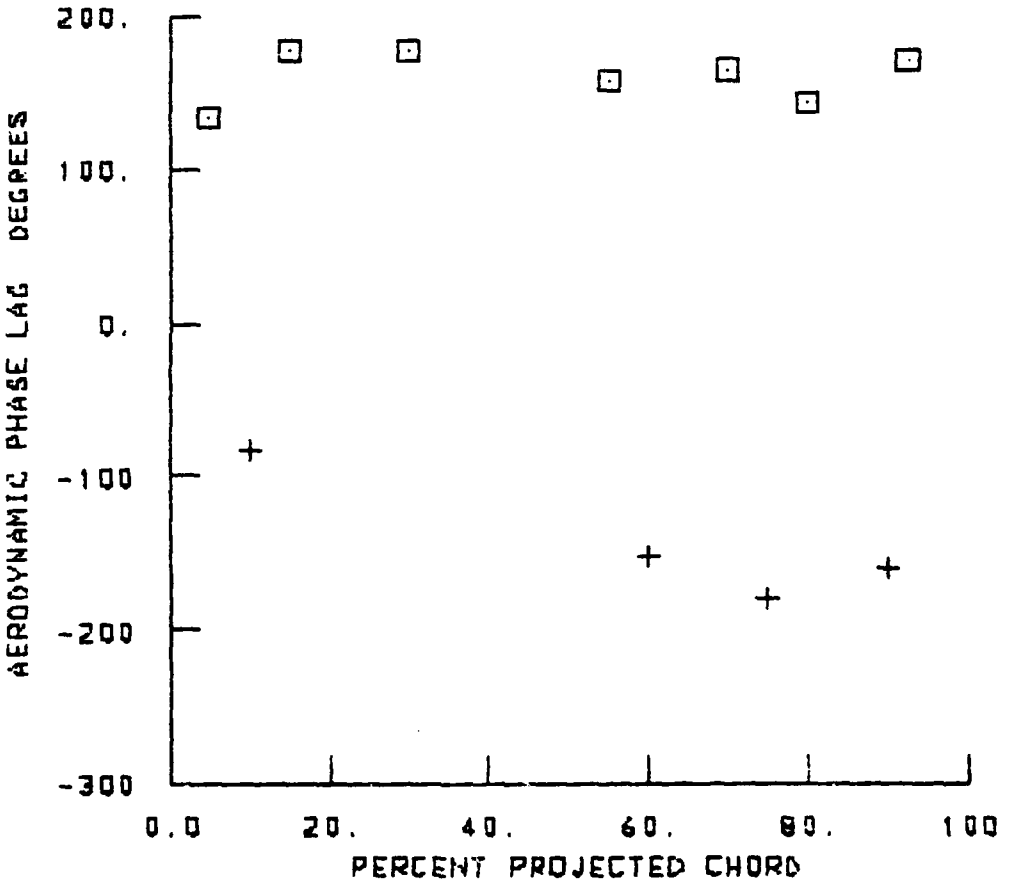

1 FEB., 1982

NORMALIZED SURFACE PRESSURE AMPLITUDES
2.8 TOTAL TO STATIC EXPANSION RATIO
90. DEGREES INTERBLADE PHASE ANGLE
+ PRESSURE SURFACE
□ SUCTION SURFACE

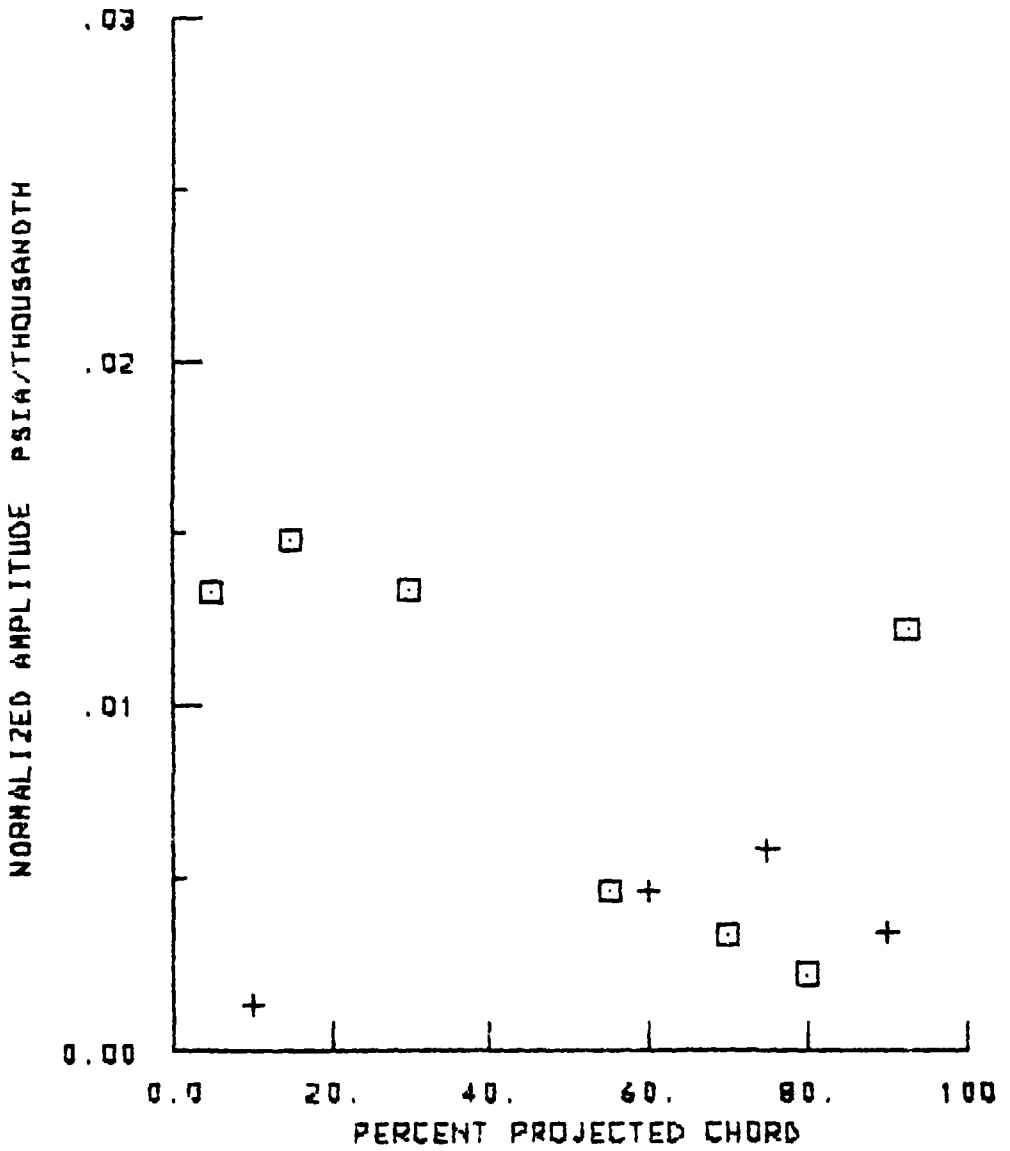

1 FEB., 1982

SURFACE PRESSURE PHASE LAGS
2.8 TOTAL TO STATIC EXPANSION RATIO
90. DEGREES INTERBLADE PHASE ANGLE
\+ PRESSURE SURFACE
□ SUCTION SURFACE

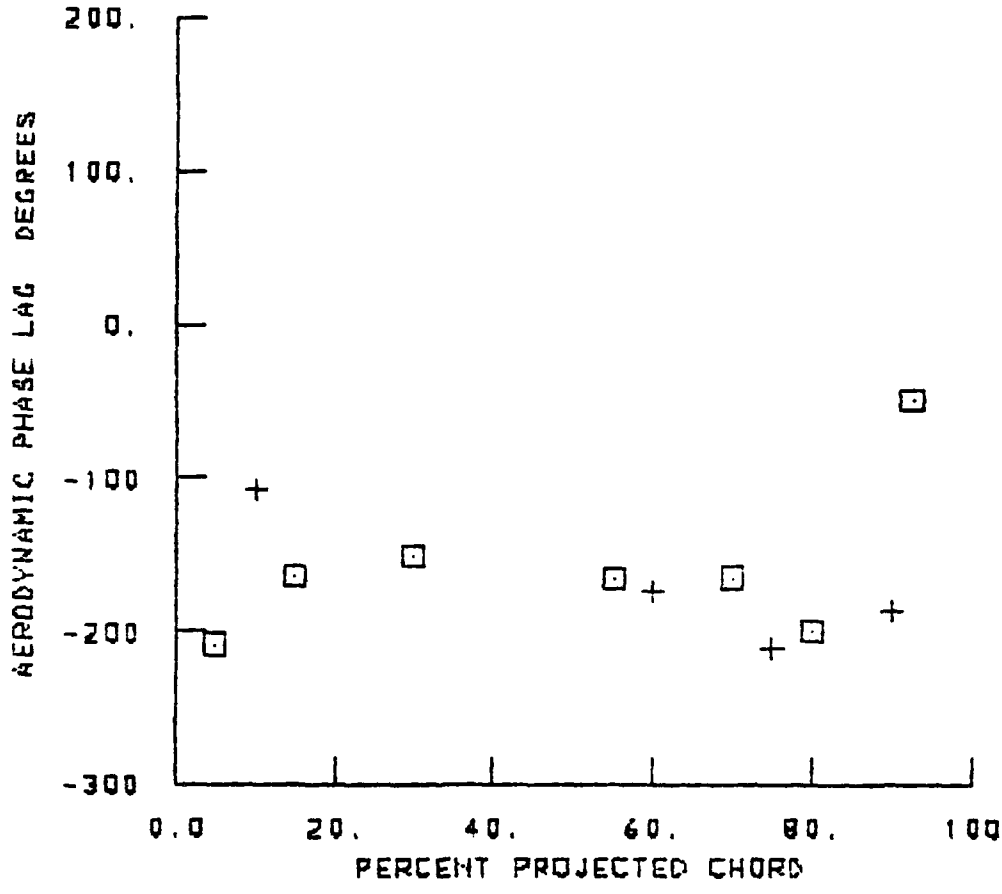

1 FEB., 1982

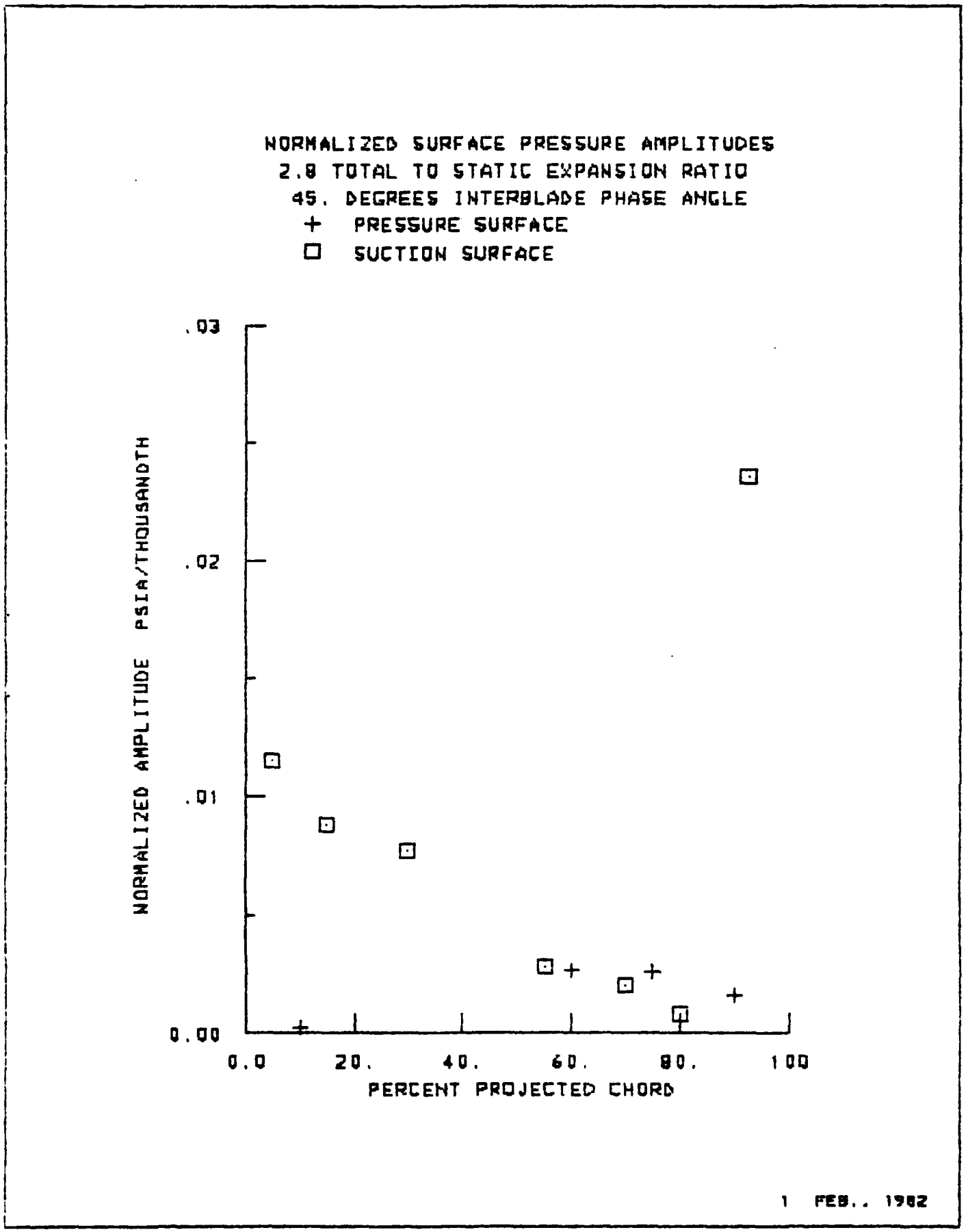
NORMALIZED SURFACE PRESSURE AMPLITUDES
2.8 TOTAL TO STATIC EXPANSION RATIO
45. DEGREES INTERBLADE PHASE ANGLE
+ PRESSURE SURFACE
□ SUCTION SURFACE
NORMALIZED AMPLITUDE PSIA/THOUSANDTH
.03
.02
.01
0.00
0.0
20.
40.
60.
80.
100
PERCENT PROJECTED CHORD
1 FEB., 1982

SURFACE PRESSURE PHASE LAGS
2.8 TOTAL TO STATIC EXPANSION RATIO
45. DEGREES INTERBLADE PHASE ANGLE
+ PRESSURE SURFACE
□ SUCTION SURFACE

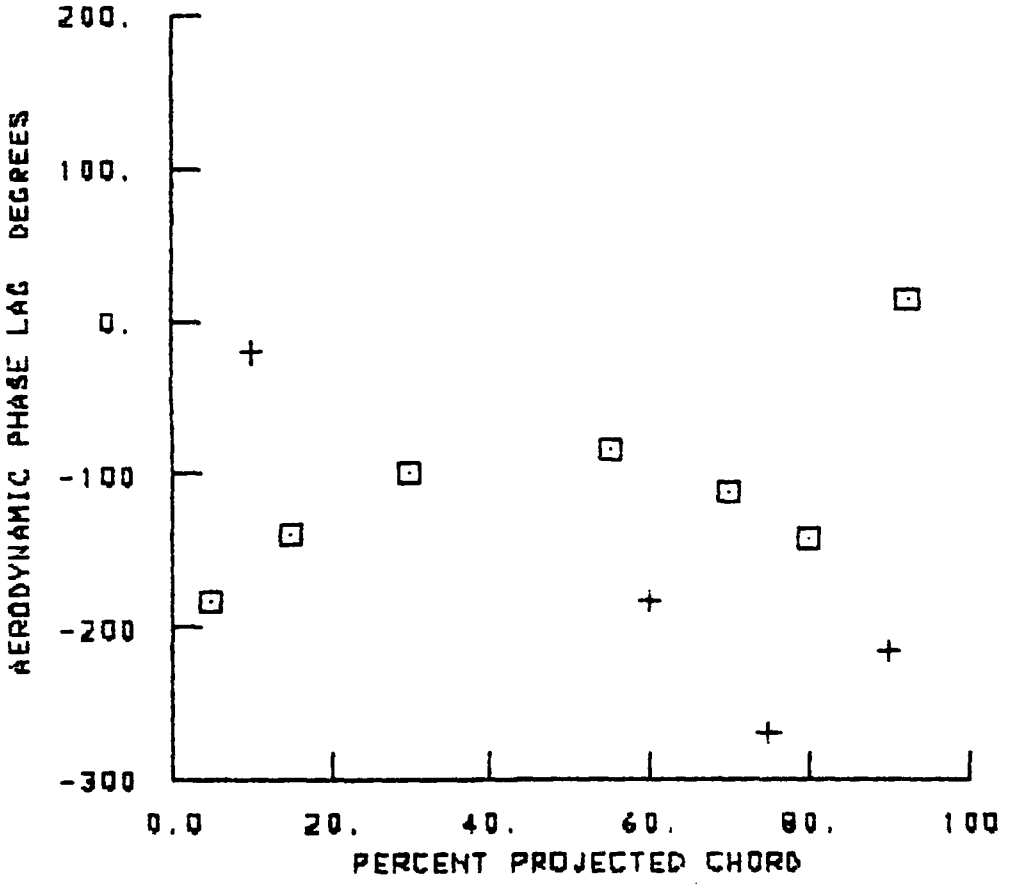

1 FEB., 1982

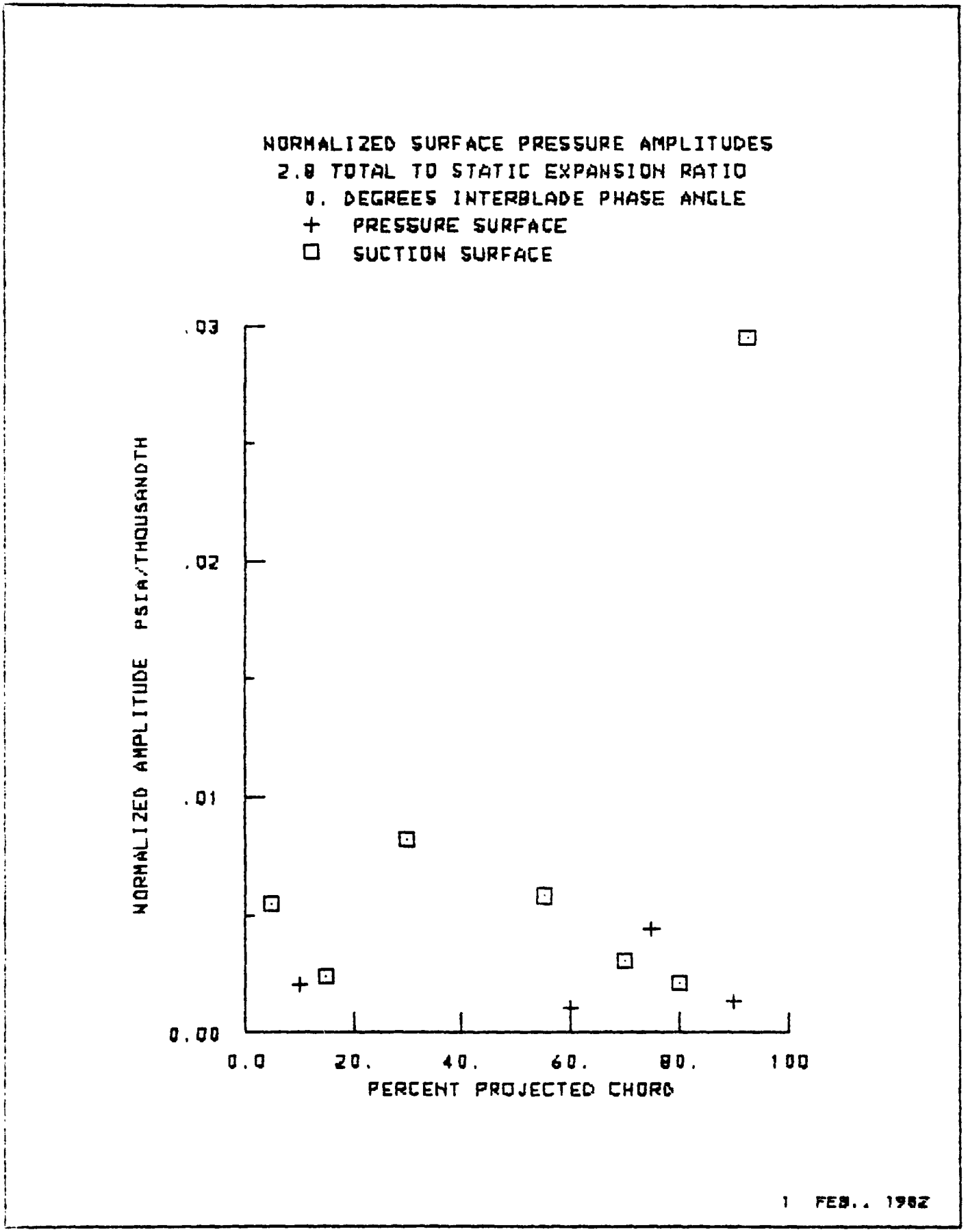
NORMALIZED SURFACE PRESSURE AMPLITUDES
2.0 TOTAL TO STATIC EXPANSION RATIO
0. DEGREES INTERBLADE PHASE ANGLE
+ PRESSURE SURFACE
□ SUCTION SURFACE
.03
.02
.01
0.00
NORMALIZED AMPLITUDE PSIA/THOUSANDTH
0.0
20.
40.
60.
80.
100
PERCENT PROJECTED CHORD
1 FEB., 1982

SURFACE PRESSURE PHASE LAGS
2.8 TOTAL TO STATIC EXPANSION RATIO
0. DEGREES INTERBLADE PHASE ANGLE
+ PRESSURE SURFACE
□ SUCTION SURFACE

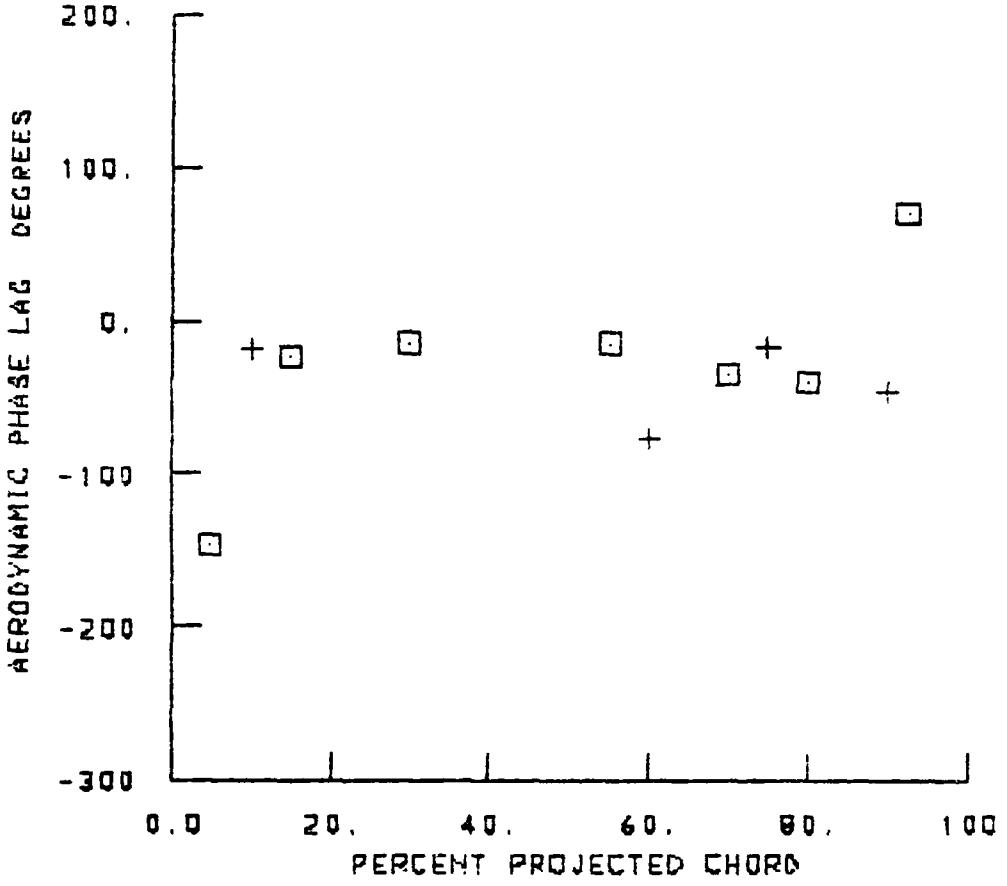

1 FEB., 1982

NORMALIZED SURFACE PRESSURE AMPLITUDES
2.8 TOTAL TO STATIC EXPANSION RATIO
-45. DEGREES INTERBLADE PHASE ANGLE
+ PRESSURE SURFACE
□ SUCTION SURFACE

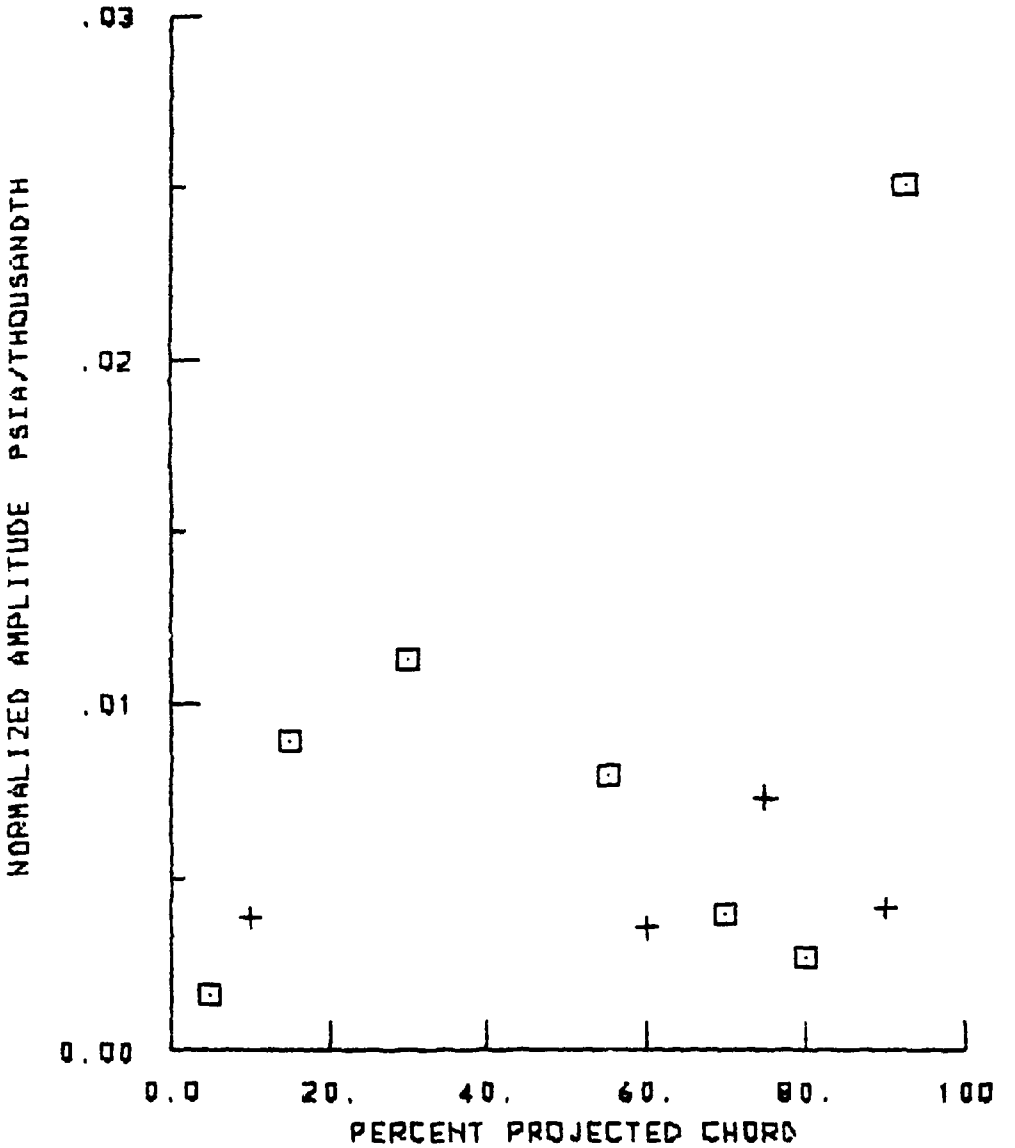

1 FEB., 1982

SURFACE PRESSURE PHASE LAGS
2.8 TOTAL TO STATIC EXPANSION RATIO
-45. DEGREES INTERBLADE PHASE ANGLE
+ PRESSURE SURFACE
□ SUCTION SURFACE

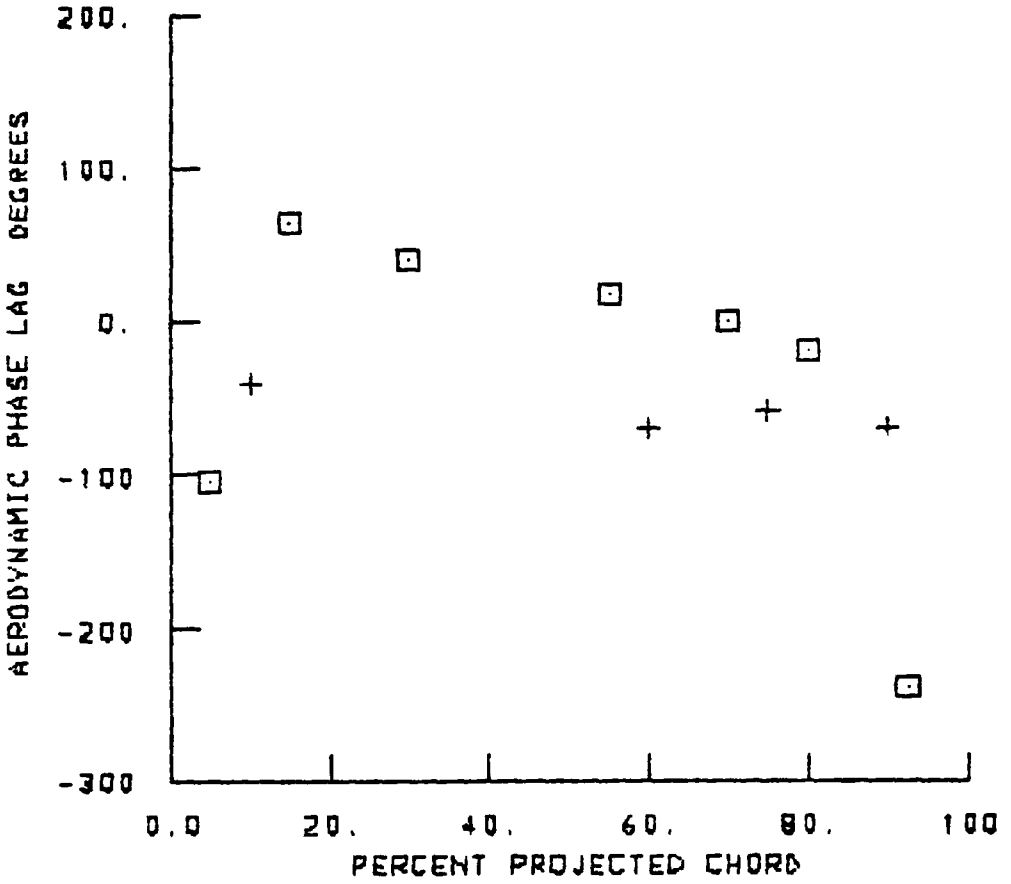

1 FEB., 1982

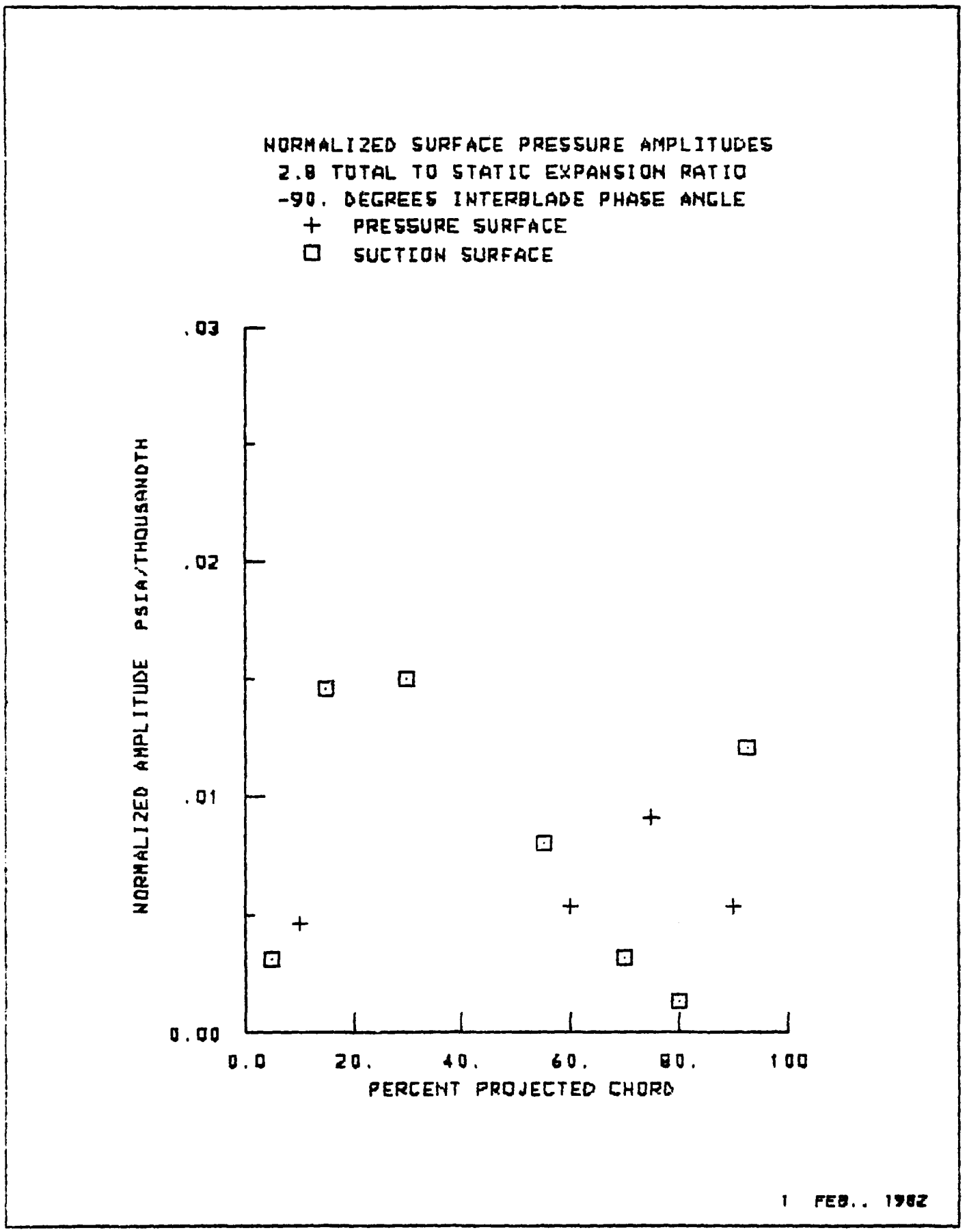
NORMALIZED SURFACE PRESSURE AMPLITUDES
2.8 TOTAL TO STATIC EXPANSION RATIO
-90. DEGREES INTERBLADE PHASE ANGLE
+ PRESSURE SURFACE
□ SUCTION SURFACE
.03
.02
.01
0.00
NORMALIZED AMPLITUDE PSIA/THOUSANDTH
0.0
20.
40.
60.
80.
100
PERCENT PROJECTED CHORD
1 FEB., 1982

SURFACE PRESSURE PHASE LAGS
2.8 TOTAL TO STATIC EXPANSION RATIO
-90. DEGREES INTERBLADE PHASE ANGLE
+ PRESSURE SURFACE
□ SUCTION SURFACE

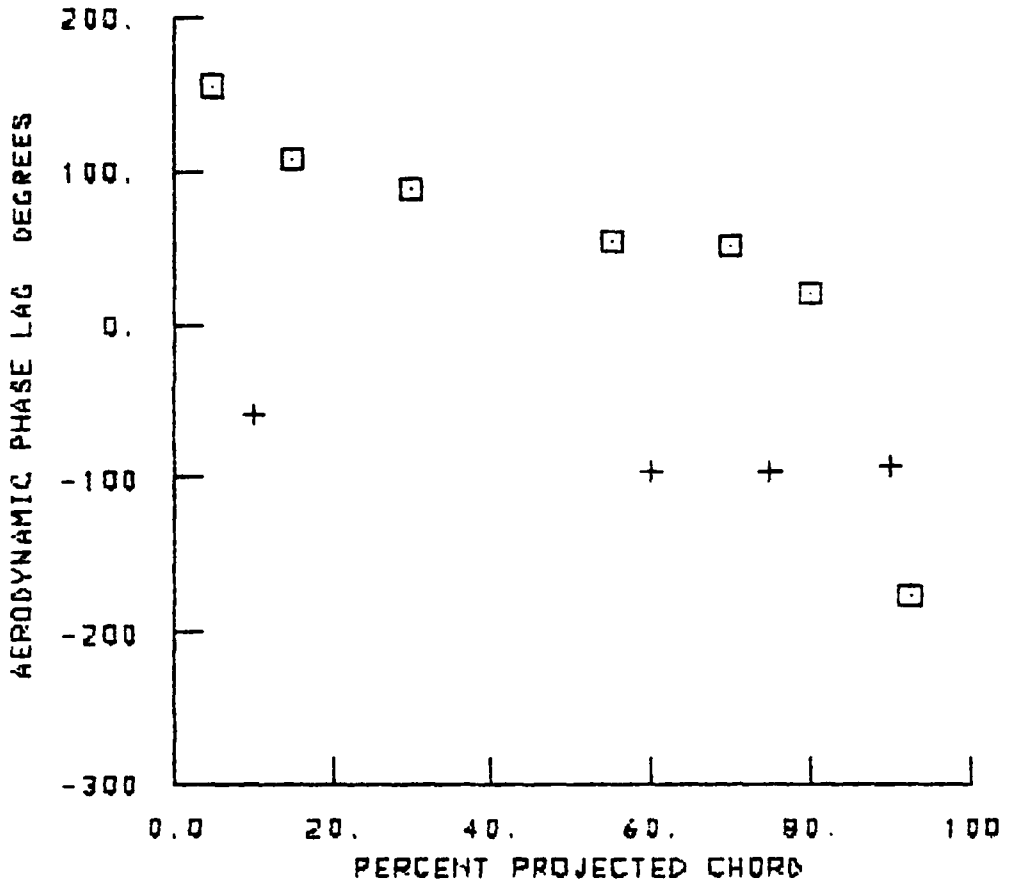

1 FEB., 1982

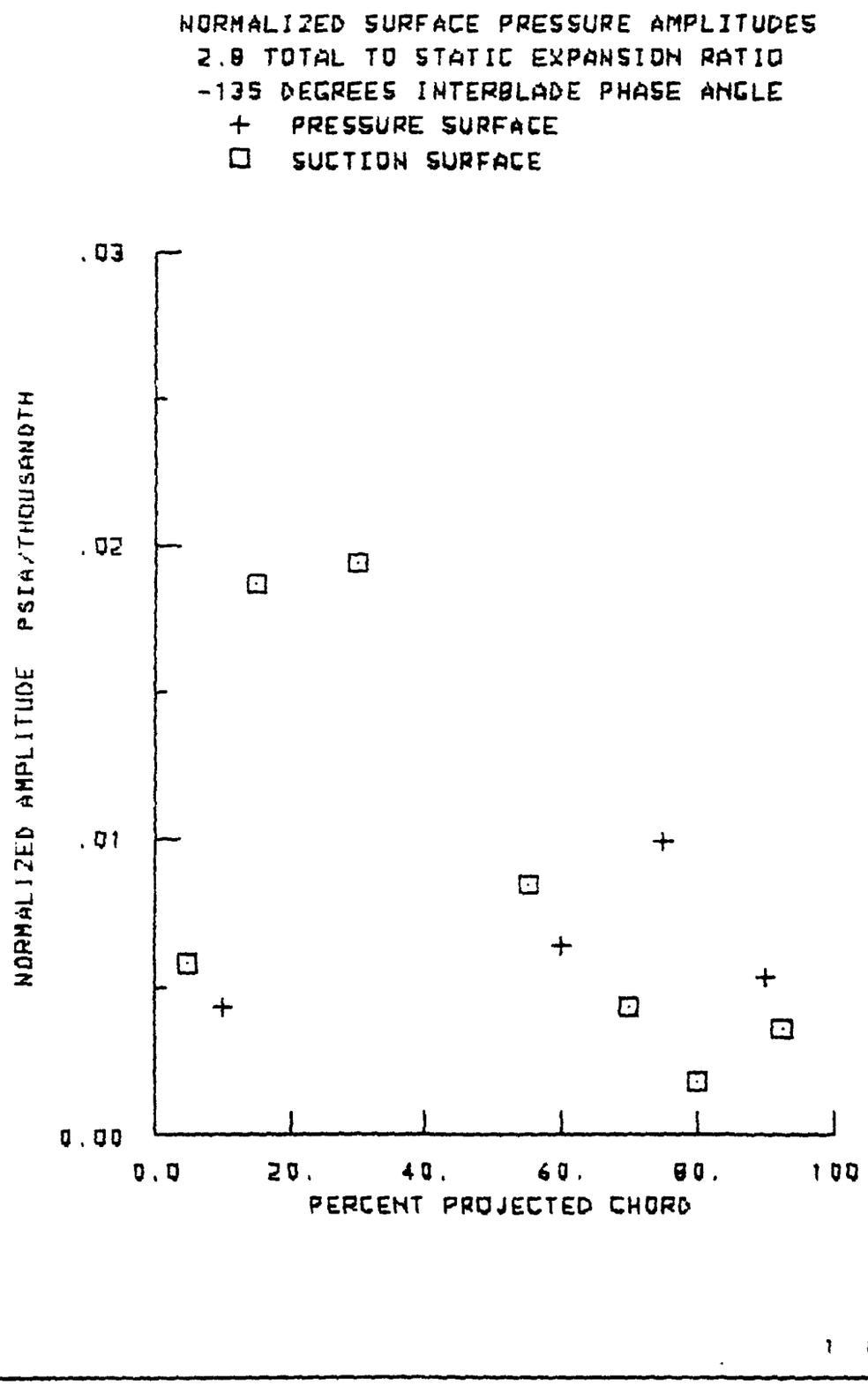
NORMALIZED SURFACE PRESSURE AMPLITUDES
2.8 TOTAL TO STATIC EXPANSION RATIO
-135 DEGREES INTERBLADE PHASE ANGLE
+ PRESSURE SURFACE
□ SUCTION SURFACE
.03
.02
.01
0.00
NORMALIZED AMPLITUDE PSIA/THOUSANDTH
0.0
20.
40.
60.
80.
100
PERCENT PROJECTED CHORD
1 FEB., 1982

SURFACE PRESSURE PHASE LAGS
2.8 TOTAL TO STATIC EXPANSION RATIO
-135 DEGREES INTERBLADE PHASE ANGLE
+ PRESSURE SURFACE
□ SUCTION SURFACE

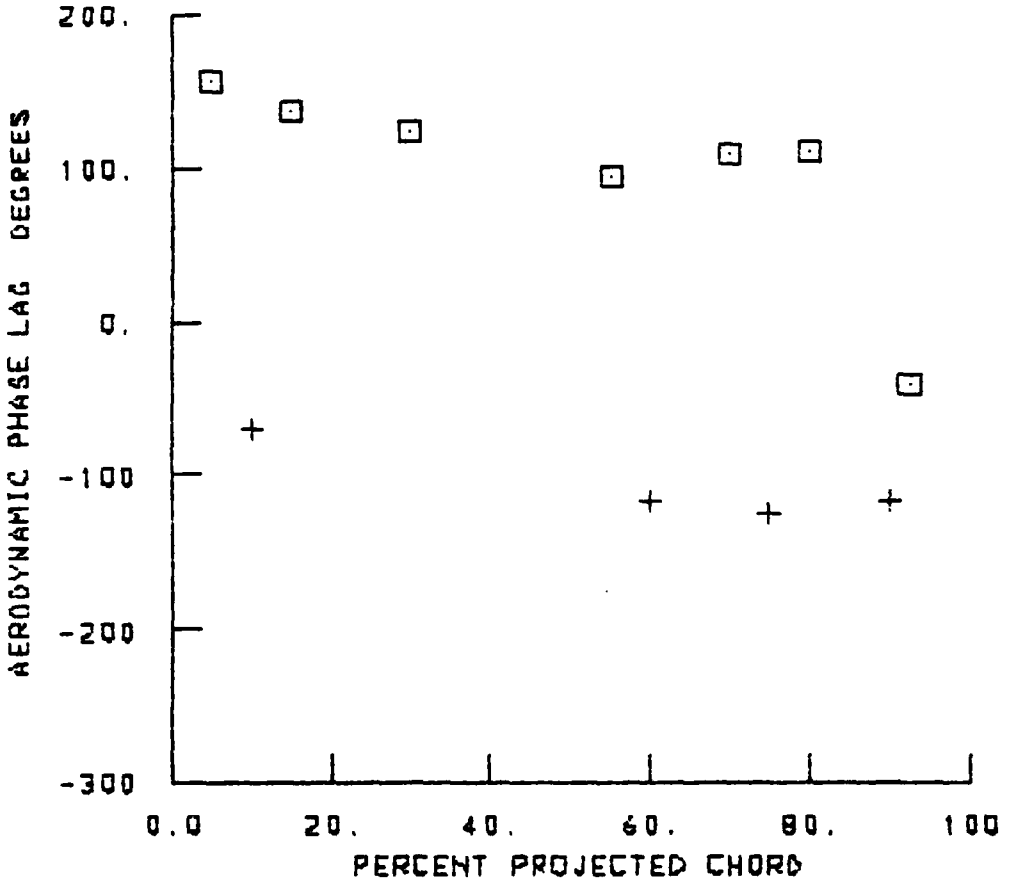

1 FEB., 1982

APPENDIX B

In this Appendix, the normalized pressure difference coefficient magnitude and phase lag as referenced to the center airfoil are presented for interblade phase angles of $\pm 45°$, $\pm 90°$, and $\pm 135°$.

NORMALIZED PRESSURE COEFFICIENTS

135° INTERBLADE PHASE ANGLE

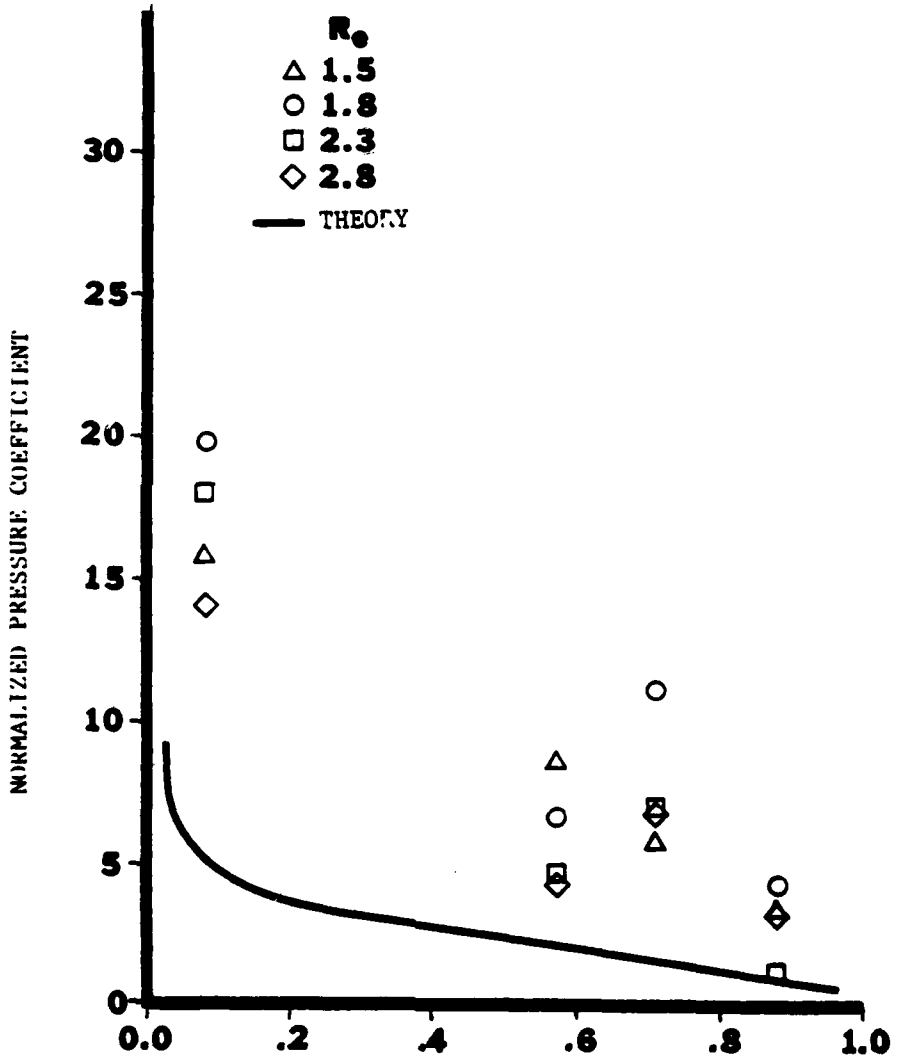

PHASE LAG

135° INTERBLADE PHASE ANGLE

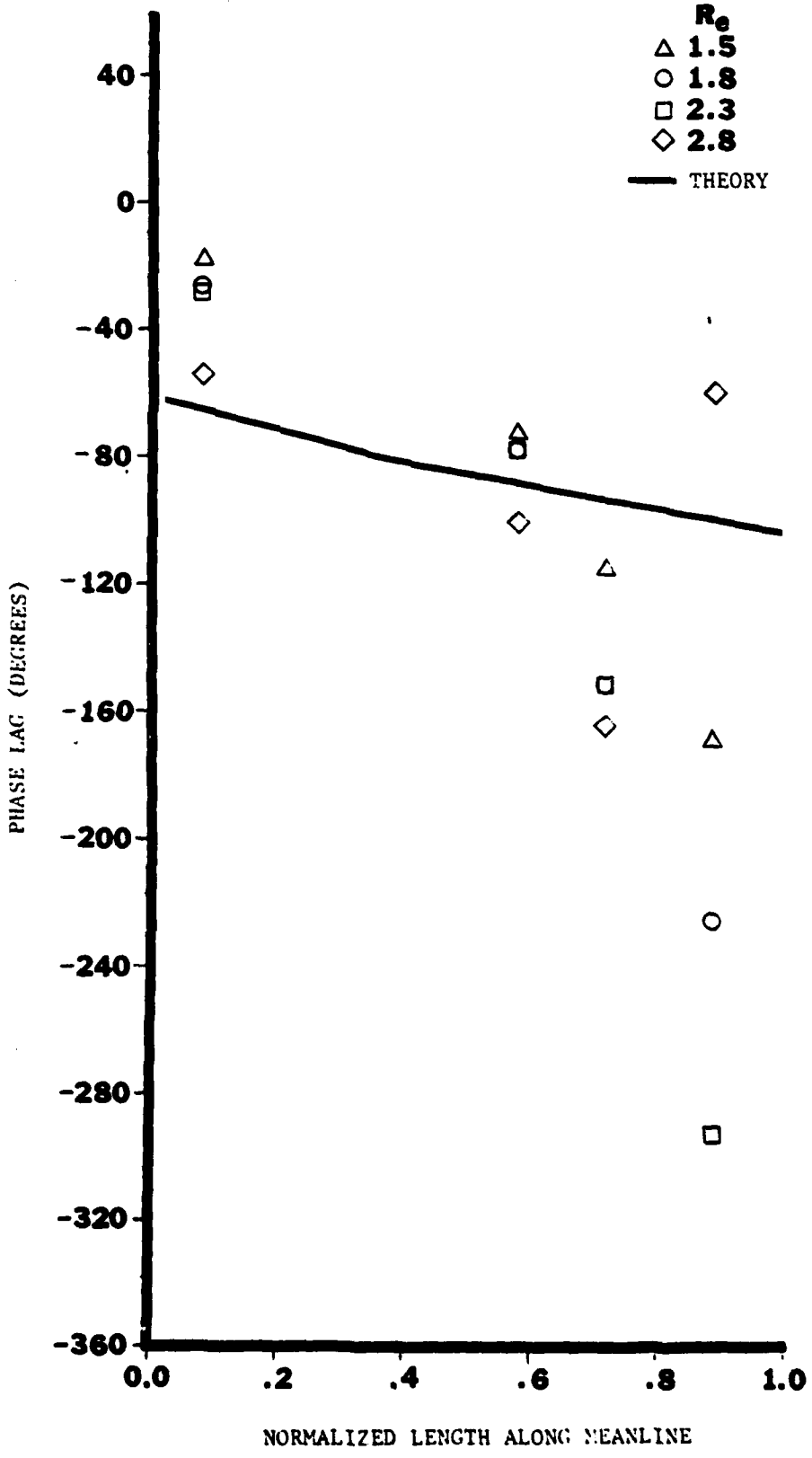

NORMALIZED PRESSURE COEFFICIENTS

90° INTERBLADE PHASE ANGLE

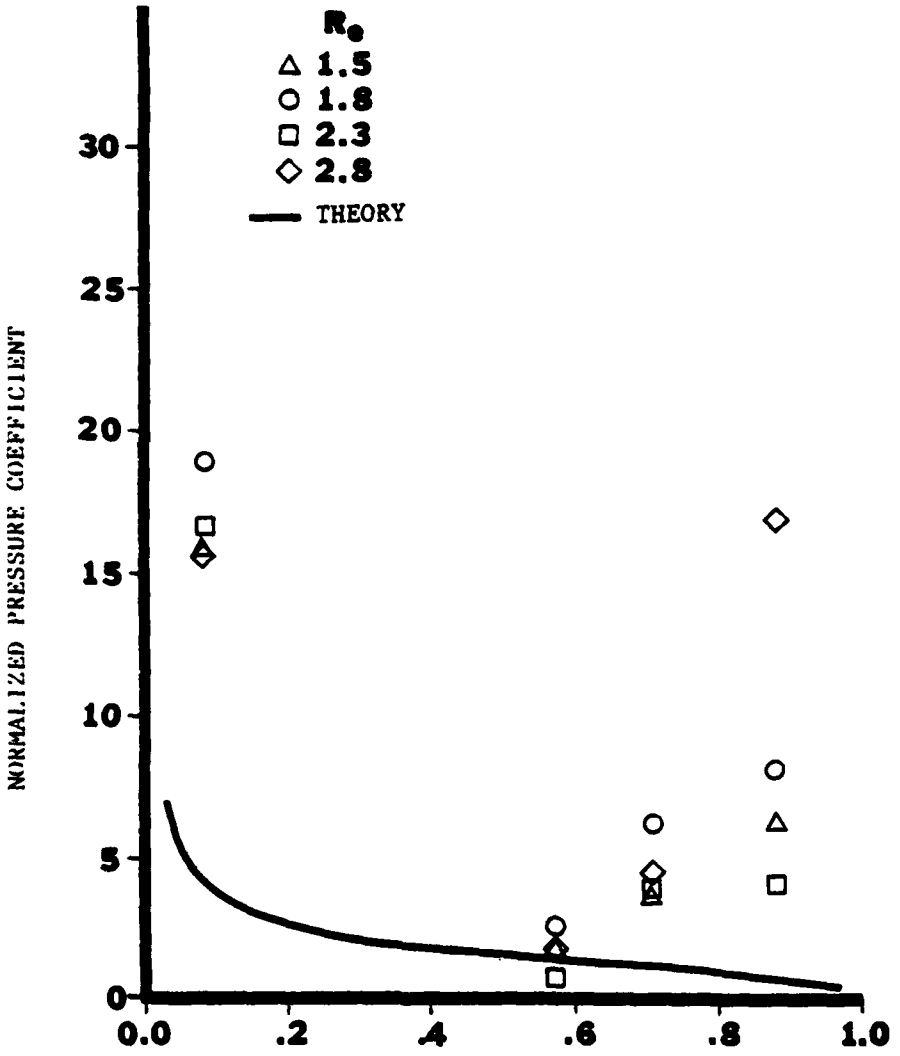

PHASE LAG

90° INTERBLADE PHASE ANGLE

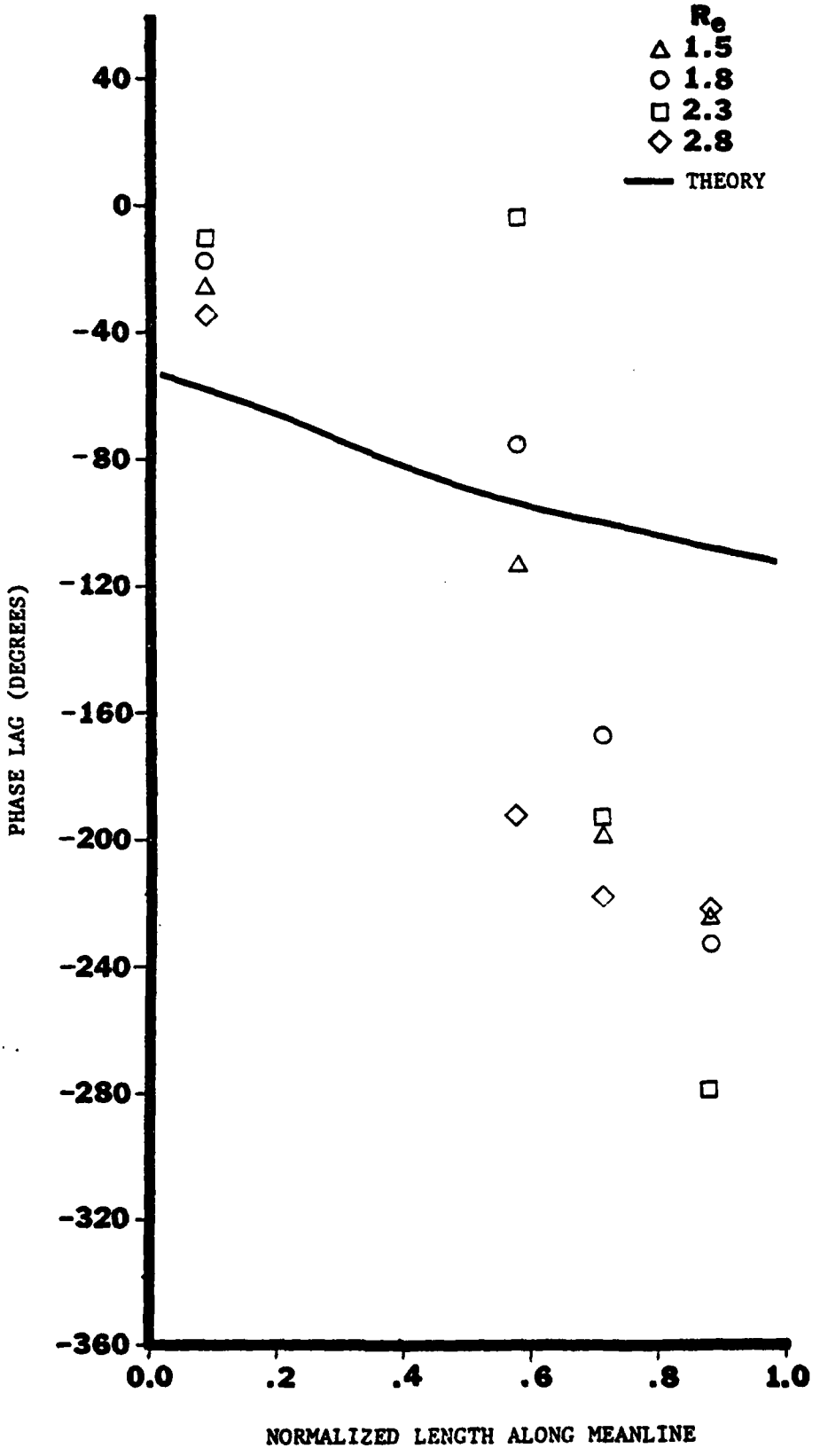

NORMALIZED PRESSURE COEFFICIENTS

45° INTERBLADE PHASE ANGLE

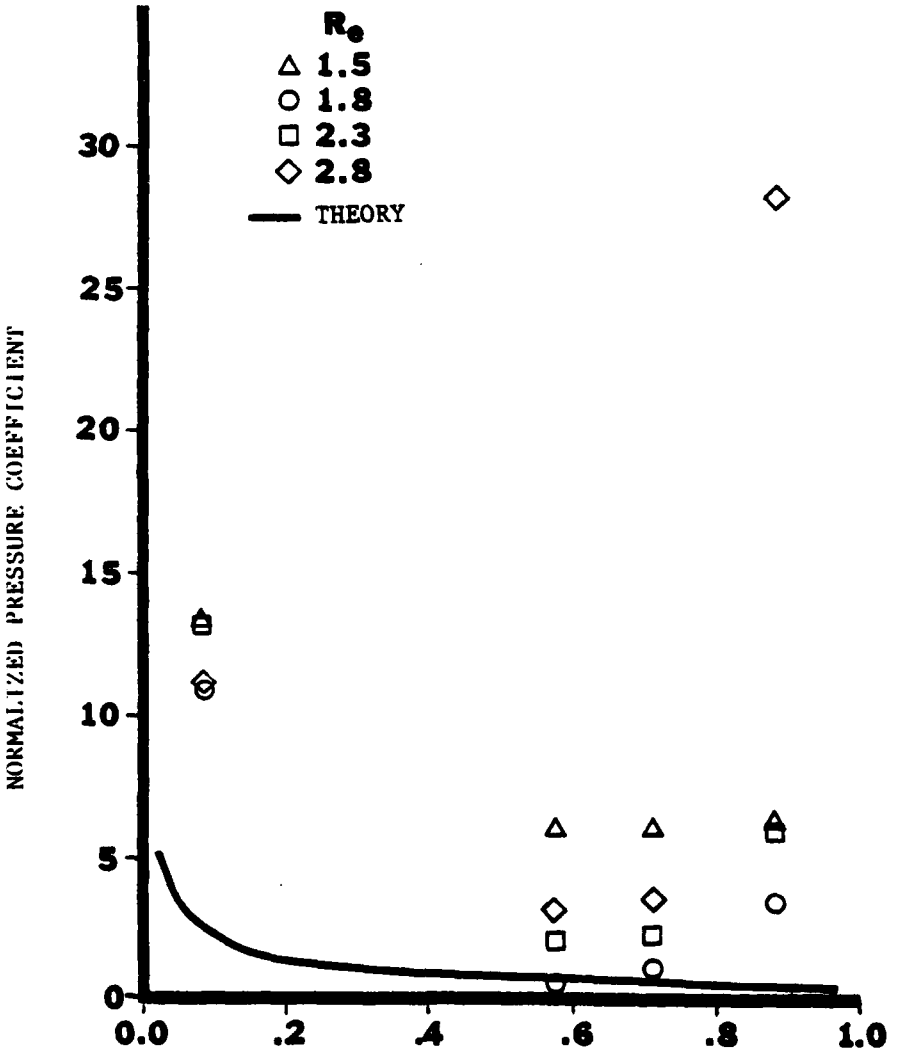

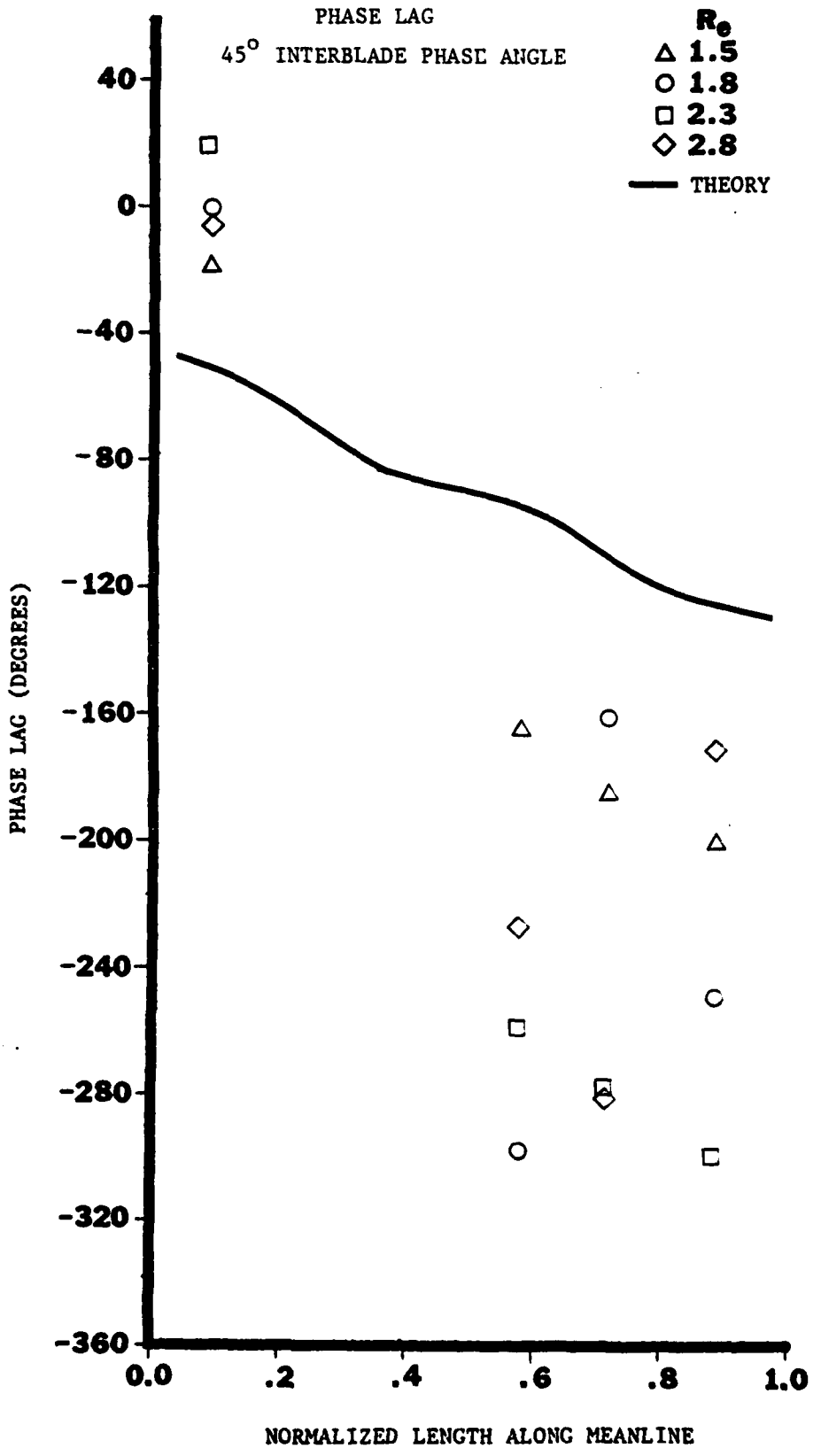
PHASE LAG
45° INTERBLADE PHASE ANGLE
R_e
1.5
1.8
2.3
2.8
THEORY
40
0
-40
-80
-120
-160
-200
-240
-280
-320
-360
PHASE LAG (DEGREES)
0.0
.2
.4
.6
.8
1.0
NORMALIZED LENGTH ALONG MEANLINE

NORMALIZED PRESSURE COEFFICIENTS

-45° INTERBLADE PHASE ANGLE

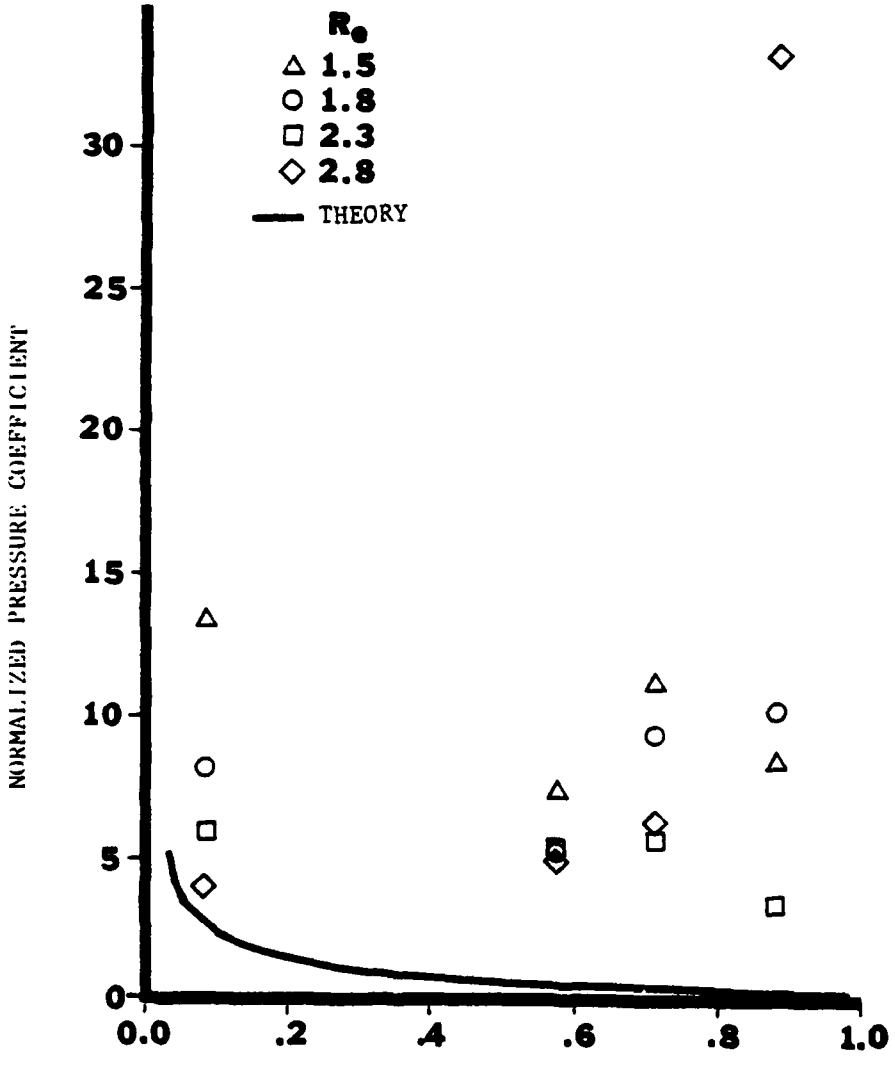

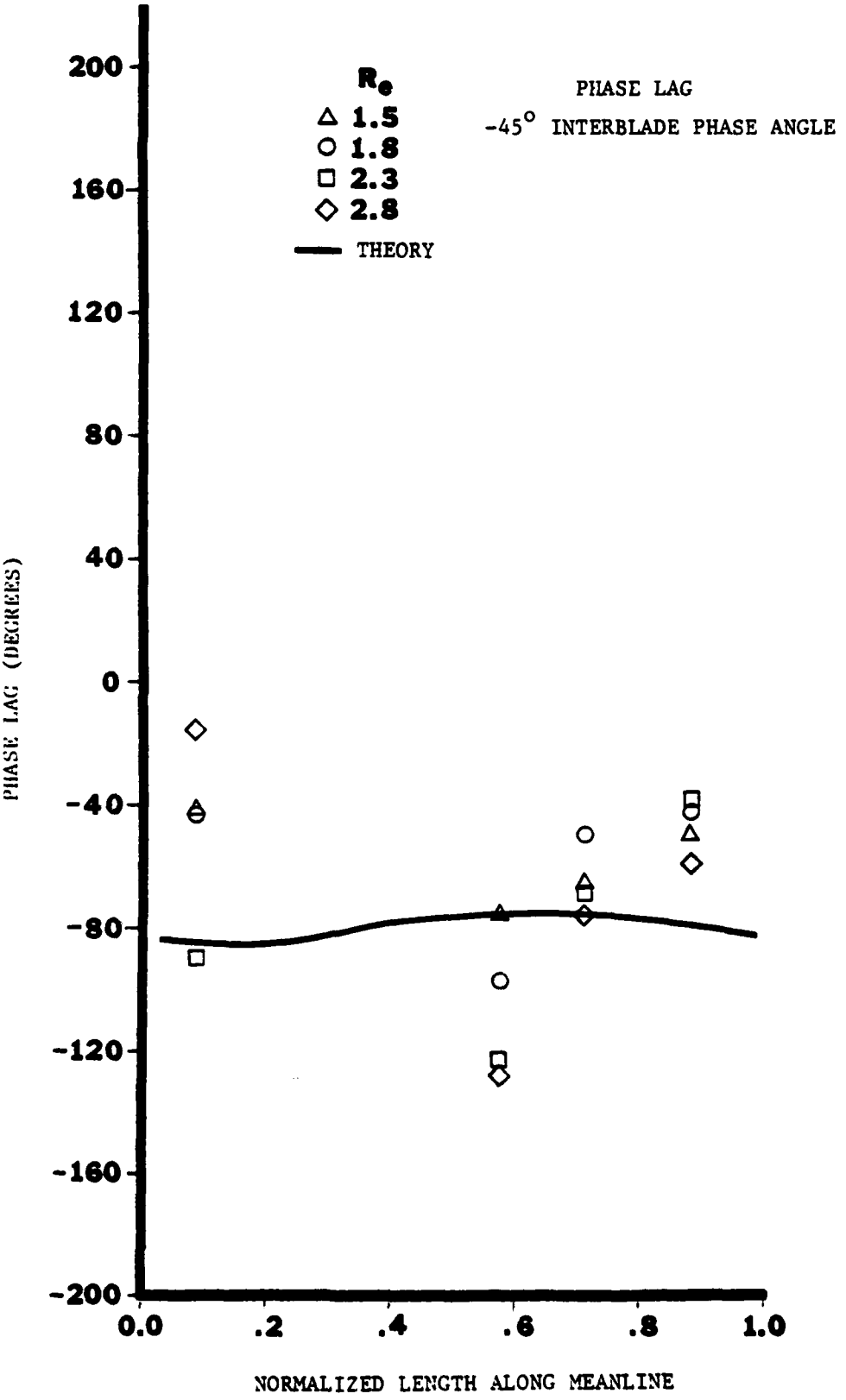
PHASE LAG
-45° INTERBLADE PHASE ANGLE
R_e
1.5
1.8
2.3
2.8
THEORY
200
160
120
80
40
0
-40
-80
-120
-160
-200
PHASE LAG (DEGREES)
0.0
.2
.4
.6
.8
1.0
NORMALIZED LENGTH ALONG MEANLINE

NORMALIZED PRESSURE COEFFICIENTS

-90° INTERBLADE PHASE ANGLE

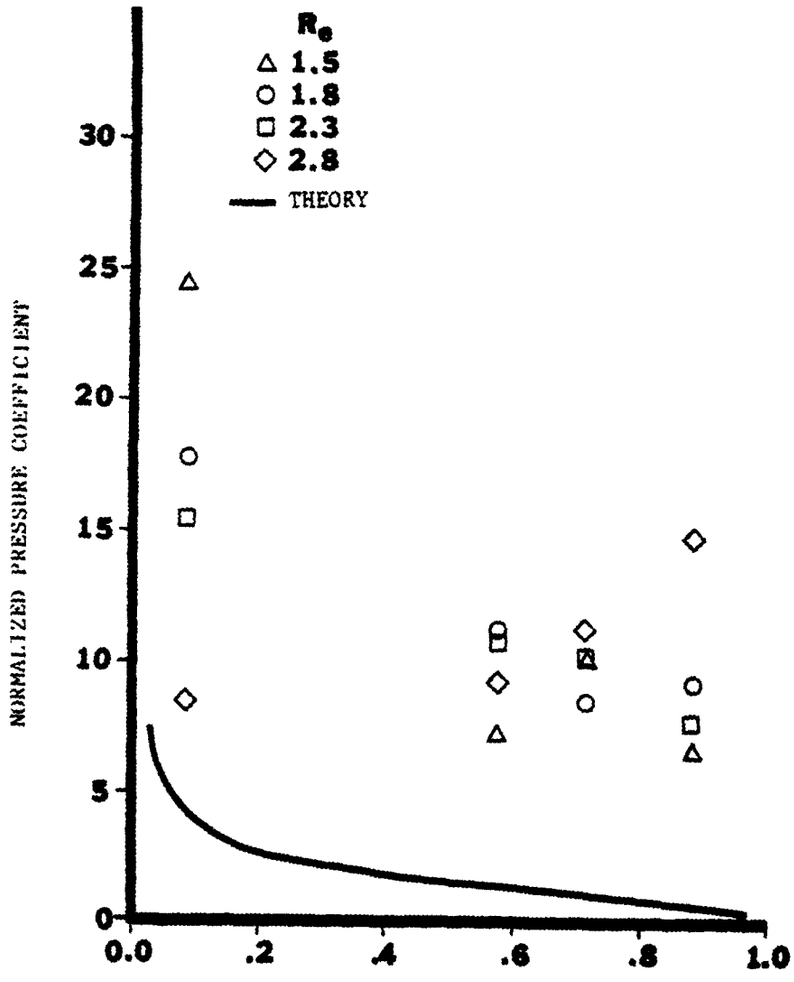

PHASE LAG

-90° INTERBLADE PHASE ANGLE

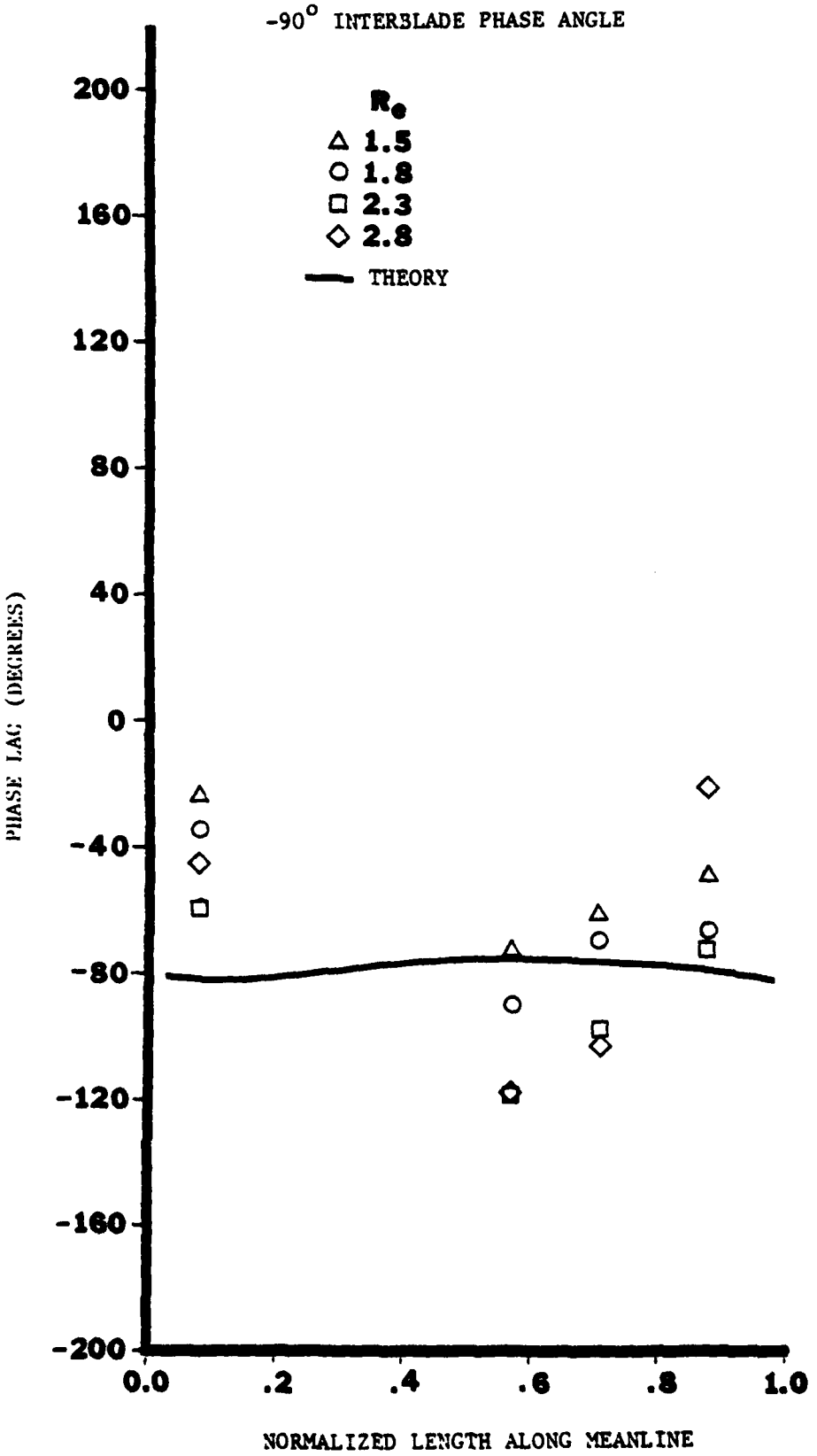

NORMALIZED PRESSURE COEFFICIENTS

-135° INTERBLADE PHASE ANGLE

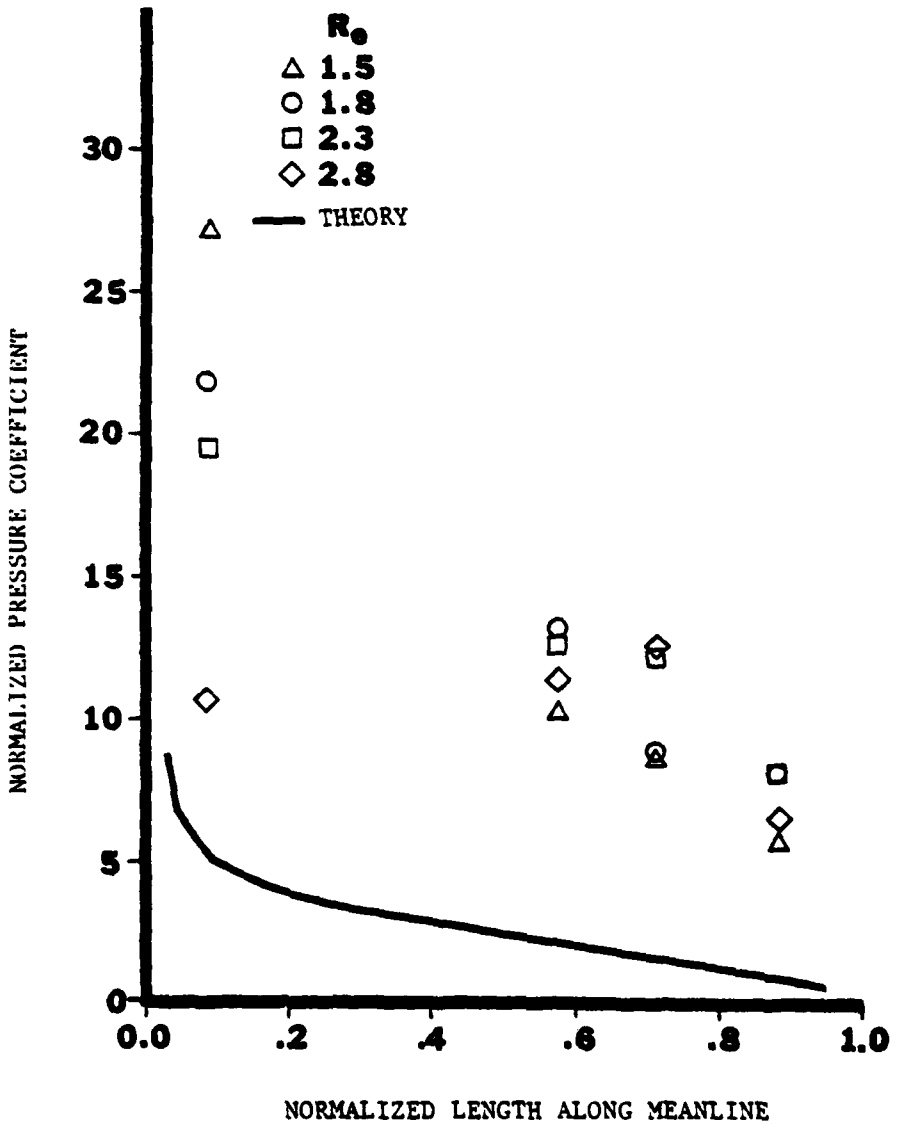

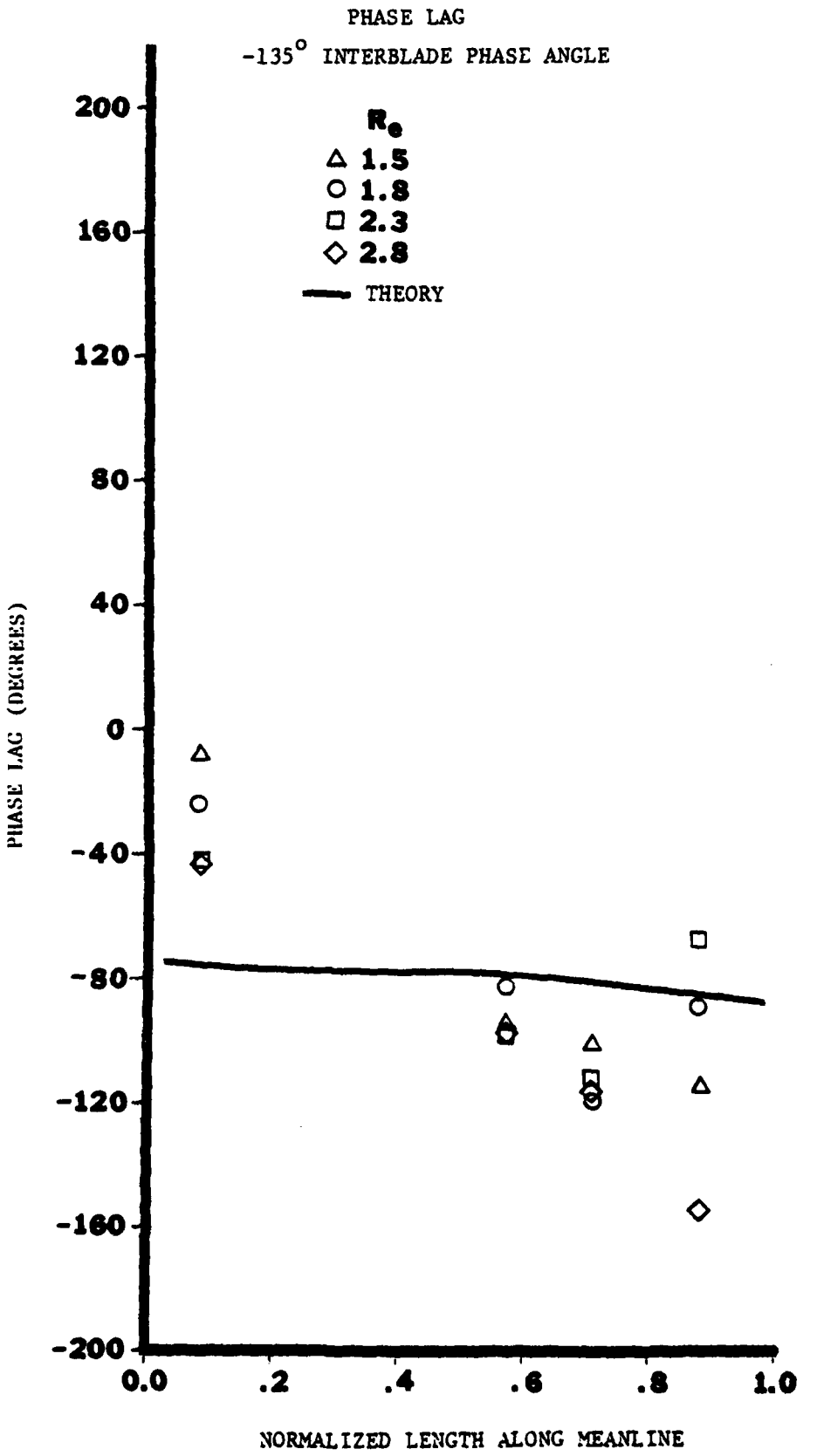
PHASE LAG
-135° INTERBLADE PHASE ANGLE
R_e
1.5
1.8
2.3
2.8
THEORY
200
160
120
80
40
0
-40
-80
-120
-160
-200
PHASE LAG (DEGREES)
0.0
.2
.4
.6
.8
1.0
NORMALIZED LENGTH ALONG MEANLINE


FILME
-8